Drug Delivery to the Hair Follicle:

Role of Follicular Tight Junctions as a Biological Barrier and the Potential for Targeting Clobetasol Nanocarriers

Christiane Mathes

Saarbrücken

2015

Drug Delivery to the Hair Follicle:

Role of Follicular Tight Junctions as a Biological Barrier and the Potential for Targeting Clobetasol Nanocarriers

Helmholtz-Institut für Pharmazeutische Forschung Saarland

HELMHOLTZ ZENTRUM FÜR INFEKTIONSFORSCHUNG

UNIVERSITÄT DES SAARLANDES

DISSERTATION

zur Erlangung des Grades

des Doktors der Naturwissenschaften der

Naturwissenschaftlich-Technischen Fakultät III

Chemie, Pharmazie, Bio- und Werkstoffwissenschaften
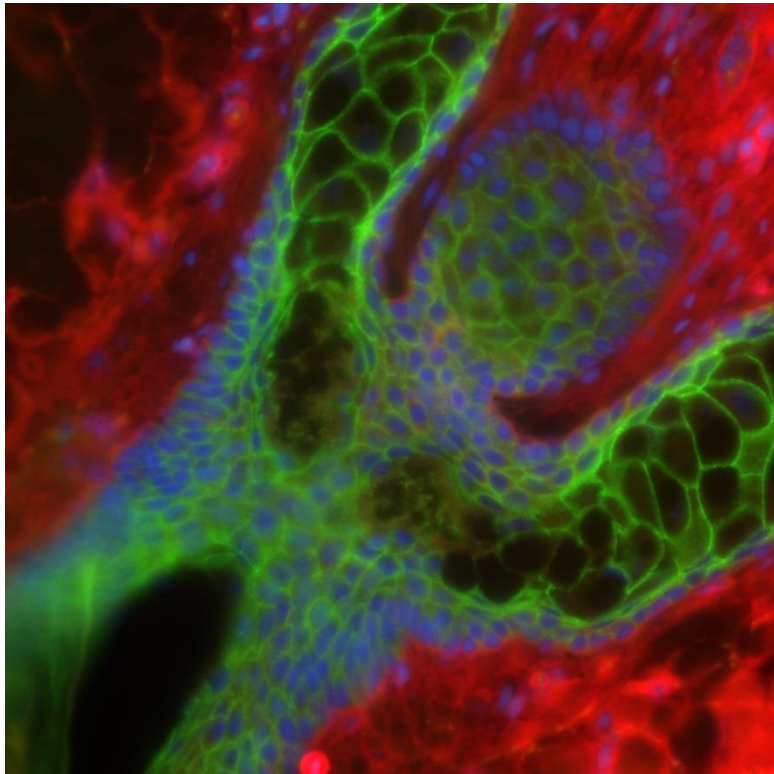
der Universität des Saarlandes

von

Christiane Mathes

Saarbrücken

2015

Tag des Kolloquiums: 03.02.2016

Dekan: Dr.-Ing. Dirk Bähre

Berichterstatter: Prof. Dr. Claus-Michael Lehr

     Prof. Dr. med. Thomas Vogt

Vorsitz: Professor Dr. Marc Schneider

Akademischer Mitarbeiter: Dr. Martin Frotscher

Für meine Familie.

"Happiness only real when shared."

Christopher McCandless

Table of Contents

Short Summary

The porcine ear skin model has become a well-accepted *in vitro* model for follicular uptake studies of nanoparticle-based drug delivery systems. The present study further confirms the suitability and transferability of this model to human tissue regarding chemical composition of various hair follicle (HF) components, as well as expression and localization of follicular tight junction (TJ) proteins claudin-1, -3, -4, occludin, and ZO-1, by means of confocal Raman microscopy, qPCR, and immunostaining, respectively. Moreover, combining confocal Raman microscopy and optical profilometry allowed for a 3-D analysis of cyanoacrylate biopsies, the main analytical method to quantify follicular uptake, showing the removal of intact HFs and thus only further corroborating suitability and reliability of this technique. Furthermore, functionality of follicular TJs was investigated and a continuous TJ barrier was detected throughout the HF via an extracellular tracer molecule, confirming a second line of defense for xenobiotics. Modification of this barrier using EDTA was feasible. Lastly, the interplay of follicular uptake and interfollicular, transdermal permeation of three different nanocarriers for Clobetasol was evaluated. Although differing in the molecular architecture, all three particles displayed similar drug-releases and a similar reduction in skin permeation as opposed to dissolved drug. Follicular uptake, however, was particle-dependent. Massage amplified this uptake.

Kurzzusammenfassung

Das Schweineohr-Hautmodell ist ein anerkanntes *in vitro*-Modell für follikuläre Aufnahmestudien von Nanopartikel-basierten Wirkstoffträgersystemen. Die vorliegende Arbeit bestätigt die Übertragbarkeit dieses Modells auf den Menschen hinsichtlich chemischer Zusammensetzung der verschiedenen Haarfollikel (HF)-Komponenten, sowie der Expression und Lokalisierung der follikulären Tight Junction (TJ) Proteine Claudin-1, -3, -4, Occludin und ZO-1, welche mittels konfokaler Raman Mikroskopie, qPCR und Immunfärbung gezeigt werden konnten. Durch die Kombination von konfokaler Raman-Mikroskopie und optischer Profilometrie wurde zudem eine 3D-Analyse von Cyanoacrylatbiopsien durchgeführt. Diese Analyse zeigte eine Entfernung des gesamten, intakten HF, wodurch Nutzen und Zuverlässigkeit der Technik bewiesen wurden. Ebenfalls wurde die Funktionalität der follikulären TJs untersucht. Mit Hilfe eines extrazellulären Tracermoleküls wurde eine intakte, kontinuierliche TJ-Barriere über den gesamten HF festgestellt, welche durch EDTA geöffnet werden konnte. Schließlich wurde ein Zusammenspiel zwischen follikulärer Aufnahme und Hautpermeation durch Verwendung dreier verschiedener mit Clobetasol-beladener Nanopartikel gezeigt. Obwohl sich diese in ihrem molekularen Aufbau unterscheiden, erzeugten alle ähnliche Arzneimittel-Freisetzungsprofile, sowie eine vergleichbare Minderung der Hautpermeation. Die follikuläre Aufnahme war jedoch Partikelabhängig. Massage verstärkte diese Aufnahme stets.

1. General Introduction

1.1. The Skin

The skin is the largest visible organ of the mammalian body (in humans about 2 m^2) and, due to its easy accessibility, a very attractive site for drug administration. It represents the interface between the body and the external environment. Due to its complex structure it is indispensable in its function as a barrier, regulating heat and water loss from the inside, as well as invasion of exogenous substances from the outside. Furthermore, the skin is important for xenobiotic metabolism and sensation [1].

It can be roughly divided into three sections: the epidermis, the dermis, and the subcutis. Detailed information about anatomy, organization, and function of human skin can be found in references [2, 3].

1.1.1.   The Epidermis

The epidermis is the heterogeneous, outermost layer of the skin and due to its composition it is mainly in charge of barrier function. It can again be subdivided into the hydrophobic *stratum corneum* (SC) and the rather hydrophilic viable epidermis (the *stratum granulosum*, the *stratum spinosum*, and the *stratum basale*, a.k.a. *stratum germinativum).*[1]

The *stratum corneum,* the outermost layer of the epidermis, is also known as the rate-limiting barrier in skin permeability. It is composed of large, keratin-based, non-viable, cornified plate-like cells (corneocytes), which are embedded in intercellular lipids [4]. Due to this organization and its graphic resemblance, it can often be found in literature described as the brick-and-mortar model (see Figure 1), even though the *in vivo* structure is more complicated [5].

Like other renewable tissue, the epidermis maintains its structural stability through a continuous process of cell renewal (starting at the basal cell layer) balanced by desquamation (shedding of the terminally differentiated corneocytes of the SC), exhibiting a turnover time of ~28 days [6]. During this time the cells (keratinocytes) undergo a differentiation process in which expression of many epidermal differentiation markers is initiated; as differentiation proceeds they move from the *stratum basale* towards the SC, where they eventually become corneocytes. Besides providing nutrients for this differentiation process, the viable epidermis also provides protection against exposure to

---

[1] Another layer, the *stratum lucidum*, is only present in some anatomical areas like the sole of the feet or the palm of the hand, e.g. areas of "thick skin". It is a thin, clear layer of dead skin cells present between the *stratum corneum* and *stratum granulosum.*

ultraviolet light via melanin production by melanocytes, and is involved in the immune response (antigen presenting cells mainly present in *stratum spinosum*) [6].
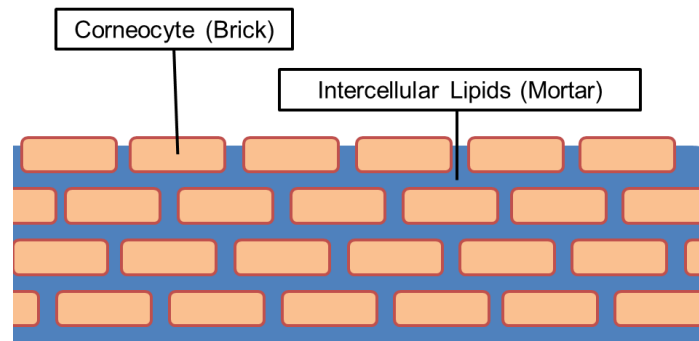
Figure 1: Diagram of the *stratum corneum* structure also known as the brick-and-mortar model (modified from [2]; not drawn to scale).

Another cell type present in the basal layer of the epidermis and epithelial sheath of the hair follicle is the Merkel cell [7]. These sensory cells are in charge of transmitting signals via synaptic contacts to somatosensory neurons thereby allowing the sensation of touch.

1.1.2.   The Dermis

The dermis is mainly composed of collagen and elastic fibers, giving rise to the skins' pliability, elasticity, and tensile strength [8]. These fibers plus cells like fibroblasts (mainly responsible for the synthesis of collagen and elastin), macrophages, or mast cells, are embedded in a matrix made up of proteoglycans and gelatin. Additionally, the dermis contains vascular channels (providing nourishment and waste removal for dermal and epidermal cells), lymph vessels and nerves, as well as skin appendages like the hair follicle or secretory glands [2].

1.1.3.   The Subcutis

The subcutis, or hypodermis, is located beneath the dermis and is mainly responsible for insulating the body, providing an energy reservoir, and for acting as a shock absorber or cushion for the body. It is mainly composed of loose fat, connective tissue, blood vessels, and nerves.

1.2. The Hair Follicle

Anatomically, the hair follicle (HF) embodies a tubular invagination of the epidermis. At birth, each person is covered with around 5 million HFs [9]. This number does not increase with time, although the size of the follicles, as well as the hairs, can be subject to change throughout a person's life.

Already during embryogenesis, the formation of the HF occurs and is dependent upon a series of signals that are sent between dermal cells and underlying epithelial cells [10]. These signals are responsible for triggering fate changes in both cell populations, which in turn results in the differentiation of the hair shaft, the root sheaths, and the dermal papillae. Once the HF is established, hair growth is a cyclic process with every HF undergoing an active growing phase (anagen), a regression and shortening phase (catagen), and a resting phase (telogen). Based on this, the mature HF can be divided into an "upper part", which does not cycle visibly, and a "lower part", which undergoes continuous remodeling during each hair cycle [11].

1.2.1. Anatomy of the Hair Follicle

The HF itself can be considered a complex miniorgan of the skin, which includes the pilosebacious unit, the apocrine gland and the arrector pili muscle [11]. For the purpose of this work, however, the term HF only refers to the structure made of the inner and outer root sheaths, as well as the hair shaft. As a whole, the HF can be divided into five sections when starting at its bottom and going up towards the skin surface: the bulb, the suprabulbar region, the central region, the isthmus, and the infundibulum (Figure 2).

1.2.1.1. The Bulb and Suprabulbar Region

The bulb represents the deepest, most distal part of the HF and is the site where biological synthesis of the hair takes place. It consists of the hair matrix (i.e. the germinative zone) and the dermal papilla, which is mainly composed of mesenchymal cells, and is believed to regulate the growth cycle of the hair [12]. The matrix cells[2] ultimately differentiate into the inner root sheath (IRS) and the hair shaft (see Section 1.2.2.2 & 1.2.2.3, respectively) [13].

The suprabulbar region is located just superior to the bulb. This is the site where the various layers of the hair begin to differentiate, and is also known as the keratogenous zone. As cell division unfolds and the matrix cells proliferate rapidly, they move up into this zone where they increase in volume, elongate, become larger, and begin to 'keratinize' [14]. Furthermore, melanin synthesis by melanocytes begins here, resulting in pigmentation of the hair.

1.2.1.2. The Isthmus and Central Region

The isthmus section of the HF marks its most superior point at the insertion point of the sebaceous gland, and reaches down to the insertion point of the arrector pili muscle (see Figure 2), including the

---

[2] The distal matrix cells are also sometimes referred to as trichocytes

so-called bulge of the HF [13, 15]. This region is of special interest to many researches, as the bulge is known to contain putative follicular epithelial and melanocytic stem cells which are, for example, involved in epithelial regeneration during wound healing [16-19]. Spanning from below the arrector pili muscle to the suprabulbar region of the HF is the so-called central region. In this region the hair undergoes its final stages of keratinization.
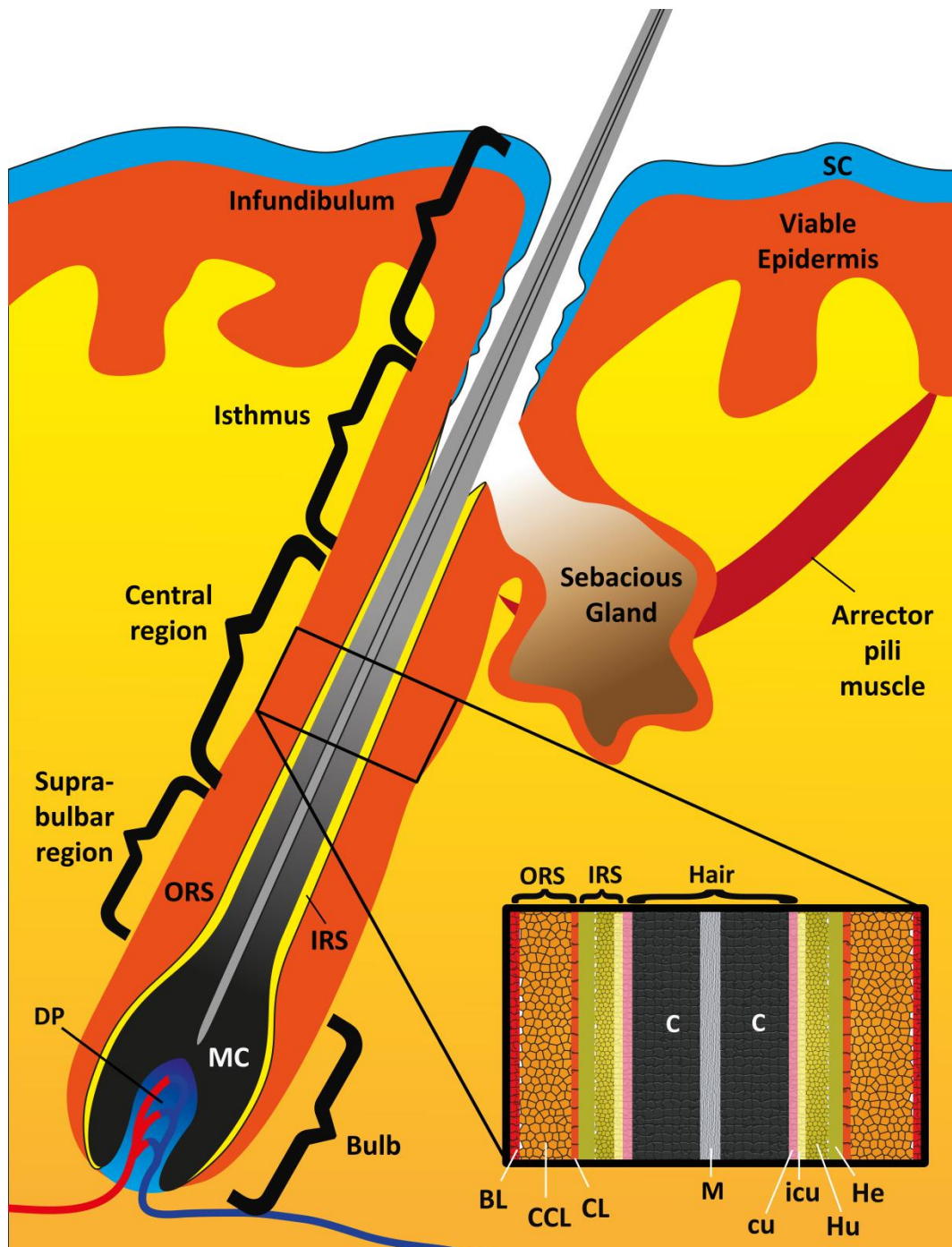
Figure 2: Schematic overview showing the anatomy of the hair follicle. BL = basal cell layer of ORS, C = cortex of hair, cu = cuticle of the hair shaft, CL = companion cell layer of ORS, CCL = central cell layer of ORS, DP = dermal papilla, He = Henle's layer of IRS, Hu = Huxley's layer of IRS, icu = cuticle of IRS, IRS = inner root sheath, M = medulla of hair, MC = matrix cells, ORS = outer root sheath, SC = *stratum corneum* (not drawn to scale).

1.2.1.3.   The Infundibulum

The infundibulum is the uppermost segment of the HF starting at the epidermis, and reaching down to the beginning of the sebaceous duct. It is a continuation of the interfollicular epidermis, thus it represents the interface between the skin epithelium and the outside world. Even though this part of the HF is often regarded simply as a canal whose duty is to only guide the outwards passage of the hair shaft, it actually harbors a rich microflora. Many cells are found in this region dealing, among many other functions, with antigen recognition and presentation due to a dense network of antigen presenting cells [20-22]. Since the HF is an invagination of the epidermis, and the infundibulum is the uppermost region of it (see Figure 2), the SC is still present and intact in the upper region; however, in the lower part of the infundibulum it is already less developed and more permeable [23].

1.2.2.   Compartments of the Hair Follicle

The HF itself is composed of several morphologically distinct and concentrically organized compartments: the outer root sheath (ORS), the inner root sheath (IRS), and the hair shaft (see Figure 2 & Figure 3).
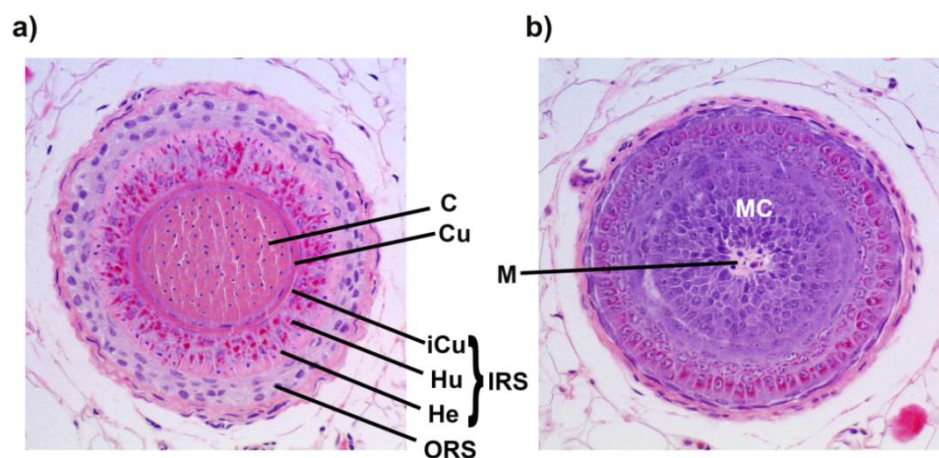
Figure 3: Coss-sections stained using haematoxylin & eosin (H&E) depicting the central region (a) and the bulb (b) of a terminal anagen hair. C = cortex Cu= cuticular layer of hair shaft, He = Henle's layer of IRS, Hu = Huxley's layer of IRS, icu = cuticle of IRS, IRS = inner root sheath, M = medulla, MC = matrix cells.

All three compartments are further subdivided into sub-compartments, which will be explained in detail below. Using protein gel electrophoresis, a lot of insight was gained on the morphologic diversity of the HF in the past, as the diverse protein pattern of keratins (hair keratins vs. epithelial keratins) was shown to mirror this situation nicely [24].

1.2.2.1. Outer Root Sheath

The outer root sheath (ORS) comprises the most peripheral epithelial cell layers of the follicle and is contiguous with the interfollicular epidermis [13]. It envelopes almost the entire HF (except the dermal papilla) and contains various cell types including melanocytes, Langerhans cells (dendritic cells responsible for antigen presentation; mostly located in infundibulum), and Merkel cells [9]. Thus, this section allows the HF to act as a sensory organ, as well as being the immunological gate-keeper for the skin.

It is structurally divided into three layers (Figure 2). The outermost layer is known as the basal cell layer (equivalent to the basal cell layer of the epidermis), followed by the central cell layer (CCL) and the innermost monolayer, known as the companion cell layer (CL).

1.2.2.2. Inner Root Sheath

As previously described, the inner root sheath (IRS) is a development which stems from the matrix cells in the bulb of the HF. It starts at the bulbar zone of the HF and abruptly desquamates in the middle of the isthmus [14, 24]. The IRS connects distally to the CL of the ORS and proximally to the hardening hair fiber. It can yet again be divided into three layers: Henle's layer, a monolayer located on the outside of the IRS connected to the CL of the ORS, Huxley's layer in the center, and the cuticle of the IRS which is in close contact with the hair shaft (Figure 2 & Figure 3). Interestingly, the order of differentiation and keratinization undergoes a different sequence for these three compartments. Differentiation starts in Henle's layer, proceeds to Huxley's layer and ends with the cuticle [25]. Keratinization, on the other hand, begins in Henle's layer, followed by the cuticle and lastly occurs in Huxley's layer.

1.2.2.3. Hair Shaft

The hair shaft is the other main product of the undifferentiated matrix cells in the bulb. It is a strong fiber which is composed of terminally differentiated, dead keratinocytes. Going from the inside to the outside it can be structurally divided into the medulla, comprised of living polygonal cells, the cortex, and, most peripherally, the cuticle of the hair shaft (Figure 2).

1.3. Tight Junctions

Tight junctions (TJs) are barrier-forming paracellular junctions composed of various TJ transmembrane proteins (e.g. claudins, occludin, tricellulin, and junctional adhesion molecules

(JAMs)), cytoplasmic linker or adaptor proteins, which connect them to the actin cytoskeleton (e.g. ZO-1, -2, -3, cingulin, MAPP1), and signaling molecules (e.g. Protein kinase C) which control the paracellular transport (see Figure 4) [26-28].

They were first identified on the ultrastructural level by Farquhar and Palade in 1963 in various simple epithelia [29]. In that study, they were shown to be part of a tripartite junctional complex consisting of *zonula occludens* (tight junctions), *zonula adhaerens* (intermediary junctions), and *macula adhaerens* (desmosomes). Although differing in the precise arrangement of the complex, the existence of TJs was already then shown in epithelia of many organs including the stomach, intestine, gall bladder, as well as uterus or oviduct epithelia.

Out of the three mentioned junctional complexes (tight junctions, intermediary junctions, desmosomes) TJs are the most apical ones in simple epithelia, while being intermingled in complex endothelia, e.g. brain endothelia [27]. Under normal conditions an intercellular membrane space is not present between two neighboring cells at TJ positive sites, which can be visualized in transmission electron microscopy as a very close contact between the neighboring cells. Therefore, they are also often referred to as "sites of fusion" or "kissing points" [30, 31].
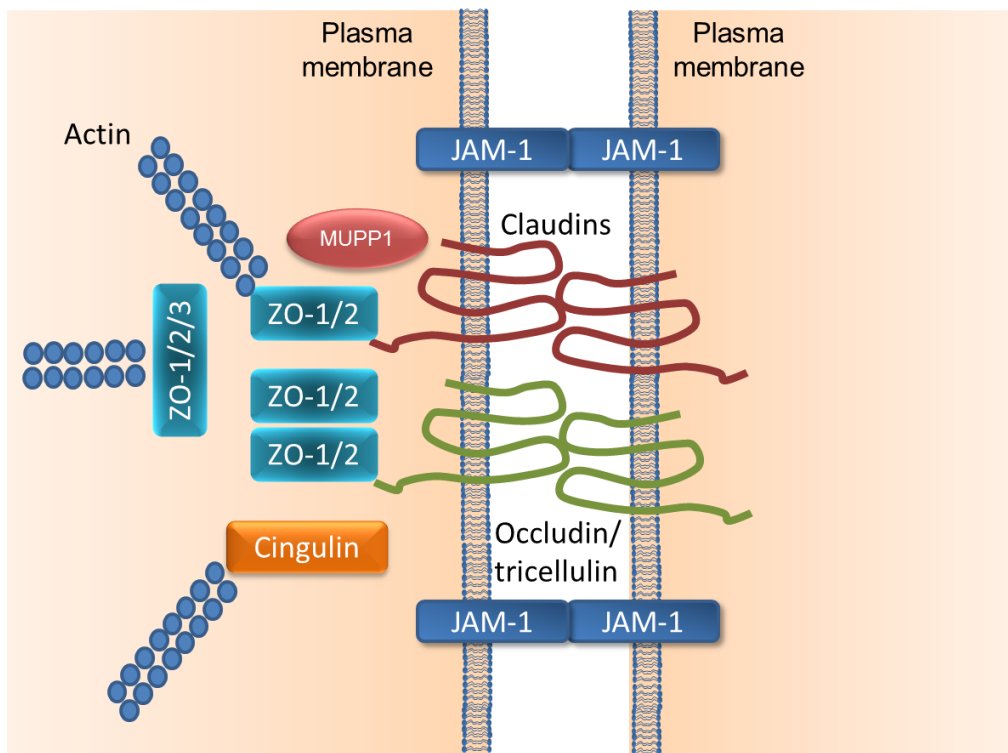

Figure 4: Schematic representation of the basic structural transmembrane components of tight junctions. Claudins and Occludin/tricellulin as well as JAMs are transmembrane proteins. ZO-1, ZO-2 and cingulin provide a direct link to the actin cytoskeleton (modified version of image in [31]).

For the purpose of this doctoral thesis, the focus was placed on five specific tight junction proteins: Occludin (Ocln), Claudin-1 (Cldn-1), Cldn-3, Cldn-4, and zonula occludens protein 1 (ZO-1).

1.3.1.   Occludin

Occludin (Ocln), a member of a larger protein family called TAMPs (TJ associated Marvel proteins (Marvel: (Myelin and Lymphocyte-related proteins for vesicle trafficking and membrane link)) has been under investigation regarding its exact function and role in TJs [32] for many years. It is a four-pass integral membrane protein (ca. 65 kDa) involved in signaling pathways and TJ assembly [33]. It was the first TJ protein to be discovered in 1993 by Furuse and colleagues [34]. Ocln is known to interact with the actin cytoskeleton by binding actin directly, or via adapters like ZO-1, -2, -3, or cingulin [28]. During TJ assembly and disassembly it can also associate with enzymes which induce post-translational modifications (phosphorylation, dephosphorylation, or ubiquitination). In order to determine whether this protein is not only structurally important, but also essential for intact barrier properties, various different studies dealing with Ocln modifications have been performed in the past. These TJ studies of structure and functionality ranged from Ocln over-expression to knock-out mutations in mice. While the over-expression studies revealed that Ocln is important for TJ assembly, and that TJ barrier integrity may even be enhanced [35], the results from the knock-out studies surprised the investigators. TJs did not appear to be morphologically affected by the lack of Ocln, and barrier function of the intestinal epithelium, evaluated based on transepithelial resistance (TER), was normal [36, 37]. There are two possible explanations for this. Either Ocln is dispensable for TJ barrier function, or, in contrast, Ocln is so important that there is a backup system in charge of compensating for it by using other proteins during development. Interestingly, however, histological examinations revealed numerous abnormalities in various organs of these knock-out mice; most likely due to dramatic changes in gastric morphology and secretory function hinting at additional, non-barrier related functions.

In the skin, Ocln has been shown to be confined to the granular cell layer, or *stratum granulosum* [38]. This restricted distribution was also seen in human HFs [30]. By means of immunostaining, this TJ protein was localized in the companion cell layer (CL) and neighboring cells of the ORS in the isthmus and central region, in the CL of the lower central and suprabulbar region, and completely negative in the ORS of the bulb. The IRS of human HF was positive for Ocln from the bulbar to the lower central region.

1.3.2.   Claudins

Cldn-1, -3, and -4 are also integral membrane proteins which span the lipid bilayer four times with the N- and C-termini oriented towards the cytoplasm and two extracellular loop domains [39]. They belong to a family of (as of now) 27 members, the first ones also identified by Furuse *et al.* in 1998 [40]. Compared to Ocln they are smaller in size (22-27 kDa) and give rise to completely different amino acid sequences. Especially Cldn-1 and Clnd-4 have been recognized as important regulators of paracellular transport in various epithelia. Their C-terminus binds to the PDZ domains[3] (for detailed review please refer to reference [41]) of TJ adapter proteins like ZO-1 and cingulin, which allows them to indirectly interact with the actin cytoskeleton. In the past, many studies have involved the over-expression, knock-down, or knock-out of claudins, which all consistently resulted in large changes in paracellular permeability in simple epithelia. While the role of Clnd-1 regarding skin barrier function in mice was shown to be vital (see Section 1.3.4), involvement of TJ protein Cldn-4 in barrier function has to date only been demonstrated in lung cells. There, inhibiting this protein resulted in an increase in paracellular permeability in healthy lung, yet an increase in Clnd-4 expression was seen in a lung injury model [42]. Thus, normal expression levels of this protein seem to be extremely important regarding its correct function.

Distribution of these two TJ proteins in skin differs greatly. While Cldn-1 is localized throughout the entire viable epidermis, Cldn-4 is mainly found in the *stratum granulosum* and upper *stratum spinosum* [43]. In human HF their localization has also been investigated and Cldn-1, similarly to the epidermis, is found in all layers of the ORS throughout the HF [30]. In the IRS, Cldn-1 is mainly seen in Henle's and Huxley's layers from the bulb to the lower central region. Localization of Cldn-4 in human HF is confined to the CL of the ORS and some neighboring cells. In the lower central region, suprabulbar region and bulb Cldn-4 staining is present in the CL of the ORS. IRS staining of Cldn-4 is positive in Henle's and Huxley's layers except for the highly keratinized cells.

The last claudin discussed in this work, Cldn-3, has been shown to be a good indicator and target for detecting and targeting cancers of various types, however its role as a tightening agent for functional TJs is only assumed as of now [44-47]. Nonetheless, as it has previously been shown to be expressed and localized in mouse skin and HFs [48], we chose to investigate its distribution and involvement in barrier function here as well.

---

[3] PDZ domains are protein-interaction domains often found in multi-domain scaffolding proteins

1.3.3.   ZO-1

Connecting the integral membrane proteins to the underlying actin cytoskeleton, plus other signaling proteins, is a meshwork of densely packed peripheral proteins like zonula occludens protein 1 (ZO-1), ZO-2, and ZO-3. They are members of the MAGUK (membrane-associated guanylate kinase) protein family, and represent an essential subgroup of the PDZ proteins of TJs [49]. It has been shown that interaction between ZO-1, ZO-2 and claudins plays an essential role in assembling TJ strands, and, with that, give rise to TJ barrier function [50].

In human skin, ZO-1 is located in the *stratum granulosum* and the upper layer(s) of the *stratum spinosum* [30]. Expression and localization of this TJ protein was also investigated in human HFs, where it was shown to be present mainly in the CL of the ORS and somewhat more weakly in surrounding cell layers from the isthmus down to the suprabasal region. The IRS from the bulbar region to the lower central region also gave rise to positive staining in Henle's and Huxley's layers, except for highly keratinized cells.

1.3.4.   Tight Junctions as a Barrier in Skin

The role of TJs as a barrier in simple epithelia and endothelia has been characterized in detail over the years. There they have been shown to regulate the transit of ions and macro-molecules via the paracellular route [49, 51]. This barrier function can, in part, be measured as an electrical resistance (transepithelial resistance, TER), and is a prerequisite for directional transepithelial transport [41]. Furthermore, TJs have been attributed a so-called 'fence function' within the cell membrane because of their capability to mechanically restrict diffusion of lipids and proteins by separating the two components of the plasma membrane into the apical and basolateral compartment [31, 38]. This, in turn, results in cell polarity. However, their involvement in this 'fence function' was challenged recently [52].

The existence of typical barrier-forming TJ structures in the epidermis of fish, amphibians and reptiles has been known for decades. Yet, the existence of functional TJs in mammalian epidermis was for long a topic of general disagreement (e.g. [53-56]). Only in recent years first barrier properties were confirmed [43, 57, 58]. A continuous, intact barrier to an extracellular tracer molecule (Sulfo-NHS-LC-Biotin (Biotin-SH; 557 Da); further explained in section 1.6) was demonstrated in healthy human skin at Ocln and Cldn-1 positive sites in the *stratum granulosum* [43, 59-61]. Moreover, Cldn-1 was shown to have a great impact on paracellular permeability of the stratified epithelium of the skin, as Cldn-1 deficient mice died of dehydration within one day after birth [62, 63]. Also in human keratinocytes the importance of this specific TJ protein (Cldn-1) for maintaining an intact epidermal

barrier was shown as knock-down experiments revealed a decrease in the TER, plus an enhanced paracellular tracer flux for sodium fluorescein [64]. Similarly, a knock-down of Ocln resulted in decreased TER values in human keratinocytes [64]. Thus, in healthy skin, the previously described SC and epidermal TJs seem to interact in a dynamic manner to assure that a formidable barrier is given.

The importance of this TJ barrier, or rather the lack thereof, has further been elucidated in various skin diseases. In atopic dermatitis, the most common inflammatory skin disease, consensus has long been reached that the SC barrier is dysfunctional as a result of a variety of possible defects (e.g. decreased levels of SC lipids [65]). In 2011, De Benedetto *et al.* showed significantly reduced expression of TJ proteins Cldn-1 and Cldn-23 in non-lesional atopic dermatitis skin in a Northern American Cohort [66]. This could, however, not be confirmed in a Central European Cohort. Nonetheless, it was recently revealed that Cldn-4 is upregulated in non-lesional skin and Cldn-1 is down-regulated in lesional skin [67]. Thus, in general, changes of TJ composition can be observed in atopic dermatitis. In Psoriasis, a skin disease characterized by hyperproliferation of keratinocytes, a broader localization was observed for TJ proteins Ocln, ZO-1 and Cldn-4 when compared to normal skin, while Cldn-1 and Cldn-7 were down-regulated [68]. This, again, highlights the involvement of TJs in skin barrier function.

As was shortly described for each individual TJ protein above, Brandner *et al.* performed a study in 2003, investigating the expression and localization of various TJ proteins (ZO-1, claudin-1, claudin-4, claudin 12, claudin 17, occludin) in human HFs [30]. In this study all proteins were localized throughout the entire HF, reaching from the infundibulum down to the bulb, thus including areas where no SC is present. These results were extremely important as they suggest that TJs in the HF, similarly to TJs in the epidermis, may serve as biological barrier. However, the fundamental functionality of mammalian follicular TJs with respect to barrier properties had not been investigated until now.

1.4. Transport Pathways through the Skin

The transdermal delivery route is a very attractive technique to administer drugs for several different reasons:

- it provides an alternative for drugs which would normally undergo a significant first-pass effect in the liver,

- it usually entails a non-invasive approach resulting in increased patient compliance,

- drug release can be modified in order to optimize therapy outcome [69].

Even though epidermal TJs have been given increased attention over the last years regarding their potential as a second invasion barrier, in healthy skin the SC is still considered the bottleneck, or limiting barrier, for invasion of drugs. Consequently, drugs have to surpass this brick-and-mortar structure in order to reach the viable epidermis and/or the blood circulation. There are two basically different, yet feasible, non-destructive invasion pathways through the skin which have to be considered (see Figure 5):

- Diffusion across the intact SC, also known as the transepidermal route.
- Invasion via skin appendages such as hair follicles (or glands).

1.4.1.   Transepidermal Route

The transepidermal route can be further subdivided into the transcellular and intercellular pathways (Figure 5). Both involve the passage of an exogenous substance from the surface of the skin into the SC under the influence of a concentration gradient and subsequent diffusion through the various skin layers [70].
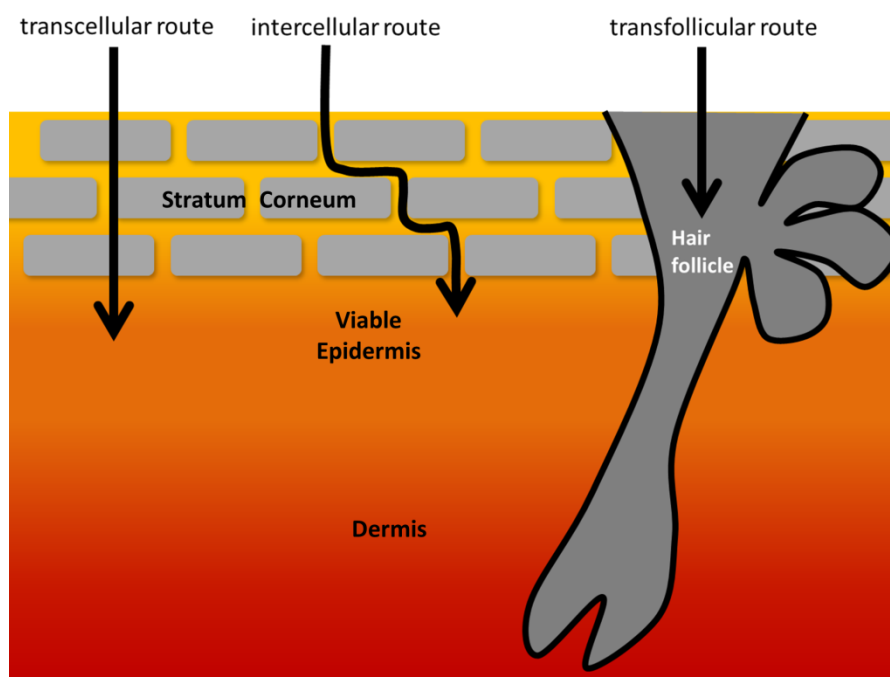

Figure 5: Graphic displaying the three discussed transport pathways through the skin: transcellular diffusion, intercellular diffusion, and the transfollicular route. Not drawn to scale.

The transcellular route represents the more direct route through the SC into the viable epidermis, as can be seen in Figure 5. Nevertheless, this pathway is normally regarded as negligible because

substances will have to undergo substantial partitioning between the lipid bilayer and the rather dense and hydrophilic corneocytes, resulting in highly reduced diffusion and penetration [71].

The intercellular (or paracellular) route is thus considered the predominant diffusion route for most substances, and leads through the lipid matrix located between the corneocytes. As this matrix is composed of liquid crystalline structures, the intercellular route provides lipophilic as well as hydrophilic domains, offering the possibility for substances of both natures, lipophilic and hydrophilic, to passively diffuse along this pathway. Although this path is very torturous and much longer than the direct transcellular route ($\sim$ 500 µm in length as opposed to approximately 20 µm [72]), the diffusion is relatively fast and can easily be modified by aplying chemical penetration enhancers like propylene-glycol, DMSO, or others [73-75].

One thing to keep in mind for both transepidermal routes, however, is that passive diffusion through the SC without any penetration enhancers only occurs for relatively small molecules (< 500 Da) of a rather lipophilic nature (log P value ranging from 1-5), significantly limiting the possibilities of application. Due to these physicochemical restrictions, the encapsulation of various substances into nano- or micro-sized carriers, and subsequent transdermal delivery, has also been under investigation (for a comprehensive review on this topic the reader is kindly referred to [76]). Consensus has meanwhile been reached that particles (polymer-based or made of zink oxide) > 20 nm are unable to cross the SC and hence are unable to reach the viable part of the epidermis [77, 78]. While this is comforting regarding the safety aspects of nanomaterials which should not enter the skin, it restricts their use for drug delivery through the interfollicular epidermis.

1.4.2. Trans-follicular Pathway

In the past, the trans-follicular pathway was considered only a secondary route of transdermal penetration, as in average only 0.1% of the skin surface is affected [79]. However, this rationale was quickly changed when researchers from France demonstrated that percutaneous penetration of various drugs was significantly higher in hairy mice relative to hair-less mice [80]. In the years to come, other groups followed their lead and were able to show similar results on human skin *in vivo* [81, 82].

In the early 2000s, many researchers also focused their efforts on the development of nanocarriers and the possibility of targeting the HF using these drug delivery systems. As the HF represents an invagination, or extension, of the epidermis it gives rise to an increased available surface area, much higher than what was initially assumed. Furthermore, this region is surrounded by numerous blood capillaries and immunocompetent cells, facilitating the absorption of drugs and/or immunologic response [21, 22].

There is convincing evidence that particles ranging between ~100-900 nm can penetrate into HFs, even more pronounced than dissolved molecules [83, 84]. Additionally, depending on particle characteristics like size, charge, or surface functionalization, differences in the degree of follicular uptake were observed [84-86]. In 2006, Lademann *et al.* also discovered that the HF shaft acts as a long-term reservoir of these particles for a maximum of 10 days [87]. This new information was revolutionizing, as it means that upon accumulation in the hair shaft, drugs can be released over time and continuously diffuse to the surrounding follicular and perifollicular cells (e.g. immunocompentent cells), or cross the capillary walls and reach the blood stream.

Current research efforts in the field of targeted delivery of drugs to the HF span a broad field of different applications, ranging from cosmetic products for acne treatment to non-invasive transcutaneous vaccination [88-92]. In the dermatologic practice, this route of penetration would also be of benefit for the administration of e.g. glucocorticosteroids. These drugs entail a wide scope of skin disorders, ranging from atopic dermatitis or psoriasis, to various inflammatory-based scalp diseases for which targeting the HF is one of the goals, yet biggest challenge [93-97]. However, potent glucocorticosteroids are also known to bring along a wide range of side effects, even when only applied topically [98, 99]. Fortunately, the developments in nanotechnology over the years have not only enabled researchers to target specific sites in the body by using functionalized particles, but many researchers have also been able to show that the encapsulation of various drugs allows for a sustained and controlled release over time [100-106]. Thus, the combination of both, nanoparticles capable of releasing the drug in a controlled manner and simultaneous targeting of the HF would be of great benefit and immensely increase the possibilities of treating the above mentioned diseases.

1.4.2.1. The Pig as an *in vitro* Model

For skin absorption and percutaneous penetration studies, porcine ear skin has been evaluated as a valuable *in vitro* model [107]. Specifically for *ex vivo* follicular uptake studies, porcine ear skin has even become known as the 'gold standard' and may be considered superior to human skin for the following reasons: for one, it is difficult to obtain sufficient amounts of human tissue at the time points when they are needed for experiments, while this is not the case for porcine ear skin. Secondly, and more importantly, HFs in human skin are known to contract immediately upon excision, whereas in porcine ear skin the cartilage prevents contraction of tensile fibers, and therefore no subsequent closure of the HFs occurs [108]. Nevertheless, applicability and a good correlation between *in vitro/ex vivo* studies on pig and *in vivo* studies on human needed to be investigated in order to establish suitability of this model.

Anatomically, HFs of both human and porcine descent, show an inner and an outer root sheath, a sebaceous gland associated with the HF, and sweat glands in the dermal layer [109, 110]. The

thickness of the SC and the viable epidermis, as well as density and follicle diameter of the terminal hairs, were also found to be similar [109].

In 2014, a series of experiments on human forearm skin and pig ear skin was performed using five different types of nanoparticles in order to determine the correlation of *in vivo* and *in vitro* follicular uptake data, respectively [86]. They concluded that, even though the pig ear model slightly overestimated differences between the particles, the general trend observed was similar for both species (*in vitro-in vivo* correlation: $r^2 = 0.987$).

Based on all the published data discussed, one can assume that the porcine ear skin model is a reliable tool for mimicking the *in vivo* situation in follicular penetration studies. Nonetheless, further comparability studies concerning e.g. chemical components in, or TJ protein distribution throughout human and porcine HFs would only strengthen this assumption.

1.5. Experimental Methods to Investigate Skin Permeation and Follicular Uptake

In vitro permeation studies on skin, as well as *in vivo* or *ex vivo* follicular uptake studies on human or pig skin, respectively, have been optimized over the past couple of decades in order to get robust and most reliable data. In the next section, two state of the art techniques used by researchers all over the world, as well as for this thesis, will be introduced shortly.

1.5.1. The static Franz Diffusion Cell

For skin permeation experiments, the state of the art technique is the Franz Diffusion cell model. In this experimental setup, which is depicted in Figure 6, the donor and acceptor compartments are generally separated by a membrane, which usually consists of one or more layers of excised skin (e.g. whole skin, heat-separated epidermis, SC only). The cells are typically made of glass and can be classified into flow-through, or static cells [111]. Only the latter will be explained in detail, as the research performed for this doctoral thesis involved the static Franz Diffusion cell only.

Before starting the experiment, one must be sure that the composition of the acceptor fluid does not limit the extent of permeation of the analyte, thus total solubility should be guaranteed. Moreover this fluid should not affect nor alter the integrity of the membrane used; meaning normal permeability properties of the skin should be given [112-114].

Upon addition of the test substances in a desired formulation (e.g. solution/suspension, semisolid preparation, etc.) into the donor compartment, samples are withdrawn from the sampling port at pre-determined time intervals and subsequently analyzed for cumulative amount of permeated substance. In order to guarantee a homogeneous distribution of drug, a magnetic stirrer is placed into the acceptor compartment before begin of the experiment. Furthermore, the whole system is thermostatically controlled throughout the entire length of the experiment in order to mimic the *in vivo* situation as good as possible.
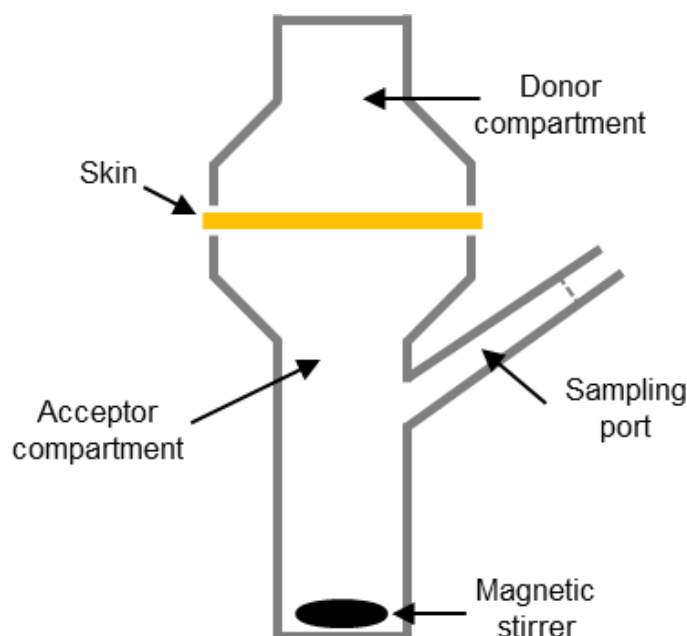
Figure 6: Sketch of a static Franz Diffusion cell (modified version of image from [111])

Based on the amount of substance added into the donor compartment, one can differentiate between two scenarios: finite and infinite dosing. For finite dosing only a limited amount of substance (< 10 µl/cm^2 of a liquid formulation, or 1-5 mg/cm^2 of a semisolid formulation according to the Organisation for Economic Co-Operation and Development (OECD) guidelines on percutaneous absorption studies [114]) is added to the donor compartment. In contrast, infinite dosing means that the applied dose is so large that for the length of the experiment an unlimited amount of substance is available to permeate from the donor into the acceptor compartment. Under the latter conditions the data may permit the calculation of a permeability constant (Kp) [114]. The amount of substance left in the skin is usually not quantified for this experimental set up.

1.5.2. Differential Stripping Method

The Differential Stripping (DS) method is the most straightforward technique to determine follicular uptake quantitatively [86]. For reasons mentioned above the *in vitro* studies are performed on porcine

ear skin. Thus, the allocation of porcine ears is required, and only ears with immaculate skin surface (no abrasions, inflammation, etc.) are to be used.

In the past, various different approaches had been attempted in order to distinguish between the transepidermal pathways and follicular penetration. These approaches included (i) confocal laser scanning microscopy methods for investigating the distribution of various fluorescently-based substances in different skin layers and/or appendageal structures [115], or (ii) analyzing histology-derived sections [116, 117]. The term 'Differential Stripping' was first introduced in 2005 by Teichmann *et al.*, and described the combination of the tape stripping technique (cleaning of skin surface) with cyanoacrylate skin surface biopsies (removing the follicular cast) [118, 119]. However, back then the method was rather a qualitative analysis than a quantitative way of determining follicular penetration. In 2014, Raber *et al.* modified and optimized this method, and ultimately obtained a protocol which made it feasible to fully quantify follicular uptake of nanoparticles [86].

The first step of this protocol entails applying the formulation (e.g. solution, nanoparticles in suspension or nanoparticles in a hydrogel) onto a predetermined area on the outer auricle of the pig ear followed by an optional massage, depending on the experimental setup. After a predetermined incubation time under constant temperature conditions, ten subsequent tape strips are taken in order to clean the skin surface and remove the SC layer by layer. To analyze the extent of follicular drug penetration, cyanoacrylate skin surface stripping is performed. This step implies the application of superglue to the pretreated skin area covered by a tape strip. Upon polymerization of the glue, the tape strip is quickly peeled off, removing the entire follicular cast [118]. For quantification and mass-balance purposes the substance of interest is extracted from the tape strips, cyanoacrylate biopsies, as well as all application devices, and skin rest are analyzed for drug content via an analytical method of choice.

1.6. Experimental Method to Determine Tight Junction Functionality

Measuring TJ barrier integrity has become the main method for determining whether TJ structures are indeed functional. Several different methods have been employed for investigating TJ functionality, as has been mentioned shortly above.

Under cell culture conditions, barrier properties of TJs have mostly been evaluated based on electrical and flux approaches in which the transepithelial resistance (TER) of the monolayer, or transport of model substances from the apical into the basolateral compartment were measured, respectively

[e.g.47, 120, 121, 122]. However, one has to be aware that the TER measures the ion barrier of the whole cellular sheet, i.e. it takes paracellular as well as transcellular ion flux into account [e.g.123]

In 1997, Chen *et al.* introduced a new technique of measuring TJ tightness by using a polar, biotin-labeled molecule called succinimidyl-6-(biotinamido)hexanoate (NHS-LC-Biotin) of 455 Da [59]. In order to obtain better solubility, this compound was later modified by adding a charged sulfo-NHS group, as is depicted in Figure 7 [124].
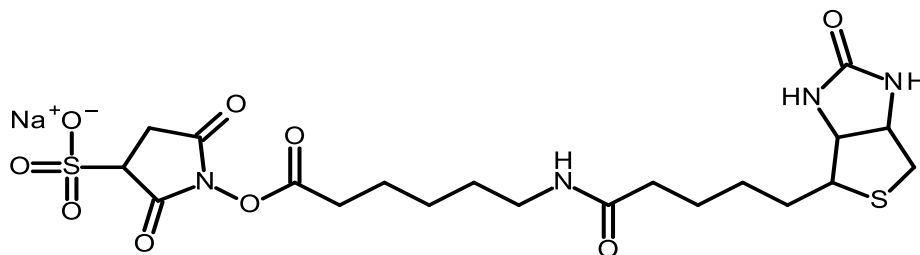
Figure 7: Structure of tracer molecule Sulfo-NHS-LC-Biotin (557 Da)

Due to its structure, this molecule (with and without the added sulfo group) does not enter intact cells and does not penetrate through intact TJs, yet it irreversibly binds primary amine groups of proteins, which makes it easily traceable. Its usefulness in determining TJ tightness, and thus functionality, has been demonstrated in various studies over the years. In 2002, Furuse and colleagues were able to reveal an inside-out barrier stop to this tracer molecule in newborn mouse skin at Ocln-positive sites, whereas in Cldn-1 deficient mice this stop was diminished [58]. Shortly thereafter, various other groups were able to reproduce these experiments on human and porcine skin demonstrating its applicability for determining TJ barrier function in various species under various conditions [125-127].

1.7. Aims of This Work

Over the last decade, the surging interest of nanoparticle-based drug delivery to the hair follicle has opened many novel possibilities to researchers all over the world. Especially the field of transcutaneous vaccination has gained a lot of promising insights about new applicable formulations which embrace a non-invasive approach by using this technology. As already mentioned in previous chapters, porcine ear skin is widely accepted as the 'gold standard' for follicular penetration studies. Nonetheless, the crucial question as to whether this pig ear model, or more specifically the porcine hair follicle, is indeed equivalent in e.g. chemical composition or tight junction protein distribution, and thus suitable for representing the *in vivo* situation in human skin, remains to be further elucidated. Moreover, the biology of the hair follicle itself needs further clarification. Specifically the question as to whether follicular tight junctions are functional with regard to barrier properties, and if so, the ability of modulating, or opening this potential biological barrier, has not been addressed up to now. Also, not much is known about the fate of nanomaterials (i.e. toxins or drug delivery systems) upon penetration into the hair follicle. Questions about whether these particles stay intact or immediately disintegrate upon penetration, what specific region in the hair follicle they reach, or what types of barriers (besides the well-known *stratum corneum*) they may encounter, remain to be answered. Lastly, it is important to further explore the types of effects concerning release, transdermal permeation, and follicular uptake that can be observed as a result of encapsulating drugs into various carrier systems.

In order to address these questions, the aims of this thesis were (i) to first evaluate and compare the chemical composition of porcine and human hair follicles using confocal Raman microscopy, and assess intactness and distribution of these components in cyanoacrylate skin surface biopsies in order to determine if, in fact, the entire follicular cast is removed during this process; (ii) to investigate expression and localization of tight junction proteins in porcine hair follicles via qPCR & immunohistochemical staining in order to compare results to previously published data in human and thereby determine equivalency, plus to investigate functionality of these structures using the tracer molecule Sulfo-NHS-LC-Biotin, and the ability to modulate barrier properties; (iii) to gain insights on follicular penetration depth of model polymeric nanoparticles via transmission electron microscopy, and simultaneously determine whether particles stay intact upon penetration or not; (iv) to study the effect of nanoencapsulation on the release, follicular uptake, and transdermal permeation of Clobetasol, a potent glucocorticosteroid, by using three different types of nanocarriers.

Based on these aims, the thesis will be organized into three main chapters:

Chapter 2.1:   ***Porcine Ear Skin as a Surrogate for Human Tissue: An Analysis using Confocal Raman Microscopy***

Chapter 2.2:   ***Follicular Tight Junctions as a Biological Barrier***

Chapter 2.3:   ***Nanocarriers for Optimizing the Balance between Interfollicular Permeation and Follicular Uptake of Topically Applied Clobetasol***

2. Experimental Section

2.1. Porcine Ear Skin as a Surrogate for Human Tissue: An Analysis Using Confocal Raman Microscopy

The authors of the publication made the following contributions:

L. Franzen:	planned and performed all experiments, analyzed data, and wrote manuscript
C. Mathes:	planned and performed all experiments, analyzed data, and wrote manuscript
S. Hansen:	designed and planned study, analyzed data, and wrote manuscript
M. Windbergs:	designed and planned study, analyzed data, and wrote manuscript

2.1.1.   Abstract

Hair follicles have recently gained increasing interest in the field of transdermal drug delivery. They have shown to provide a facilitated uptake into the skin, as well as a high potential to enable a drug depot. In this area of research, excised porcine ear skin is widely accepted as an *in vitro* model to assess penetration of drug delivery systems into hair follicles. However, a comparison of porcine and human hair follicles in terms of chemical composition has not been reported so far. In this study, confocal Raman microscopy was applied as a chemically selective imaging technique in order to compare human and porcine hair follicle composition, and to visualize individual component distribution within follicular cross-sections. Based on measured and processed human and porcine Raman spectra, optical similarity was successfully confirmed for both species. Moreover, cyanoacrylate skin surface biopsies, which are generally applied to measure the extent of follicular penetration, were imaged using a novel complementary analytical approach which combines confocal Raman microscopy and optical profilometry. This all-encompassing analysis generates a 3-D image which permits investigation of component distribution, and intactness of the removed hair bulb. Overall, confocal Raman microscopy proves its high potential as a non-invasive and chemically selective analytical approach for the investigation of trans-follicular drug delivery.

2.1.2.   Introduction

Many different studies in the field of pharmaceutical technology have recently demonstrated the importance of the transfollicular route for drug administration, especially with regard to drug delivery systems in the nano-sized range [88-90]. Varying in applicability from treating skin or hair diseases to transcutaneous vaccination, the HF and its ability to provide a depot effect (i.e. sustained release of drug) has widened the spectrum of new potential drug delivery systems [87, 91, 92].

In Chapter 1 it was already discussed that the general application of the pig ear as an *in vitro* model for these types of follicular uptake studies (due to closure of the HF in excised human skin [108]) has been widely accepted. It has also been shown that both species express anatomically equivalent structures and compartments in the terminal anagen HF, ranging from the inner and outer root sheaths and their individual subdivisions, to an attached sebaceous gland and arrector pili muscle. In addition, thickness of the SC and the underlying viable epidermal layers, as well as follicle density and thickness are similar in both species [109, 110]. Also, concerning experimentally obtained data on porcine (ear) skin, many studies on skin absorption, percutaneous penetration, as well as follicular uptake have been evaluated and deemed suitable when compared to equivalent studies on human tissue [86, 107, 109, 128]. By using the so-called skin sandwich method, it was shown that porcine HF

absorption of various solutes differing in their physicochemical properties mirrored previously accumulated absorption data on human tissue [129, 130].

Nevertheless, one specific comparison between the two species, which has not at all been discussed in literature up to now, is the composition of various follicular components, most importantly porcine sebum vs. human sebum. In humans, hamsters, rats, and mice the composition has previously been investigated and thoroughly characterized. It mainly consists of triglycerides, sterol- or wax-esters, diol-diesters, free sterols, and free fatty acids [129, 131]; only human sebum additionally contains squalene. Yet the composition of porcine sebum has not been examined at all. Considering, however, that the sebum represents the release medium for drugs delivered via the transfollicular route, we considered this information, or the lack thereof, very important and necessary to investigate further.

A suitable technique to obtain an all-encompassing analysis concerning chemical composition of sebum and other major HF components, or visualization of spatially resolved component distribution (sample mapping) in porcine and human HFs, is confocal Raman microscopy. It is a chemically selective and non-destructive technique, thus optimal for biological samples. In the past, this technique has been used for qualitative analysis of substance penetration into the skin *in vivo* [132] and *in vitro* [133, 134], as well as for an evaluation of drug distribution on the skin surface, via sample mapping [135]. One study also dealt with the visualization and characterization of human hair revealing information about the secondary structure of proteins and the disulfide bridges [136].

In this study, confocal Raman spectroscopy was applied in order to evaluate the chemical similarities between human and porcine HFs. Thus, the spectral properties of the four key follicle-associated components—hair, sebum, dermis and follicular epidermis—were analyzed and compared for both species. Furthermore, confocal Raman microscopy was used to image cross-sections of HFs, visualizing the individual component distribution. Finally, a novel complementary analytical approach combining confocal Raman and optical profilometry was applied to visualize cyanoacrylate biopsies of HFs, used to determine follicular uptake, in 3-D.

2.1.3.   Materials and Methods

2.1.3.1. Materials

Tesafilm® kristall-klar (Tesa, 33 m × 19 mm, cut to 30 × 19 mm sections) was obtained from Tesa AG, Hamburg, Germany. UHU superglue (UHU, blitzschnell Pipette) was kindly provided by UHU GmbH & Co, KG, Bühl/Baden, Germany. For nuclear staining, Mayer's haematoxylin was purchased from Carl Roth GmbH+ Co. KG, Karlsruhe, Germany.

2.1.3.2. Porcine and Human Skin

All porcine ears used for the herein described experiments were acquired from Emil Färber GmbH & Co. KG, a local slaughterhouse in Zweibruecken, Germany. The ears were excised immediately before the brewing step, and brought to the lab where they were thoroughly cleansed.

The human skin used for all *in vitro* experiments was donated from the department of Plastic and Hand Surgery at the Caritaskrankenhause in Lebach, Germany. The study was performed on thigh skin which was acquired after plastic surgery performed on a 48 year old female donor who had previously consented to the donation. Immediately upon arrival of the skin, all subcutaneous adipose tissue was carefully removed, leaving only the dermis and epidermis for further investigations. The remaining skin was cut into pieces of 10 x 20 cm, covered in aluminum foil and stored at -20°C until further use. This study was approved by the ethical commission of Saarland, Germany (Aerztekammer des Saarlandes, 204/08).

2.1.3.3. Longitudinal-Sections of Hair Follicles

Longitudinal sections of HFs were obtained by excising 8 mm biopsies out of the 20 x 30 mm intact frozen human thigh skin sections or porcine ear skin. Next, cryosections with a thickness of 15 μm were cut using a cryomicrotome set at -20°C (MEV Cryostat, Slee, Mainz, Germany). For nuclear staining, sections were immersed in Mayer's haematoxylin solution for 8 min followed by the blueing step which entails leaving the section under running water for 10 min.

Visualization of the sections was performed on a Zeiss AXIO Scope A1 light microscope (Carl Zeiss Microscopy GmbH, Oberkochen, Germany), equipped with a digital camera (Axio-Cam ERc 5 s) for the taking of the images. Taken images were then edited and labeled using the software Zen lite 2011 (Carl Zeiss Microscopy GmbH, Oberkochen, Germany).

2.1.3.4. Cyanoacrylate Skin Surface Stripping

As shortly described in Section 1.5.2 (General Introduction: Differential Stripping Method), cyanoacrylate skin surface stripping was performed by first applying a drop of UHU superglue onto a predetermined and pre-cleansed area on the outer auricle of the excised pig ear, followed by immediately placing a tape strip on top. Upon complete polymerization of the glue (approx. 10 min), the tape strip is quickly ripped off in one continuous movement, removing the entire content of the HF. For further analysis, all biopsies were fixed upside down onto a glass slide, leaving the HFs facing upwards.

2.1.3.5. Confocal Raman Microscopy & Optical Profilometry

For all confocal Raman microscopic evaluation, the 15 μm sections, as well as the cyanoacrylate biopsies, were fixed onto calcium fluoride slides. Measurements were performed using a Witec alpha 300R+ (WITec GmbH, Ulm, Germany). As excitation source a diode laser with an emitting wavelength of 785 nm was used. The power of the laser, placed right in front of the objective, was set to 50 mW, as this strength had previously been tested and shown to not harm biological tissue. The light microscopic images obtained were taken with a 10x objective (Epiplan Neofluar N.A. 0.5, Zeiss, Germany), whereas Raman single spectra and maps recording was done using a 50x objective (Epiplan Neofluar N.A. 0.8, Zeiss, Germany). In order to reject signals from out-of-focus regions, a confocal pinhole of 100 μm was employed. Raman spectra were recorded using a spectral resolution of 4 cm^{-1} over the range of 400 - 1780 cm^{-1}. For a single spectrum, three measurements, which were taken over a 10-s integration time, were averaged. Raman mapping was done by collecting data at every 5 μm in x and y directions for a total of 10 s. The obtained data was then processed using WITec Project Plus software (WITec GmbH, Ulm, Germany). After applying a cosmic ray removal, a spectral baseline correction was performed using a polynomic fit. Finally, all spectra were normalized to the most intense peak (1430 to 1480 cm^{-1} representing ν(C─H)) [137].

For surface topography measurements, a True Surface Microscopy sensor incorporated in a Witec alpha 300R+ confocal Raman microscope (WITec GmbH, Ulm, Germany) was implemented. With a high accuracy of 1 μm, this sensor is able to resolve an elevation difference of 3 mm. Data points were collected every 5 μm in x and y directions, generating a lateral resolution equivalent to Raman mapping.

2.1.4. Results & Discussion

2.1.4.1. Comparison of Porcine and Human Hair Follicle

The first part of this study was a composition comparison between human and porcine tissue of the four major chemical components (sebum, dermis, epidermis, hair) by confocal Raman spectroscopy. In Figure 8, longitudinal sections of porcine (a) and human (b) HFs are depicted, showing optical and dimensional similarities between the two species. For each image one can clearly differentiate between the hair (blue cross), the follicular epidermis (yellow cross; outer root sheath and inner root sheath are not differentiated here), deeper skin layers (green cross), and the sebaceous gland (red cross). To assess spectral comparability between the two species, Raman spectra were acquired for each of the four components in porcine and human HFs and are shown in (c) and (d), respectively. Here, the

Raman spectra measured at the areas marked by the colored crosses from (a) and (b) are shown in corresponding colors, thus human and porcine epidermal spectra are shown in yellow, the hair in blue, the dermis in green, and sebum in red.
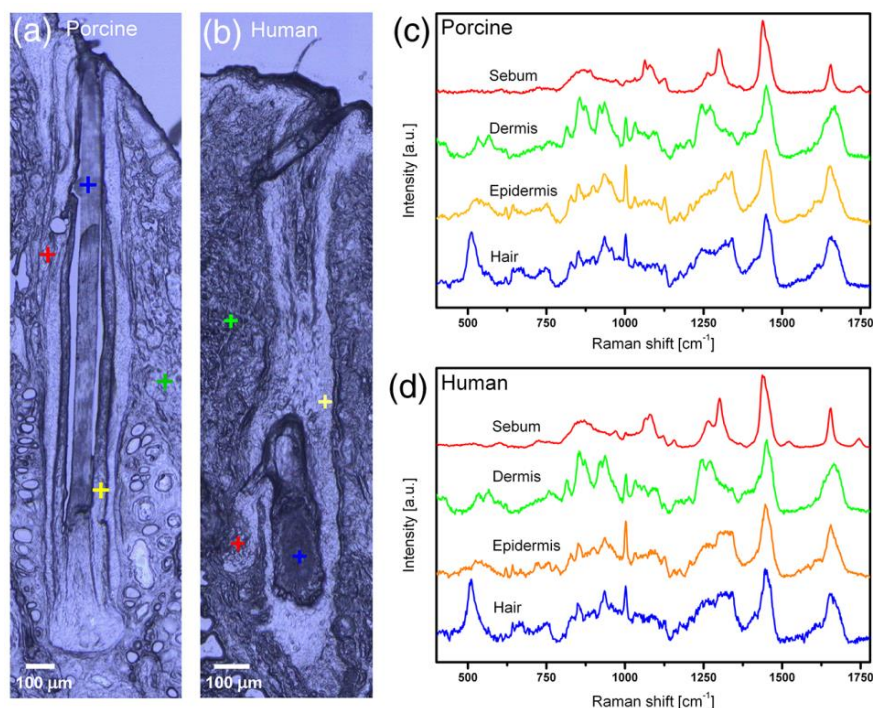

Figure 8: Microscopic pictures of porcine (a) and human (b) hair follicle cross-sections. Raman spectra obtained from the areas marked by the colored crosses displayed in corresponding colors from porcine (c) and human (d) follicles (image taken from [138]).

The follicular epidermis spectrum is mainly composed of unspecific bands indicating protein at ~1003 cm^{-1} (aromatic amino acids), 1440 cm^{-1} δ(CH), and at 1650 cm^{-1} (amide I) with keratin being the main component [137]. The dermis spectrum has two additional characteristic double peaks. The first one is located at 815 to 850 cm^{-1}, and the second one at 920 to 940 cm^{-1}. This specific pattern is representative for collagen, which is one of the main components of the dermis layer in the skin [139]. Concerning the hair spectrum, both species give rise to a prominent peak at 509 cm^{-1}, known to be specific for disulfide bridges [136, 140]. These types of bonds are characteristic for keratotic tissue like hoof, horn, and hair.

For an evaluation concerning similarity of the recorded spectra from both species, a statistically robust method was necessary. Thus, spectral subtraction was performed, followed by a calculation of the area under the curve (AUC) of the obtained graphs. For the references, three spectra of each component from varying positions were subtracted from each other. The resulting graphs specify the internal spectral variability for each individual component. Figure 9(a) displays these graphs for hair (blue), follicular epidermis (yellow), dermis (green), and sebum (red). The 95% confidence interval (CI) of

spectral similarity for each of the four components was then calculated based on the absolute AUC of the spectral subtraction graphs. In the last step, the component spectra of human and porcine HFs were subtracted from each other and the resulting AUC was calculated. The values for all AUCs, along with the confidence intervals obtained, can be found in Figure 9(b). A significant difference was observed for the hair, which displayed a much higher AUC (49,03) than the reference (27,99). However, as can be seen in Figure 9(c), upon subtraction of the two spectra only high noise, yet no major differences, was observed. Moreover, no significant difference was detected for the follicular epidermis or the dermis. The sebum was analyzed extra carefully, as it represents the potential release medium for drug delivery systems. Yet, between human and porcine sebum, no significant difference was observed. All minor discrepancies were only intensity related and thus negligible concentration differences of sebum components. For this study, the inter-individual variability of porcine and human HF composition was not taken into account, as it would have been necessary to test an immense number of individuals to gain valid results. However, by means of Raman spectroscopy, chemical composition of the four main HF constituents were analyzed and evaluated, confirming similarity between the two species.
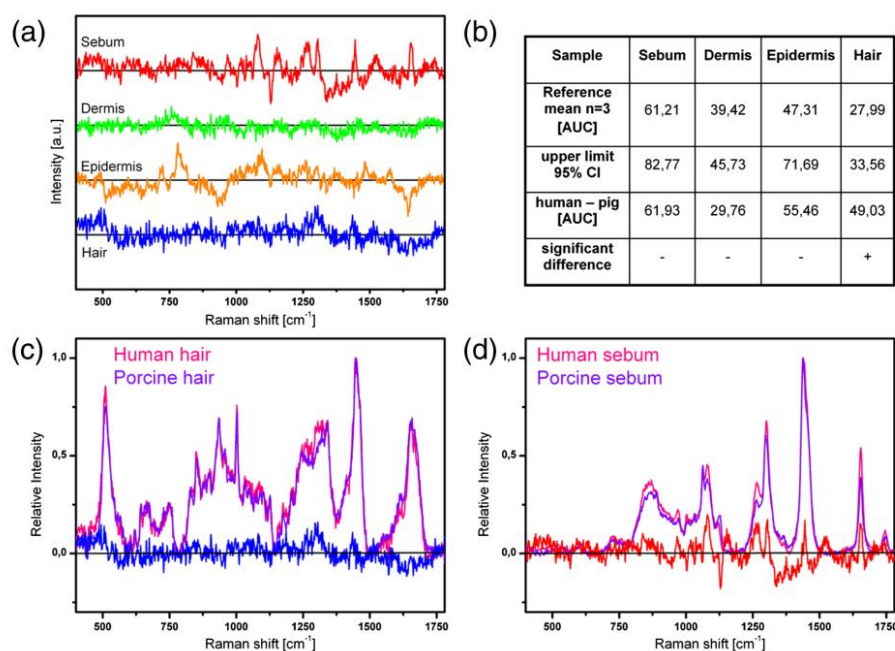

Sample	Sebum	Dermis	Epidermis	Hair
Reference mean n=3 [AUC]	61,21	39,42	47,31	27,99
upper limit 95% CI	82,77	45,73	71,69	33,56
human – pig [AUC]	61,93	29,76	55,46	49,03
significant difference	-	-	-	+

Figure 9: (a) Spectral subtraction graphs derived from porcine and human Raman spectra of the four main chemical components. (b) Statistical evaluation of the absolute area under the curve (AUC) of the spectral subtraction graphs. Comparison of single Raman spectra and the subtraction graphs for human and porcine hair (c) and sebum (d) (image taken from [138]).

The staining procedure based on haematoxylin and/or eosin is one of the most common techniques used to differentiate between various components in tissue sections. In Figure 10(a) a longitudinally cut porcine HF is displayed after undergoing haematoxylin nuclear staining. In this image one can clearly differentiate between the follicular epidermis, the dermis, and the hair. The entry duct to the

sebaceous gland can be assumed in this specific image (red arrow), but the sebum is undetectable via this method.

Figure 10(b) depicts a longitudinal section of a similar location in a porcine HF, yet unstained. In that image, the red square indicates the area which was mapped using Raman in (c), and (d). Raman mapping is a method which allows discriminating between various components based on their obtained Raman spectra without the need of a previous staining procedure. Thus, it permits visualization of the component distribution without the need to treat the sample prior. For this study, the spectra of the region of interest were recorded with a step size of 5 µm. After measuring the spectral data, a processing step was performed using multi-variant analysis algorithms, in order to identify the component distribution. From that data a false-color Raman image was obtained where each picture pixel was assigned one color that represents a similar Raman spectrum (see Figure 10(c)). During this binary processing method, pixels with a spectrum which represents the follicular epidermis are displayed in yellow, dermis in green, sebum in red, and hair in blue. A similar, yet more sophisticated procedure was performed for Figure 10(d).
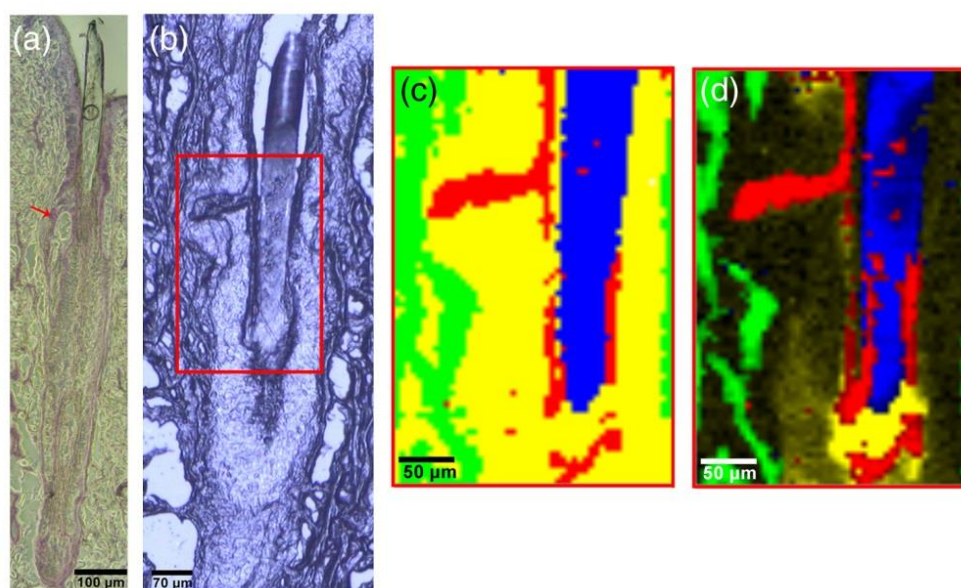

Figure 10: (a) Transmittance-light microscopy pictures of a haematoxylin nuclear stained porcine hair follicle cross-section. The red arrow indicates the location of the sebaceous gland. (b) Incident light microscopic picture of an unstained porcine follicle cross-section. (c) and (d) Raman map of the area indicated by the red rectangle in (b). The hair is displayed in blue, the sebum is depicted in red, whereas epidermal and dermal structures are shown in yellow and green, respectively (image taken from [138]).

However, this method includes visualizing intensity differences, plus the possibility of displaying multiple components (colors) simultaneously in one pixel. Thus, this type of processing method allows for a more specific and detailed depiction of the real component distribution. When taking a closer look at Figure 10(c) and Figure 10(d), one can see the advantage of the latter method. For examples, in

(d) traces of sebum (shown in red) can be identified on parts of the hair (shown in blue), whereas looking only at the binary image in (c), or the light microscopy image in (b), this conclusion cannot be drawn. Thus, Raman mapping allows for a more specific and more accurate components distribution analysis, which is not feasible by conventional microscopy. Furthermore, this methodology needs no labeling or previous staining, and would therefore be ideal for tracking the penetration of drugs with and without drug delivery systems into the HF.

2.1.4.2. Visualization of Cyanoacrylate Skin Surface Biopsies

For the qualitative and (semi)quantitative analysis of drug penetration into the HF, cyanoacrylate skin surface stripping represents the most common analytical technique. It involves removing the hair plus the entire follicular cast in a cyanoacrylate biopsy which can later be analyzed and quantified for drug content. Nevertheless, an actual quality assurance for the removal of the entire follicular cast cannot be given by using conventional light microscopy, as information about only one focal plane is gained via this method. This problematic is depicted in Figure 11(a) and (b), where each image displays a light microscopic picture acquired from two different focal planes of a porcine cyanoacrylate biopsy. In these images the tape strip, which was beforehand placed over the drop of glue in order to remove the follicular cast, is turned upside down, and the removed hairs are pointing upwards. However, as only one focal plane can be visualized via this method, only parts of the hairs can be analyzed.
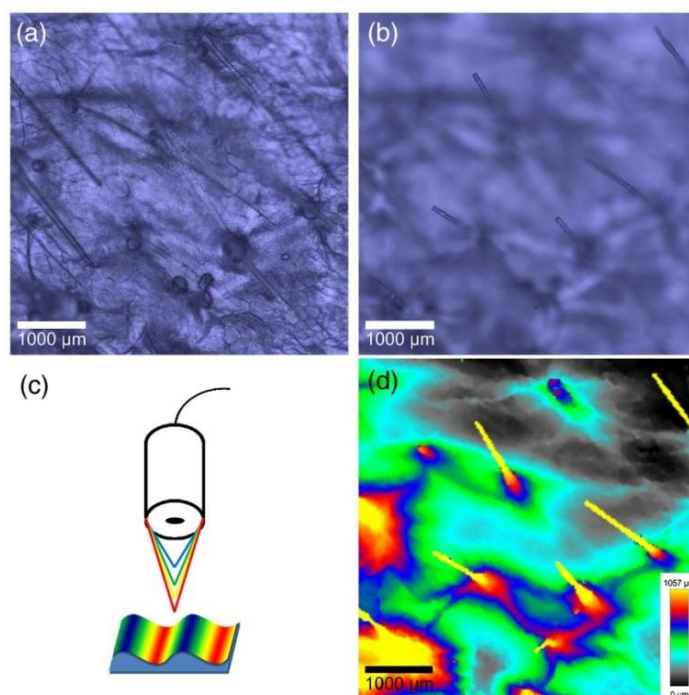

Figure 11: (a) and (b) depict light microscopy pictures of a cyanoacrylate skin surface biopsy recorded from two different focal planes. (c) Schematic of the basic principle of optical profilometry. (d) Color-coded surface map of the biopsy area corresponding to (a) and (b) (image taken from [138]).

To get a complete analysis of the entire follicle, a three-dimensional (3-D) analytical approach is needed. Optical profilometry presents itself as a useful method for this type of analysis. It represents a non-contact interferometric-based method which is used for characterizing surface topography. The basic principle which underlies this methodology relies on the effect of chromatic aberration. Using a set of hyperchromatic lenses, one obtains very good mapping-point capabilities, along with a high chromatic error. Consequently, the white light, which gets focused through this lens assembly, is split into its different colors, resulting in the assignment of a specific, yet different, color for each focal length. Detection of the light occurs in the confocal pinhole, and, as a result, a topography map is generated, as can be seen in Figure 11(c). Applying this method to the above mentioned sample, the whole cyanoacrylate biopsy, including the interfollicular epidermis rests plus the entire HF, can be visualized (Figure 11(d)).

Another possible application of this method is to overlay the obtained sample surface topography map with Raman spectroscopic information. Thus, after measuring the surface structure, the same sample surface can be used to obtain Raman spectra. This is done by diminishing weak signal intensities produced by out-of-focus effects. Therefore, this technique makes it possible to apply Raman mapping to highly structured specimen like an individual HF obtained from a cyanoacrylate surface biopsy (see Figure 12).
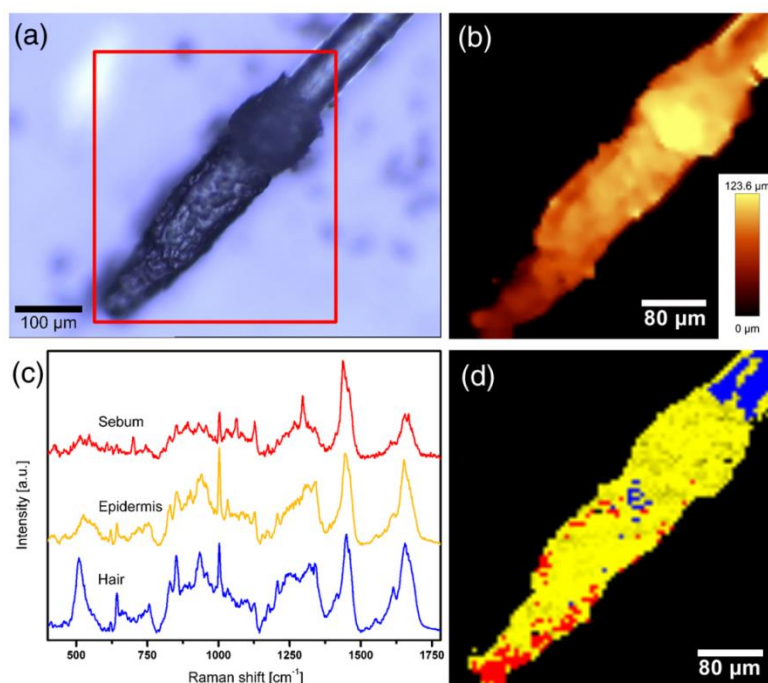

Figure 12: (a) Light microscopy picture of an excised hair follicle. (b) Surface topography map of the area indicated by the red rectangle in (a). (c) Raman spectra of the individual chemical components in the hair follicle. (d) Raman map displaying the component distribution on the excised hair follicle (image taken from [138]).

The red square in (a) indicates the area which was measured by optical profilometry and is shown in Figure 12(b). For the same area that was mapped in (b), individual Raman spectra were recorded and are shown in (c). Overlaying the information obtained from (b) with the spatially resolved information gained from the Raman spectra in (c), a 3-D components distribution map of the HF is generated and displayed in (d). In this false-color image, the sebum is shown in red, the epidermis in yellow and the hair in blue. The information that is acquired from combining these two methods is that the hair shaft is completely enclosed by an intact follicular epidermis (inner and outer root sheath) and, thus, the whole follicular cast was successfully removed by this cyanoacrylate skin surface stripping method. Also visible are traces of sebum along the HF, especially in the bottom areal hinting at a possible thinning of the epidermal layers in this region. Overall, this analytical evidence is an important finding because it only further corroborates the suitability of this technique (cyanoacrylate skin surface stripping) which is (up to date) the only measure for quantifying drug content in the HF. Furthermore, the novel combination of confocal Raman microscopy and optical profilometry in this setting proves its worthiness in evaluating biological samples, opening the possibility for other similar analytical approaches.

2.1.5.   Conclusion

In this study, confocal Raman microscopy has proven to be an excellent tool for investigating the equivalency and suitability of porcine HFs as a model for the evaluation of trans-follicular drug delivery. It entails a non-destructive and chemically selective analytical approach, and was shown to be very successful in proving the similarities between human and porcine tissue. Based on the individual Raman spectra, the four main components (hair, dermis, sebum, and follicular epidermis) were effectively identified in both species and found to be equivalent. Moreover, a comparison between the common histologic staining procedure and Raman mapping was performed, and demonstrated the advantages of the latter. Also, based on the novel combination of confocal Raman microscopy and optical profilometry, a 3-D chemically resolved analysis of cyanoacrylate skin surface biopsies was achieved, only further proving the suitability of this analytical approach. These results corroborate the potential of this methodology in the field of drug delivery, like visualizing the penetration behavior of drug delivery systems into the HF or non-invasive depth profiling.

2.2. Follicular Tight Junctions as a Biological Barrier

Personal contributions to this chapter were as follows:

- ❖ Tissue preparation for experiments performed on porcine ear skin
- ❖ Performance, analysis and interpretation of tight junction experiments
- ❖ Performance and analysis of H&E stainings described
- ❖ Sample preparation for transmission electron microscopy experiments
- ❖ Analysis and interpretation of all described results
- ❖ Writing of chapter

2.2.1. Abstract

Follicular penetration has recently been given more attention regarding i) safety concerns of nanomaterials which should not enter the skin, and ii) the possibility for nanoparticle-based drug delivery. However, potential barriers in the hair follicle (HF) that a substance will encounter upon uptake and/or penetration into surrounding tissue remain undetermined up to now. In the interfollicular epidermis, functional tight junctions (TJs) have been revealed before. Moreover, several TJ proteins have previously been localized in human HF. However, the functionality of these follicular TJ has not been investigated this far. Hence, this work investigates and elucidates for the first time a continuous, intact TJ barrier from the infundibulum down to the suprabulbar region of mammalian HF. In the upper region a double-barrier comprising the *stratum corneum* and functional TJs was revealed, while in lower areas TJs likely act as the only barrier. Moreover, by modulating the permeability using EDTA, the dynamic character of this TJ barrier was verified. In the bulb, however, no TJ barrier was detected, which proves the importance of free supply for e.g. hormones or nutrients from the dermal microenvironment to this hair-forming part. Lastly, transmission electron microscopy revealed that model, polymeric nanoparticles (154 nm), which had previously been applied to the skin, were mainly found in the upper part of the HF where the previously mentioned double-barrier is present. Few particles penetrated deeper; however, they were only found in areas where functional TJs are present. Thus, no particles reached areas without an intact TJ barrier. To summarize, follicular regions of high accessibility for external substances – here model polymeric nanoparticles – are protected by two barriers, while areas with lower accessibility are lined with one functional barrier, TJs.

2.2.2. Introduction

The hair follicle (HF) represents a potential entry route for topically applied substances, or (exogenous) substances present in the environment [141, 142]. This entry route may be of advantage on one hand (e.g. for drug delivery purposes), or of disadvantage concerning the uptake of allergens or toxins. In the past few years, there has been an extensive debate around the topic of nanomaterials and toxicity, especially concerning the question whether certain particles may or may not penetrate, or even permeate, mammalian (in particular human) skin. General agreement has meanwhile been reached that nanoparticles (NPs) (both polymer-based or made of metal oxides) > 20 nm do not penetrate the *stratum corneum* (SC), and are therefore unable to reach the viable part of the epidermis, let alone the bloodstream [76-78, 143]. Alternatively, several studies have shown that particles in the size range of ~100-900 nm accumulate in hair follicles (HFs) to a higher extent than dissolved molecules, and even exhibit a size-dependent effect on follicular uptake [83, 84]. Furthermore, it was

demonstrated that various nanoparticulate-based delivery systems penetrate into the HF shaft, and can serve there as a long-term reservoir for a maximum of 10 days [85-87]. Thus, a possible, yet undesired, uptake of toxins needs to be considered. On the other hand, the possibility of targeting the HF has also opened novel possibilities for new drug delivery systems, like targeted non-invasive delivery of drugs and antigens [90, 92, 144-146]. Thus, for both, understanding the putative risk of unwanted uptake of substances, as well as the possibility to deliver drugs via the transfollicular route, knowledge about potential barriers present in the HF is crucial.

As was shortly discussed in Chapter 1, the SC has been identified as the first invasion barrier in interfollicular skin [147]. Beyond this structure, located in the *stratum granulosum* of the viable epidermis, are the previously introduced tight junctions (TJs) [148]. These are multi-protein complexes in charge of barrier properties. In simple epithelia and endothelia, this barrier function has been extensively characterized over the years; however, only recently their role in a stratified epithelium (e.g. the skin) has gained increasing interest [31, 57, 148-150]. In 2002, an intact epidermal TJ barrier was demonstrated by Furuse *et al.*, along with the revolutionizing discovery of the vital role of claudin-1 (Cldn-1) in mice (refer to Section 1.3.4) [58]. Shortly after, this barrier function was also revealed to exist in adult human interfollicular epidermis [43, 60, 61]. Using cultured keratinocytes, researchers were able to demonstrate that TJ proteins Cldn-1, Cldn-4, occludin (Ocln) and zonula-occludens protein-1 (ZO-1) contribute to the TJ barrier for ions, as well as small and large molecules [123]. Due to their localization underneath the SC, it seems as if TJs serve as a second-line of defense for the outside-in passage of substances, especially when the SC barrier is impaired. However, they can also actively influence the SC (e.g. abnormally shaped corneocytes, altered ceramide composition of SC lipids, altered filaggrin processing, increase in pH of SC, increase in polar lipids and decrease in nonpolar lipids), and are therefore likely to be involved in the regulation of SC barrier function[63, 123, 151].

The HF represents an invagination of the skin in which the SC barrier is interrupted, hence, an intact SC is only present in the upper part of the infundibulum [152]. Thus, researchers were wondering whether TJs are present in this region of the HF or beyond. In the early 2000s this question was answered, as expression and localization of various TJ proteins were revealed in human HFs – including lower follicular areas not covered by the SC – as well as in murine skin [30, 153-155]. Also, the importance of regular TJ protein expression for normal hair growth was demonstrated in Cldn-1 knock-out mice, patients with NISCH syndrome (deficiency of Cldn-1 in human), as well as Cldn-6 over-expressing mice, which all exhibited a peculiar hair phenotype [154, 156, 157]. However, the intriguing question whether these follicular TJs actually serve as a barrier, which may or may not compensate for the non-existing SC in deeper follicular regions, had not been addressed up to now. We therefore took it upon us to investigate TJ barrier function in mammalian HFs. We used porcine ear skin, as this model has been accepted as the 'gold standard' for follicular uptake studies, and we

were interested in comparing the localization of an extracellularly applied exogenous substance – here model NPs - with the localization of existing barriers in the HF.

In this study we therefore started by investigating expression and localization of follicular TJs via qPCR and immunohistochemical staining, respectively. To be able to compare our results to previously published clinical data on humans and preclinical data on mice, we focused our efforts on TJ proteins that have previously been localized in the HF of both species before, namely Cldn-1, -3, -4, Ocln, and ZO-1. Next, barrier function of these TJs was evaluated using the tracer molecule Sulfo-NHS-LC-Biotin (Biotin-SH), followed by the attempt to modulate this barrier using the Ca^{2+}-chelator EDTA. Finally, transmission electron microscopy (TEM) was employed to visualize our model NP in the HF.

2.2.3.   Materials and Methods

2.2.3.1. Materials

Oleic acid-coated primary magnetite particles were kindly provided by the Leibniz Institute for New Materials, Saarbruecken. Poly-D,L-lactide-co-glycolide (Resomer® RG 503 H) was purchased from Evonik in Essen, Germany. Uranyl Acetate was obtained from Polysciences Europe GmbH, Eppelheim, Germany. For tissue fixation, paraformaldehyde was purchased at VWR International in Radnor, PA, USA, and glutaraldehyde at Agar Scientific, Stansted, UK. HEPES and Eosin Y solution 0.5% in water were bought at Carl Roth GmbH + Co. KG in Karlsruhe, Germany, and RNAse Inhibitor at Fermentas, Waltham, MA, USA. Dulbecco's Modified Eagle Medium (DMEM), the Maxima First Strand cDNA Synthesis Kit, and an O'GeneRuler^{TM} 50-1000 bp DNA Ladder were purchased from Thermo Fisher Scientific, Darmstadt, Germany. The RLT buffer and RNeasy Mini Kit used for PCR experiments were bought from Qiagen, Venlo, Netherlands. All pig specific primers used were ordered from Applied Biosystems in Darmstadt, Germany: 1) Claudin-1 (CLDN1): Ss033757089, 2) Claudin-3 (CLDN3): Ss03377787, 3) Claudin-4 (CLDN4): Ss03375006, 4) Occludin (OCLN): Ss03377507, 5) ZO-1 (TJP1): Ss03373514, 6) GAPDH (Ss03375435), 7) β-2-microglobulin (Ss03391156), 8) β –actin (Ss03376160). EZ-Link^{TM}-Sulfo-NHS-LC-Biotin (Biotin-SH;557 Da) was purchased at Pierce, Rockford, IL, USA. Formaldehyde (Formafix® 4%, buffered) was obtained from Formafix Global Technologies, Duesseldorf, Germany. Mayer's haematoxyline was provided by Medite GmbH, Burgdorf, Germany. All primary antibodies were purchased from Invitrogen Carlsbad, CA, USA. The Alexa-488-coupled secondary antibody (F(ab')2 and Alexa-594-coupled secondary antibody (F(ab')2 were provided by MoBiTec, Goettingen, Germany. For the biotinylation assay, the Texas-Red®-conjugated Streptavidin was purchased at Merck Biosciences, Darmstadt, Germany. For nuclear staining DAPI was bought at Boehringer Mannheim, Mannheim, Germany and Fluoromount-G^{TM} at Southern Biotechnology Associates, Birmingham, Ala., USA. Aqueous polyvinyl alcohol, 1%

Alcian blue, phosphotungstic acid, dispase, 2-Mercaptoethanol, Hydrocortisone, fetal calf serum, penicillin/streptomycin and ethylenediaminetetraacetic acid (EDTA) were all obtained from Sigma Aldrich, St. Louis, MO, USA.

2.2.3.2. Porcine Ear Skin & Mice

Fresh pig ears (Yorkshire/German Large White crossbreed; age: 6 months) were donated by a slaughterhouse in Schleswig-Holstein, Germany. The ears were excised before brewing, immediately brought to the lab, and washed thoroughly. They were carefully examined for skin abrasions prior to use, and only ears with immaculate looking skin were selected for experiments. For control experiments on the localization of TJ protein Cldn-3 in murine HFs, C57/Bl6 mice (adult) were used.

2.2.3.3. Isolation of Hair Follicles and Epidermis for qPCR

Porcine ear skin tissue blocks of 0.3 x 0.5 cm were incubated in a solution consisting of 4.0 mg/ml Dispase and 1.0 U/µl RNAse Inhibitor in DMEM at 4°C overnight. Subsequently, whole HFs were pinched using a pair of tweezers, washed in phosphate buffered saline (PBS) and stored in 1.0 ml of RLT buffer containing 10 µl 2-Mercaptoethanol. As a control, porcine heat-separated epidermis (HSE) was used by heating normal skin at 60°C for 90 sec resulting in a distinct separation of the epidermis from the dermis [158]. HSE was then washed in PBS and also stored in RLT buffer containing 10 µl 2-Mercaptoethanol. RNA extraction was done using an RNeasy Mini Kit and tested for purity using the NanoDrop 2000C (Wilmington, DE, USA). After successful isolation of RNA, cDNA was generated by using a Maxima First Strand cDNA Synthesis Kit. qPCR was performed as previously described by Brandner *et al.* [159] using the parameters recommended by the manufacturer. Resulting amplified DNA of qPCR was then separated on a conventional 2% agarose gel using a 50-1000 bp and 100-1000 bp DNA Ladder as standards.

2.2.3.4. Biopsy Preparation and Staining Procedures

Biopsy Preparation

Biopsies of 8 mm diameter were removed from the inside of the pig ears and placed dermis down in DMEM supplemented with hydrocortisone, 2% (v/v) fetal calf serum, and 1% (v/v) penicillin/streptomycin. For TJ functionality experiments, 50 µl of 1 mg/ml Biotin-SH in 1 mM $CaCl_2$ PBS were carefully injected into the dermis and incubated for 1 h at 37°C. For barrier-modulation experiments, biopsies were bathed in 8.0 mM EDTA for thirty minutes, prior to injection of the tracer molecule Biotin-SH. After this incubation (with and without injected Biotin-SH), biopsies were fixed in formaldehyde at 4°C for 12 hours, embedded in paraffin, and 5 µm cross- and longitudinal section were cut using a Leica RM2165 Rotary Microtome (Leica Microsystems GmbH, Wetzlar, Germany).

Paraffin sections were deparaffinated and rehydrated, after which followed haematoxylin and eosin (H&E) staining or immunohistochemical staining.

Embedding Tissue in Paraffin

The protocol shown in Table 1 was used to embed the tissue in paraffin. The increasing alcohol concentrations first dehydrate the tissue. Xylol is then used to replace the alcohol. The last step, also known as the infiltration step, consists of placing the sample into a paraffin bath twice for 2 hours.

Table 1: Protocol for embedding tissue in paraffin

Time (hours)	2	2	2	4	4	6	4
Solvent	H$_2$O	EtOH 70%	EtOH 80%	EtOH 96%	EtOH abs.	Xylol	Paraffin

De-waxing Procedure of Paraffin Sections

Paraffin sections were dewaxed and hydrated using Xylol (minimum of 2 x 15 min) followed by passing the tissue through a series of decreasing alcohol concentrations (EtOH abs, 96%, 80%, 70%) and distilled water, immediately after which followed either haematoxylin and eosin (H&E) staining or immunohistochemical staining.

H&E Staining

Sections were submerged in haematoxylin for 10 min and then left under running water for 10 min (bluing step). Next they were rinsed with distilled water, placed into 0.5% Eosin for 40 sec and rinsed again. The dehydration process was finalized by passing the tissue through a series of increasing alcohol concentrations (70%, 80%, 96%, EtOH abs) followed by submersion into Xylene and mounting coverslips using Eukit.

Immunohistochemical Staining of Porcine and Mouse Paraffin Sections

After being rehydrated, sections were placed in TEC buffer (0.25% w/v Tris, 0.5% w/v EDTA, 0.32% w/v Tri-Sodium Citrate, dihydrate) at 300 W twice for 10 min for epitope de-masking purposes. They were washed thoroughly using TBST buffer (6.01% w/v Tris, 8.76% w/v NaCl, 0.5% v/v Tween, 5.67% v/v 25% HCl; pH 7.6), and incubated with a 0.001% Trypsin solution for 10 min at 37°C. Sections were washed again using TBST and soaked in blocking solution (DAKO® Protein Block Serum-Free) for 30 minutes at room temperature. Next, sections were incubated with primary anti-claudin-1 (1:3000; polyclonal rabbit), anti-claudin-3 (1:100; polyclonal rabbit), anti-claudin-4 (1:60; polyclonal rabbit), anti-occludin (1:50; monoclonal mouse), or anti-ZO-1 (1:100; polyclonal rabbit) antibody overnight at 4°C. Subsequently, sections were washed three times with TBST and incubated

with Alexa-488-coupled secondary antibody (F(ab')2 anti-mouse/rabbit (depending on primary; 1:500), or Alexa-594-coupled secondary antibody (F(ab')2, anti-mouse/rabbit, 1:500, or a mixture of the above mentioned secondary antibodies and Texas-Red®-conjugated Streptavidin for 30 min. For nuclear staining, DAPI was used. At last, slides were washed twice with PBS and distilled water and coverslips were mounted using Fluoromount-G[TM].

Light and Immunofluorescence Microscopy for H&E and Immunohistochemical Stainings

Immunohistochemical stainings of 5 µm sections were examined using a Zeiss axiophot II fluorescence microscope (Zeiss, Göttingen, Germany) with the software Openlab 5.0.2 (Improvision, Coventry, UK). H&E stainings were examined using a Leica DM LS microscope (Leica Microsystems GmbH, Wetzlar, Germany). For each analysis, at least 5 sections per skin sample were evaluated.

2.2.3.5. Model PLGA-Nanoparticle Preparation and Characterization

The magnetite-loaded PLGA-NP used for the TEM experiments were prepared via a modified single emulsion-evaporation method. In brief, oleic acid-coated primary magnetite particles, kindly provided by the Leibniz Institute for New Materials, Saarbruecken [160, 161] were dispersed in chloroform containing poly-D,L-lactide-co-glycolide (PLGA, Resomer® RG 503 H). After adding aqueous polyvinyl alcohol, particles were homogenized using sonication. Water was added to expand the volume, and the dispersion was left overnight under moderate stirring for the organic solvent to evaporate. To assure that only particles loaded with iron oxide were used for the experiments, magnetic separation was performed and agglomerates were removed by filtration. Size and polydispersity of the particles were determined by means of dynamic light scattering analysis using a Zetasizer Nanoseries (Malvern Instruments, Worcestershire, UK).

2.2.3.6. Transmission Electron Microscopy

Visualization of pure NP was done by negative staining electron microscopy [162]. Briefly, NP were adsorbed onto hydrophilized (with 1% Alcian blue) sample supports (pioloform-coated and carbon reinforced grids) by adding 10 µl of the NP suspension, and incubating for 10 min at room temperature. After three washing steps using aqua dest., samples were stained using heavy metal stains phosphotungstic acid and uranyl acetate, and left to air dry.

Visualization of NP in the HF was performed by ultrathin section TEM as previously described [162]. Beforehand, 50 µl of 2.12 mg/ml particles suspended in water were applied onto a predetermined and cleansed area of porcine ear skin. A three min massage was performed using a gloved forefinger, and, subsequently, particles were incubated on tissue for 1 h. Next, 4 mm biopsies were taken and placed

into 1% paraformaldehyde and 2.5% glutaraldehyde in 0.05 M HEPES buffer at room temperature for fixation. Biopsies were cut using a scalpel into slices of approximately 1 mm thickness.

Sample dehydration and embedding was done according to the rapid embedding procedure described in reference [162], with slightly changed incubation times on ice: ethanol 50, 70, 100, 100% for 10 min each; mixtures of resin (LR White) and ethanol 1:1, or pure resin for 10 min each; after an additional step in pure resin for 15 min, samples were embedded in fresh resin which contained 5 µl of accelerator per ml resin. Complete polymerization was achieved after 90 min on ice. To remove remaining unpolymerized resin, samples were placed at 60°C for a few hours. Thin sectioning was performed using an ultramicrotome (UC7, Leica, Leica Microsystems GmbH, Wetzlar, Germany), and ultrathin sections were placed on pioloform-coated single slot grids. No section staining was done. Semi-thin sections were collected on glass slides, stained with toluidine blue and analysed using a phase-contrast light microscope (Axiophot, Zeiss, Göttingen, Germany) equipped with a digital CCD camera (ColorviewII, Olympus Soft Imaging Solutions (OSIS) GmbH, Muenster, Germany).

TEM was done on a Tecnai12 Biotwin (FEI Corp., Hillsboro, Oregon, USA) microscope run at 120 kV acceleration voltage. Images were taken using a digital CCD camera (Megaview III, OSIS GMbH, Muenster, Germany) and a resolution of 1376x1024 pixel.

2.2.4.　Results and Discussion

For all results discussed in this paper, only terminal anagen HFs were considered. This phase was distinguished from the other growing phases based on the complete structure of the HF composed of an infundibulum, an isthmus, a central region, the suprabulbar zone and the hair bulb [14]. For a comprehensive overview of the structure of the HF see Figure 2.

2.2.4.1. Expression of TJ Proteins in Porcine Hair Follicles and Epidermis

Presence and distribution of TJ proteins have to date only been shown in human and mouse, but not porcine HFs. Therefore, the first objective was to look at the expression of the TJ proteins of interest in porcine tissue and compare them to previously published human data [30]. Using qPCR, mRNA from isolated porcine HFs encoding Ocln, ZO-1, as well as Cldn-1, -3, and -4 were identified and analyzed. Amplified DNA obtained was separated and visualized using gel electrophoresis (see Figure 13a-b).
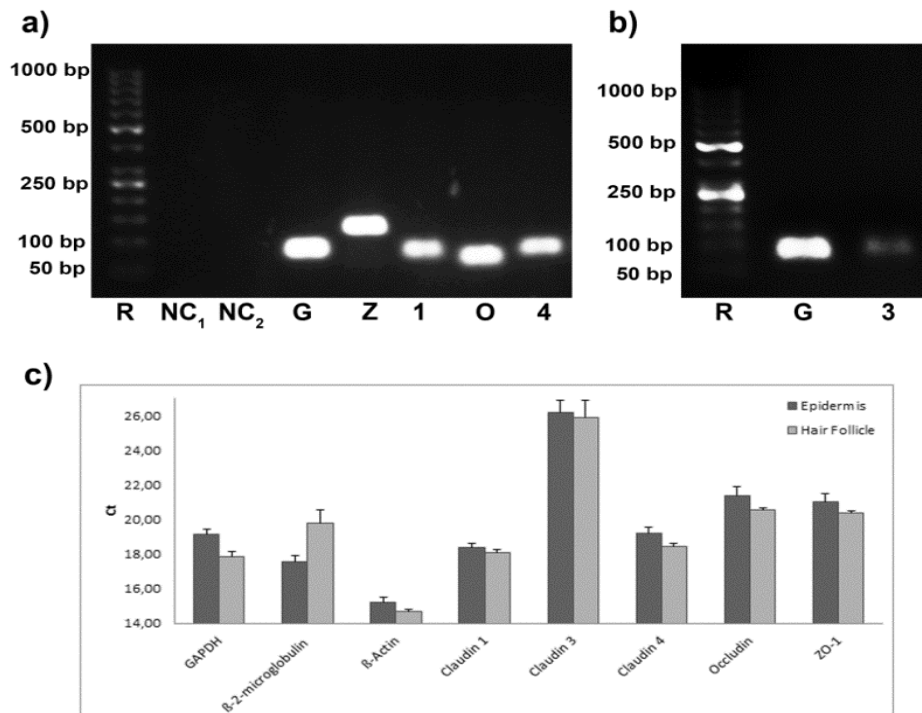
Figure 13: Expression of various TJ proteins in porcine hair follicles and epidermis. a) 2% agarose gel analysis of amplified DNA encoding GAPDH (lane G) as a control, ZO-1 (lane Z), Cldn-1 (lane 1), Ocln (lane O), and Cldn-4 (lane 4) in pinched porcine hair follicles. b) 2% agarose gel analysis of amplified DNA encoding GAPDH (lane R) as a control and Cldn-3 (lane 3) in pinched porcine hair follicles. Lanes R = 50-1000 bp ladder, Lane NC1 and NC2 = negative controls. n=3. c) Cycle threshold (Ct) values for genes of interest (CLDN1, CLDN4, OCLN, TJP1 (ZO-1)), as well as three separate housekeeping genes (GAPDH, ß-2-microtubulin, ß-actin) in porcine hair follicles compared to porcine epidermis; n≥3. Note the higher differences of Ct values for housekeeping genes between hair follicle and epidermis than for TJ proteins.

Normal expression of Cldn-1, -4, Ocln, and ZO-1 in porcine HFs could be detected and was in accordance with what had previously been shown in human HFs [30]. For Cldn-3, which had not been investigated before in human skin, only a weak signal was observed (Figure 13b). The results obtained were then compared to the expression levels in porcine epidermis, in order to determine whether the genes of interest are expressed alike in both structures. Interestingly enough, when using the same amounts of mRNA, our genes of interest, especially the ones encoding Cldn-1, were expressed more alike (determined via cycle threshold (Ct) values) in HFs and epidermis) than all three housekeeping genes used, hinting at the possibility of using CLDN1 (gene) as a more relevant housekeeping gene to compare HF and interfollicular skin (Figure 13c). The Ct value mentioned here is generally defined as the number of cycles required to obtain a fluorescence signal above the threshold (i.e. above background noise), and this number is inversely proportional to the amount of target nucleic acid in the sample [163]. When comparing our data to previously published data on TJ protein distribution in human HF [30], our Ct values were in accordance to what had been shown via immunofluorescence: Cldn-1 being expressed most and Ocln the least (Cldn-3 had not been investigated before). Overall, these findings gave a basis to believe that, as expression in both structures was similar quantitatively, function of these structures with regard to barrier properties may be similar, too. Hence TJs in the HF

may exert a significant barrier function as has been demonstrated for TJs in the interfollicular epidermis before [43].

2.2.4.2. Localization of TJ Proteins in Porcine Hair Follicles: a Comparison to Human Tissue

The next step was to investigate the distribution of the TJ proteins of interest and compare those to previously published data on human. Thus, the localization pattern for the five mentioned proteins (Cldn-1,-3,-4, Ocln, ZO-1) among porcine follicular epithelia was identified using immunohistochemistry (see Figure 14). For clarification regarding the anatomy of the HF during this section, the reader is kindly asked to refer to Figure 2.

<u>Claudin 1 & Claudin 4</u>

In porcine HF, Cldn-1 was distributed throughout all viable layers of the epidermis and the outer root sheath (ORS) of the infundibulum and isthmus (Figure 14a-b). In the upper central region, Cldn-1 staining was intense in the central cell layer (CCL) and companion cell layer (CL), but none was observed in the basal cell layer. In the lower central region, Cldn-1 was limited to the outermost layer of the CCL and the CL, while in the suprabulbar/bulbar zone staining was only positive in the CL (Figure 14c-d). Matrix cells in the bulb, as well as cortex and cuticle of the hair shaft, were faintly positive (see Figure 14c-d). In the inner root sheath (IRS), which consists of Henle's layer (He), Huxley's layer and the cuticle, all layers revealed strong staining, except for the fully differentiated and highly keratinized Henle cells (He*). These cells and their characteristic keratinization development have previously been described in detail by various hair specialists like Langbein or Alibardi and Bernd [24, 155]. For a detailed review the reader is kindly asked to refer to those references.

For Cldn-4, a typical staining of the *stratum granulosum* and upper layers of *stratum spinosum* was observed in the epidermis and infundibulum of the HF (Figure 14e). In the ORS of isthmus and upper central region, Cldn-4 was found in the CCL and CL, while in the lower central and suprabulbar region the staining was confined to only the CL (Figure 14f-g). As for distribution within the IRS of the HF, Cldn-4 staining was intense in all three compartments, yet strongest for Henle's layer, except again for He* (Figure 14h). Matrix cells and cuticle of the hair shaft in the bulbar region showed intense staining, except the ones directly enclosing the dermal papillae.

Distribution of Cldn-1 and Cldn-4 was similar to what was shown in human HFs in the upper parts, while in the central and suprabulbar ORS layers, as well as in the hair shaft region, small contradictions were observed [30]. The previous results in human HFs exhibited a broader staining for

Cldn-1 and Cldn-4 in the ORS. However, after restaining human scalp tissue under the same conditions, the same distribution as had been observed in porcine HFs was also seen in human skin. It is very likely that these differences in the staining distribution can be explained by different fixation processes[4] resulting in different antigen accessibility. Also, a new batch of antibodies, which may contain slightly different concentrations of antibody, could be a possible explanation.

ZO-1

An intense staining of ZO-1 was found in the *stratum granulosum* and the upper layers of *stratum spinosum* in the interfollicular epidermis and infundibulum (Figure 14i). In the isthmus and central region of porcine HF, ZO-1 was strongly positive in all cell layers of the ORS (Figure 14j-k). The suprabulbar region revealed a more intense staining of the CL than surrounding cell layers, yet it was visible throughout the entire ORS of the bulbar and suprabulbar region. Within the bulb the IRS exhibited strong staining of ZO-1, with the undifferentiated cells of Henle's layer being the most intense. In the suprabulbar region the IRS remained positive, but staining intensity in Henle´s layer decreased with He* being completely negative (Figure 14k-l). The matrix cells, lower cortex and cuticle of hair shaft showed an intense ZO-1 staining, whereas the upper cortex displayed only moderate staining (Figure 14k-l). The staining pattern was overall similar to that found in human HFs [30].

Occludin (Ocln)

In the interfollicular epidermis and infundibulum, Ocln was restricted to the *stratum granulosum* (Figure 14m). This narrow distribution continued on through the isthmus and central region, as only the CL of the ORS stained positive (Figure 14n-o). The suprabulbar region still exhibited staining in the CL, but no presence of Ocln in the ORS of the bulb was seen (Figure 14p). Among the IRS, Henle's layer was positive for Ocln in the bulbar, suprabulbar, and lower central region. No staining at all was observed in the matrix cells, but some was seen in the more differentiated matrix cells and medulla (Figure 14o). The staining pattern was similar to human HFs [30] except for a slightly broader localization of Ocln in the ORS of the upper parts of human HFs. Again, the difference in fixation may be an explanation for this.

---

[4] In 2003, sections were prepared via cryo fixation while for this study formalin fixation and paraffin embedding was done for better quality sections
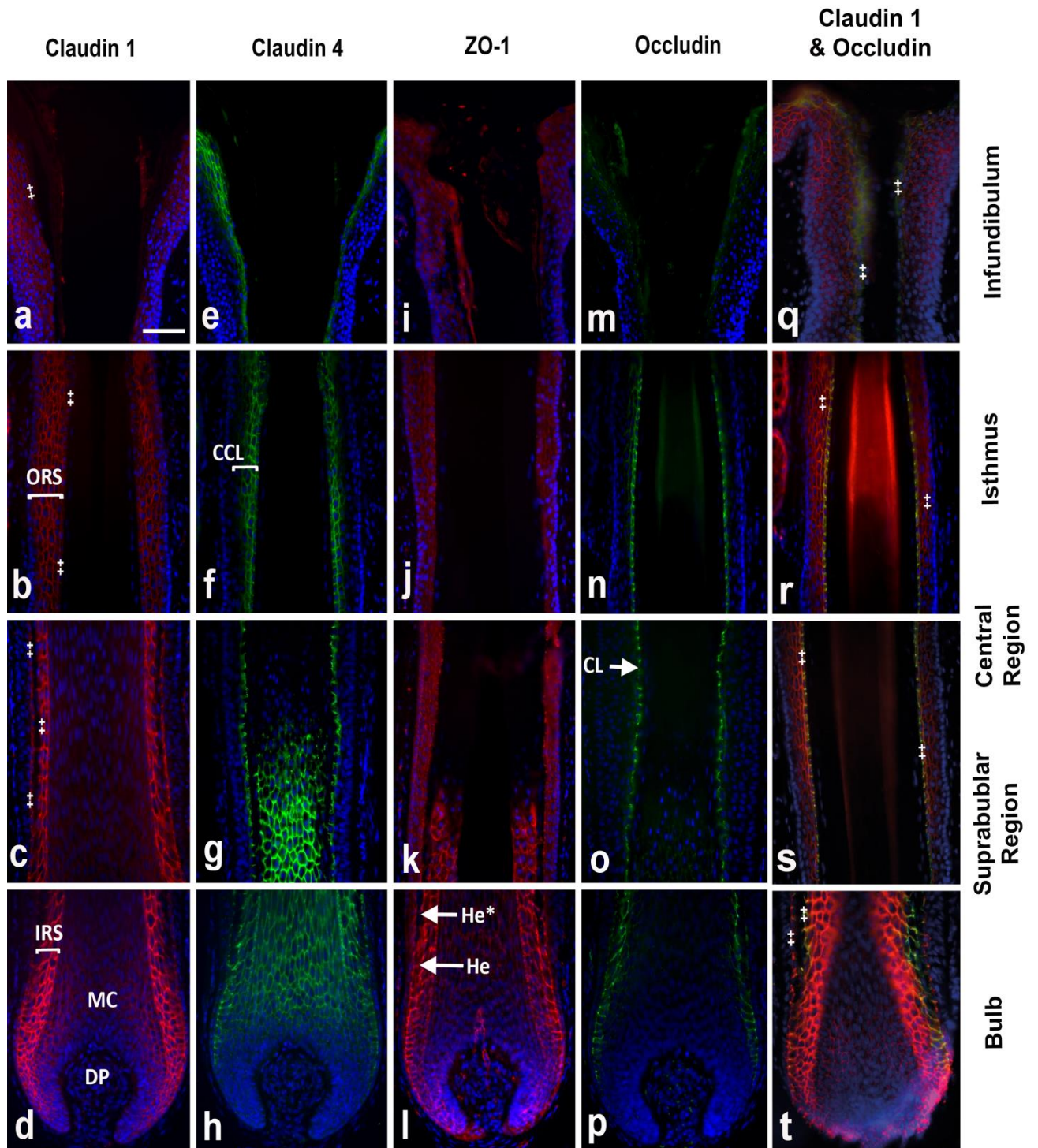
Figure 14: Localization of TJ proteins in adult porcine hair follicles. Immunofluorescence-based localization of Cldn-1 (red; a-d), Cldn-4 (green; e-h), ZO-1 (red; i-l), Ocln (green; m-p), and co-localization of Cldn-1 & Ocln (red & green;q-t) in infundibulum (a,e,i,m,q), isthmus/upper central region (b,f,j,n,r), lower central/suprabulbar region (c,g,k,o,s), and bulb (d,h,l,p,t) of HFs. Blue: nuclei; yellow: co-localization of green and red. CCL = central cell layer of the ORS, CL = companion cell layer of ORS, DP = dermal papilla, He = Henle's layer of IRS, He* = differentiated cells of Henle's layer of IRS, IRS = inner root sheath, MC = matrix cells, ORS = outer root sheath, ++ = regions of co-localization of all TJ proteins. Scalebar = 80 μm.

Claudin 3

Because Cldn-3 was shown before at cell-cell membranes in murine HFs [48], and because it had given a weak signal via qPCR (see Figure 13), it was also examined here. However, immunolocalization revealed that Cldn-3 was only found very weakly and mainly intracellularly in porcine epidermis and HFs (Figure 15a,b) , even though it was positive in porcine sweat glands and murine HFs (Figure 15b,c). These results were, again, in accordance with human data, as staining of human HFs had also given an only very weak, mainly intracellular staining (unpublished data). This was an interesting finding, as it hints at differences between porcine/human and murine HFs, with Cldn-3 not playing a part in barrier function.
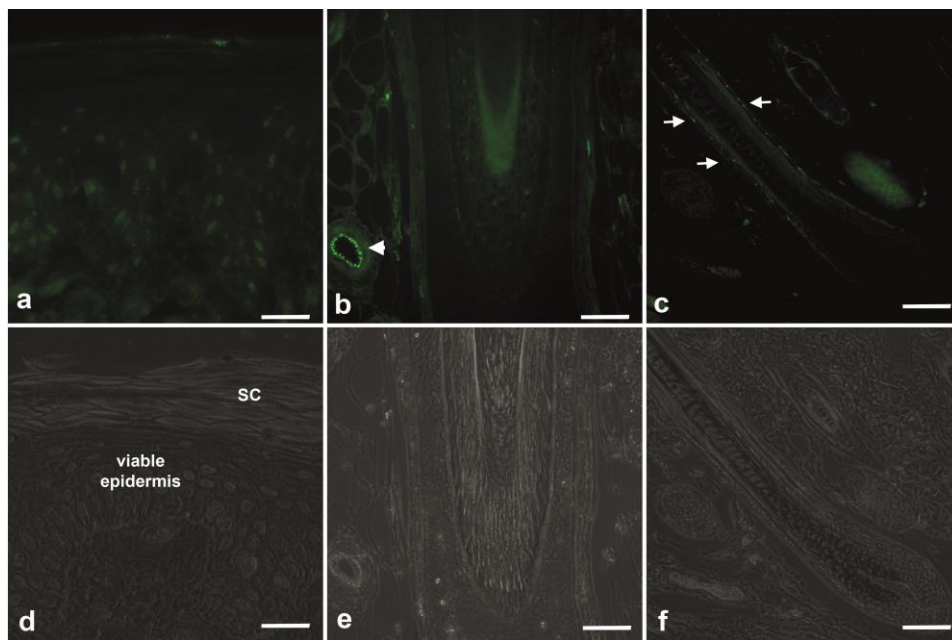
Figure 15: Localization of Cldn-3 in pig (a,b,d,e) vs. Cldn-3 in mouse skin (c,f). Cldn-3 immunolocalization (green) in porcine epidermis (a), porcine hair follicle (b) and mouse hair follicle. (d-f) represent corresponding phase contrast pictures. Note that Cldn-3 is found only weakly and mainly intracellular in porcine epidermis and hair follicles while it is clearly positive at cell-cell borders in murine hair follicles (companion cell layer of the ORS (arrows in c) and faintly in the IRS, as well as sweat glands in porcine skin (arrowhead in (b)). Scalebars = 50 µm.

Co-localization of TJ proteins

As it is likely that functional TJs are only found in areas where TJ proteins co-localize (for review see [58, 148, 164]), we took a closer look to identify those areas of co-localization throughout porcine HFs. Figure 14q-t and Figure 16 are examples which display this co-localization nicely. In the past, functional epidermal TJs in healthy skin have mainly been detected at areas where Ocln is present in the *stratum granulosum* [43, 58, 164, 165]. And although a lack of Ocln does not necessarily influence barrier function of TJs [37, 166], this protein is the most restricted one resulting in its frequent use as a surrogate marker for TJ detection in skin, as it mostly co-localizes with tracer stops at TJs in the epidermis.

In Figure 14q-t and Figure 16, Cldn-1 is shown in red and Ocln in green, resulting in a yellow/orange appearance at points of co-localization. In the infundibulum of porcine HFs, a co-localization of all four TJ proteins was detected at the *stratum granulosum* (Figure 14a,e,i,m,q) and it continued down the CL of the ORS from the isthmus to the suprabulbar region (Figure 14b-d,f-h,j-l,n-p,r-t, Figure 16). In the lower central region, suprabulbar region, and bulb the proteins were co-expressed in Huxley's layer of the IRS hinting at a possible barrier at those sites (Figure 14c-d, g-h, k-l, o-p, s-t).
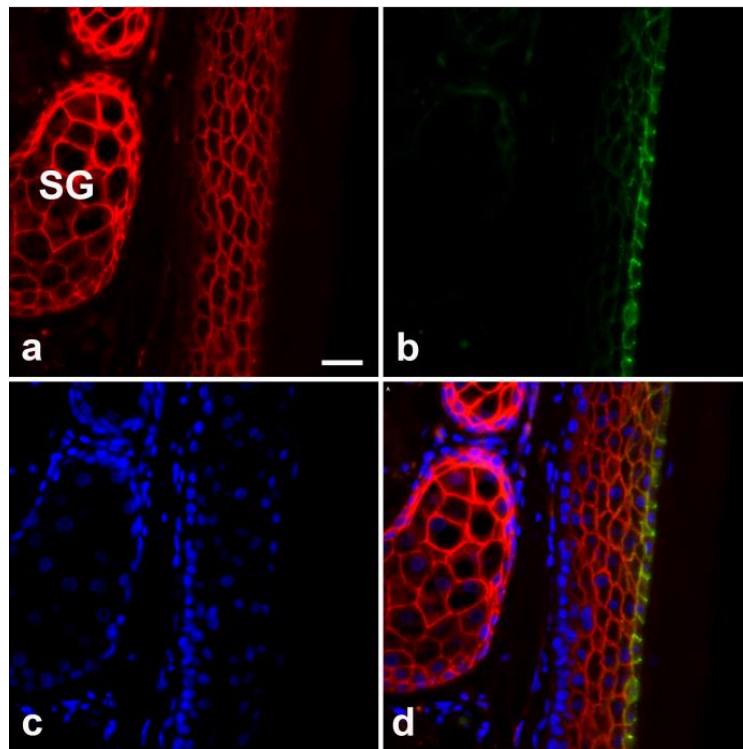
Figure 16: Co-localization of Cldn-1 and Ocln in companion cell layer of ORS in isthmus region of porcine hair follicle. (a) shows Cldn-1 in red, (b) Ocln in green, (c) DAPI in blue, and (d) represents an overlay of all three stainings. Scalebar = 20 µm.

Thus, it seems as if throughout the entire HF, from the infundibulum down to the suprabulbar region, a putative barrier may exists which may be involved in regulating invasion of exogenous substances from the outside, as well as loss of water and nutrients from the inside. Overall, (co)-localization of all of the investigated TJ proteins was similar between pig and human, making the porcine HF a good tool to investigate TJ barrier function in HFs.

2.2.4.3. TJs as a Biological Barrier in Hair Follicles

In healthy human skin and newborn mice, the polar, biotin-labeled extracellular tracer molecule Sulfo-NHS-LC-Biotin (557 Da, Biotin-SH) has been used to investigate TJ functionality [43, 58, 165, 167]. In newborn mice and healthy human skin, this tracer molecule was stopped, when applied from the dermis side, at the most apical sites of TJ protein co-localization. Interestingly, changing the site of co-

localization (e.g. in psoriasis vulgaris [168, 169]), or applying the TJ modulator cCPE [151], resulted in changing the localization of the Biotin-SH stop or complete abolishment of the tracer stop, respectively. Figure 17 shows reproducibility of these results in healthy porcine tissue.
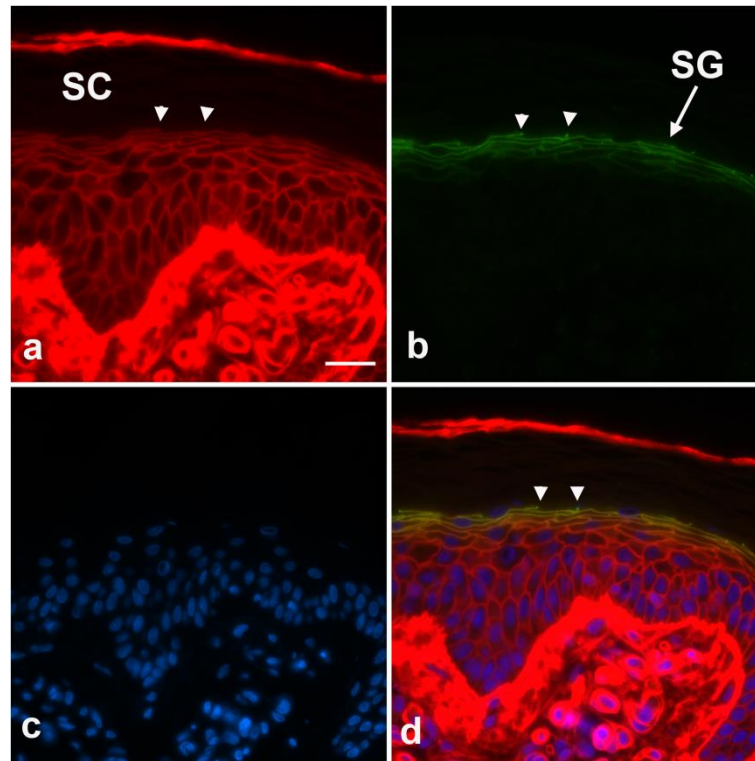

Figure 17: Biotin-SH gets halted at Cldn-4 positive sites in *stratum granulosum* of porcine epidermis. (a) Biotin-SH staining in red, (b) Cldn-4 staining in green, (c) DAPI in blue, and (d) represents an overlay of (a-c). Arrowheads denote Cldn-4-positive sites in granular cell layer where Biotin-SH stops. Scalebar = 30 µm.

Similar to human skin [43], the tracer molecule penetrates towards the skin surface and gets halted at the most apical point of TJ protein co-localization, e.g. granular cell layer. Next, this well-established and reliable assay was used to test functionality of follicular TJs in porcine skin. Thus, longitudinal-sections (Figure 18) and cross-sections (Figure 19) of porcine HFs, which had previously been injected with the tracer Biotin-SH and later stained for TJ proteins, were thoroughly investigated.

In the infundibulum, a functional barrier was to be expected in the *stratum granulosum*, similar to what was observed in the epidermis (Figure 17). As depicted in Figure 18a-c and Figure 19a-b, a tracer stop was indeed seen in this cell layer. In the longitudinal-, as well as the cross-sections, Biotin-SH spreads from the dermis into the viable part of the epidermis; yet it is not able to penetrate past the outermost site of the Cldn-1 and Cldn-4 staining, the apical part of the *stratum granulosum*. Of note, this specific localization is also the site where the narrow Ocln staining is present (Figure 18d)). Similarly, in the isthmus and upper central region of porcine HFs, a TJ barrier was observed in the CL of the ORS (Figure 19d-i)).The lower central and upper suprabulbar region give rise to two individual

barrier sites in two distinct compartments of the HF, one in the CL of the ORS (Figure 18f-g) arrowhead pointing to the left & Figure 19j-k), and one in Huxley's layer of the IRS (Figure 18f-g) arrowhead pointing to the right & Figure 19j-k)). The tracer spreads from the dermis into the ORS of the HF to the point of co-localization of at least four (Cldn-1, Cldn-4, Ocln, ZO-1) TJ proteins in the CL. Simultaneously, the tracer molecule permeates from the bulb (see below) upwards via the matrix cells, hair cortex, and cuticle into the IRS up to Huxley's layer where it is stopped.
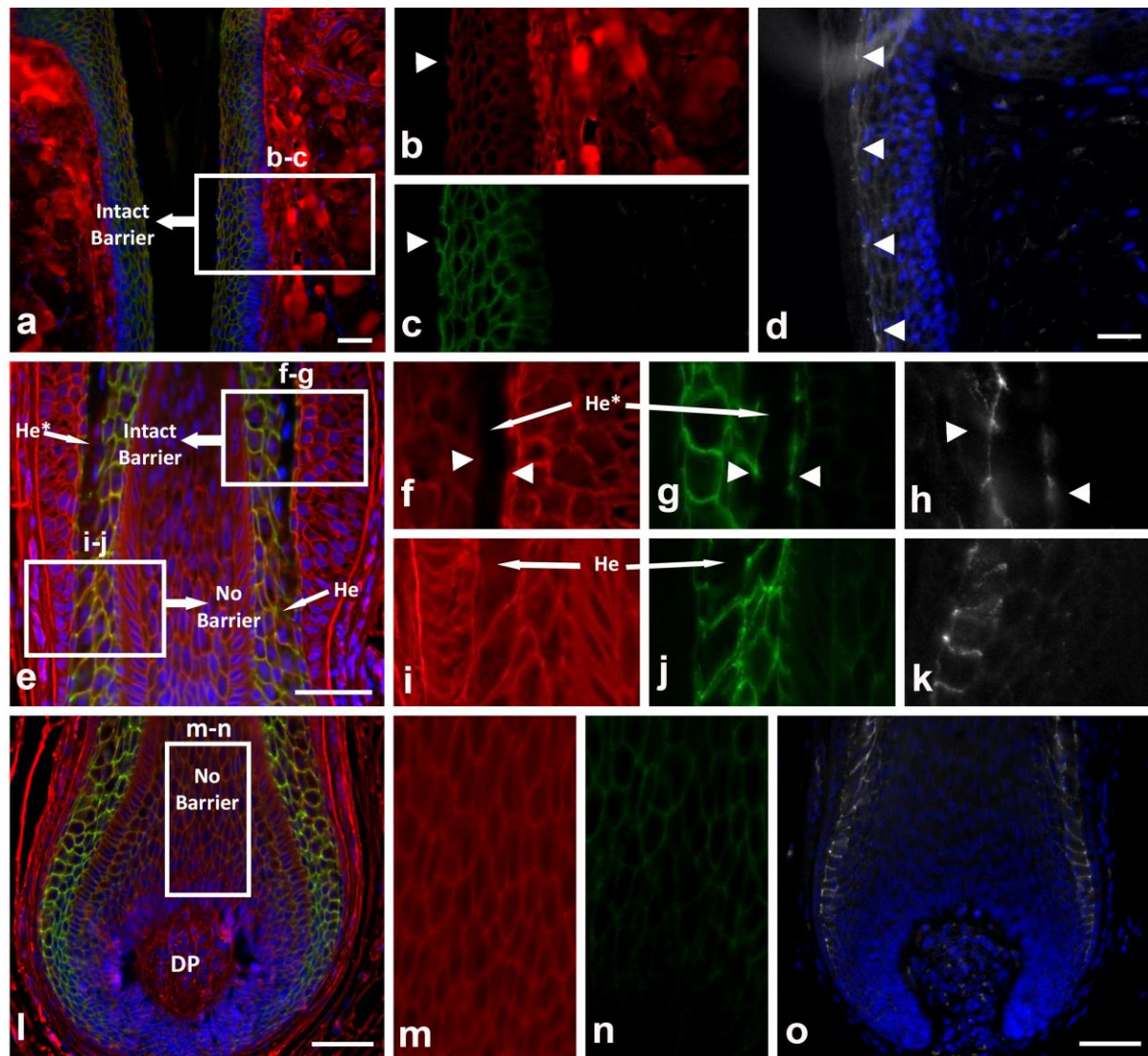
Figure 18: Barrier function of follicular TJs displayed in longitudinal-sections. Immunohistochemical stainings of Biotin-SH (red), Cldn-1 (green), Ocln (white), and DAPI (blue, nuclei). (a-d) infundibular region, (e-k) lower central/suprabulbar region, and (l-o) bulb. White boxes in a, e and l represent areas magnified in b-c, f-g, i-j, and m-n, respectively. Arrowheads highlight points where Biotin-SH is stopped (b-h) (c-d, g-h); He = Henle's layer, He* = differentiated cells of Henle's layer, DP = dermal papilla. Scalebars = 50 μm

This is in accordance with all data discussed before, as exactly in these layers, the CL and Huxley´s layer, a co-localization of various TJ proteins occurs. Of note, tracer flux into the fully differentiated and keratinized cells of Henle's layer (He*) in the IRS [24, 155] is blocked from two sides: the most proximal layer of the ORS (CL) and the most distal layer of the IRS (Huxley). For that reason, the He*

cells appear black in Figure 18f & Figure 19g-f. For a simplified depiction of this situation, please refer to Figure 20a.

Figure 19: 5 μm cross sections of porcine HFs from infundibulum (A-C), upper central region (D-F), lower central region (G-I), suprabulbar region (J-L) and bulb (M-O) demonstrating intact barrier properties from the infundibulum down to the suprabulbar region. The bulb was freely permeated. Sections on the left represent Cldn-1 (green), Biotin-SH (red) and DAPI (blue). Middle sections show Cldn-4 (green), Biotin-SH (red) and DAPI (blue). Sections on the right are H&E stainings of representative regions shown to the left. ** highlight examples of intact barrier, °° denote no barrier. SG=*stratum granulosum*, SC=*stratum corneum*, M=Medulla, ORS=outer root sheath, He=Henle's layer of IRS, Hu=Huxley's layer of IRS, C=cortex, Cu=cuticle, DP=dermal papillae. Scalebar = 20 μm.

Only about 70 µm further down the hair shaft, in the lower suprabulbar region magnified in Figure 18i-j, these two barrier sites seem to not be established yet. Here, Biotin-SH permeates from two sides: 1) via the bulb into the hair shaft to the IRS, and 2) from the dermis into the ORS up to the point of TJ co-localization in the CL of the ORS. In contrast to above, however, Henle's layer gets freely permeated in this lower region. A putative explanation for this scenario could be that while two points of co-localization were observed in the upper suprabulbar region (in the IRS & ORS; see two X's in Figure 20a), only one monolayer is subject to co-expression in the lower part (located in the CL of the ORS; single X in Figure 20b). Thus, in the latter situation the tracer molecule permeates from two sides, via the IRS and ORS, and only gets halted at one 'fine line', making the stop not visible to the normal eye. However, this is only a hypothetical explanation, and, of course, another one could be that simply no TJ barrier is present in this region.
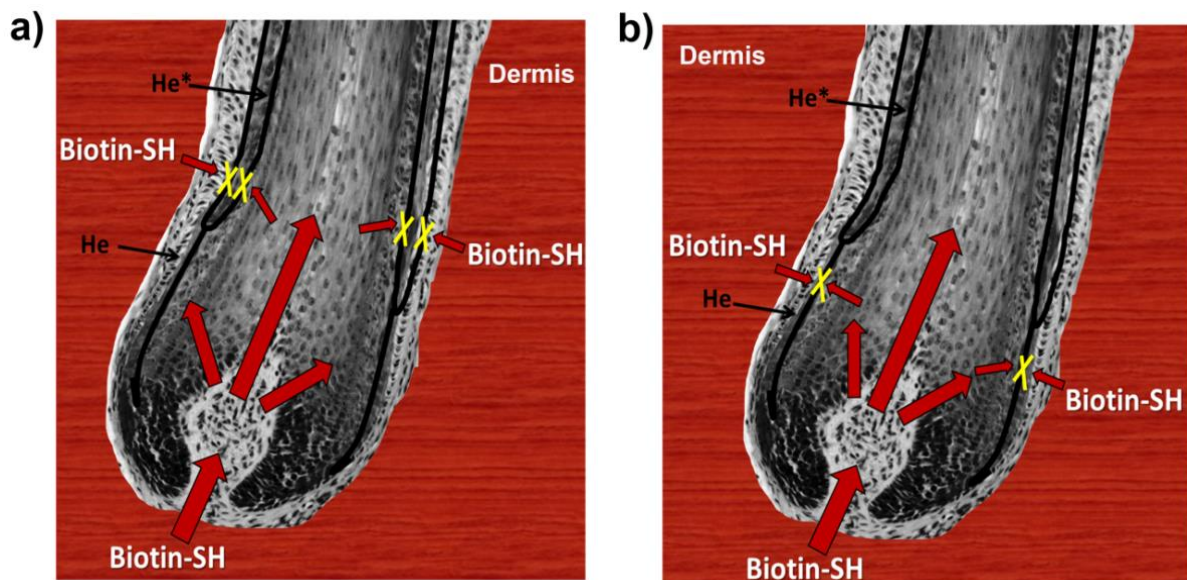
Figure 20: Cartoon depicting permeability of Biotin-SH in untreated porcine HFs at TJ borders in upper suprabulbar region (a) and lower suprabulbar region (b). Red arrows represent Biotin-SH, black lines represent functional TJs, and yellow X's display the area where Biotin-SH gets blocked (a) or hypothetically may be get blocked (b).

The bulb of the HF is not protected by a TJ barrier at all. Biotin-SH permeates from the dermis into the bulb, most likely via the dermal papilla and the matrix cells, which do not contain neither Ocln, nor Cldn-1 (Figure 18l-o & Figure 19m-n). This confirms previous work published on cell-cell communication in rat HFs in which the tracer dye Lucifer yellow was applied to demonstrate spreading of the dye after injection into the matrix region of rat HFs [170].

Noteworthy is that the manual application of Biotin-SH to the epidermis (i.e. from the outside) was also performed in order to mimic outside-in barrier conditions in the HF. This was, however, unsuccessful. The tracer molecule did not penetrate past the first layer of corneocytes in the SC (Figure 21a), and not at all into the HF (even after massaging the skin post-administration) (Figure

21b). This is in accordance with what has been reported before about solutions (in contrast to NPs) not penetrating into HFs [83].
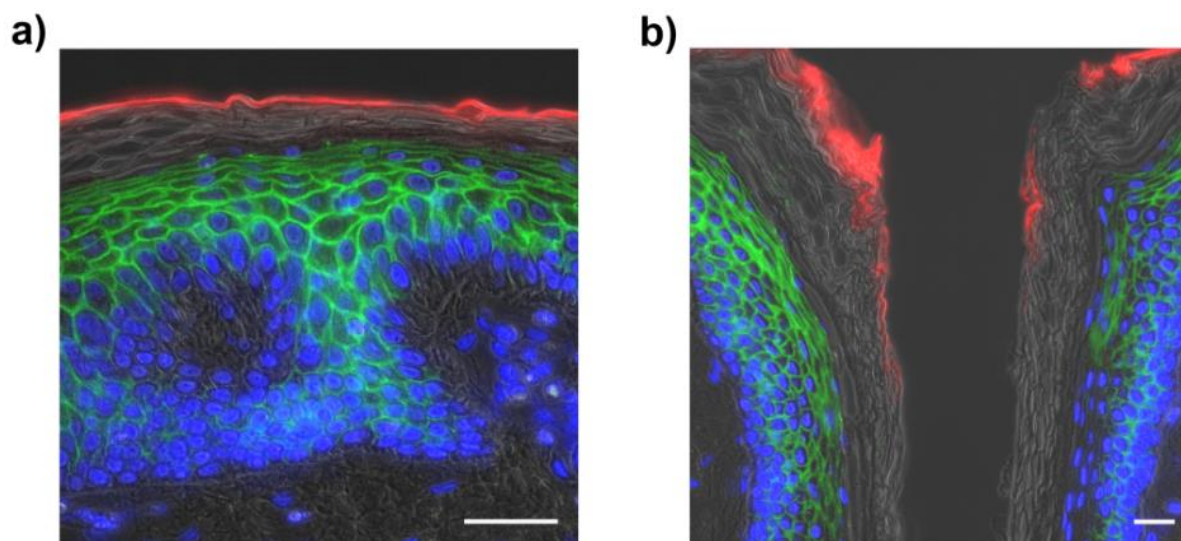

Figure 21: Intact barrier function of the "limiting barrier", the *stratum corneum,* to Biotin-SH in porcine epidermis (a) and infundibulum of hair follicle (b). (a, b) Overlay of Biotin-SH (red), Cldn-1 (green), DAPI (blue) and a transmitted light image. Scalebars = 30 µm.

Summarizing this data, barrier-forming TJs exist in the ORS from the infundibulum down to the upper suprabulbar region of the HF. In the infundibulum this TJ barrier is – similar to the epidermis – an addition to the SC, but in lower areas it is likely the only barrier. In the bulb, however, no obvious barrier hinting at functional TJs was detected, and the tracer molecule was able to permeate freely[5]. Therefore, TJs seem to compartmentalize the HF i) into areas that are freely accessible from the dermal microenvironment, i.e. the hair-forming area of the bulb and the ORS (containing the bulge area), which may be important for the supply and control of nutrients and signaling molecules; and ii) into areas that are restricted from the extracellular supply by the dermal microenvironment, i.e. the upper areas of the IRS, especially the He*. This may be important to reduce and/or prevent the loss of hormones, nutrients, or other solutes via the HF, plus to possibly keep exogenous substances from translocating into the outer layers of the HF and/or entering the bloodstream.

2.2.4.4. Modulation of Tight Junction Barrier Function using EDTA

After barrier properties of follicular TJs had successfully been demonstrated, EDTA was used to test whether this barrier can be modulated, as is displayed in Figure 22.

---

[5] Of note, even though the tracer was applied only from the dermal side (inside-out barrier function), we can conclude that TJs also form an outside-in barrier at the same sites, because the permeation of solutes through TJs is bidirectional and only dependent on the gradient of the substances. Therefore, when a barrier for permeation exists, it exists in both directions. Because TJs form a functional inside-out barrier in the HF, especially in areas where NP were found, we can conclude that they also form a functional outside-in barrier in these areas [170].
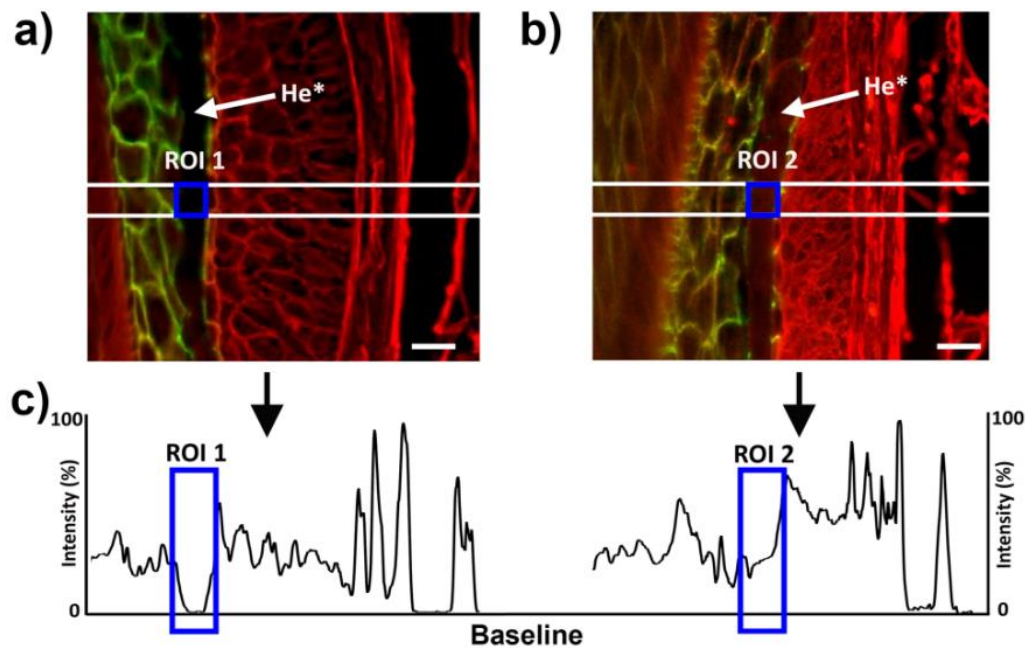
Figure 22: Direct comparison between intact barrier in suprabulbar region of untreated porcine HF (a) and impaired barrier in with 8.0 mM EDTA treated tissue (b). (c) represents an intensity curve for tracer molecule Biotin-SH in images for selected area denoted by two white lines in (a) and (b), respectively. Blue boxes in (c) highlight region of interest 1 (ROI 1) of intact barrier to Sulfo-NHS-LC-Biotin in (a) indicated by intensity curve dropping down to the baseline vs. impaired barrier in (b) indicated by a rise in intensity in ROI 2 of ~30%. He*=differentiated cells of Henle's layer, ROI=region of interest. Scalebar = 15 μm.

EDTA is a well-known Ca^{2+}-chelator and has been shown to impair TJ functionality in cells, resulting in increased permeability [171, 172]. Thus, untreated and EDTA-treated samples were analyzed simultaneously. For samples which had not been treated using EDTA, a clear stop of Biotin-SH was seen at Huxley's layer of the IRS, as well as at the CL of the ORS, leaving He* black (Figure 22a). In the EDTA-treated samples, however, the tracer permeated this layer of fully differentiated cells, making He* appear red (Figure 22b). To further examine this matter, an intensity analysis (Figure 22c) of Biotin-SH was performed at the regions of interest (ROI) highlighted in Fig. 24a-b. While the intensity curve at He* is close to the baseline in the untreated sample (ROI 1), it is significantly higher (about 30%) for the EDTA-treated sample (ROI 2), only further confirming previous results. For the sake of correctness, it has to be noted that EDTA does not only address TJs. By chelating Ca^{2+} it also disturbs adherens junctions. Nonetheless, adherens junctions are no barrier-forming junctions, hence the observed effect on barrier function is most likely TJ-mediated.

2.2.4.5. Visualization of PLGA-based Nanoparticles in Hair Follicles

Based on the newly found data discussed above, the following question aroused: can the organization of the different barriers in the HF [two barriers in the infundibular region (SC and TJs), one barrier in the isthmus/central/suprabasal region (TJs), and a complete lack of a barrier in the bulb] be interpreted

as the biological answer to the varying accessibility of exogenous substances to the hair shaft? To investigate this further, model NPs were applied to porcine ear skin, and the distribution of these particles within the hair shaft was compared with the distribution of these various barriers in different follicular regions.

Since follicular penetration of NPs with respect to drug delivery has also become a field of surging interest over the last decade, polymer-based NPs were used. Until now, only indirect detection of NPs based on fluorescence microscopy had been discussed in literature [77, 83, 85, 145]. However, for this study we used PLGA-based NP (mean diameter = 154 nm; polydispersity index = 0.02; see Figure 23) loaded with primary magnetite particles (10 nm) in order to visualize, and simultaneously evaluate, the uptake, intactness, as well as potential translocation of individual particles in the HF.

In Figure 23a) the NP depicted are completely embedded in a thin film of the heavy metal stain (phosphotungstic acid), which makes the background appear dark. The particles are spherical in shape, and homogeneous in size. The bright low-scattering PLGA matrix is clearly visible with dense magnetite particles embedded within.
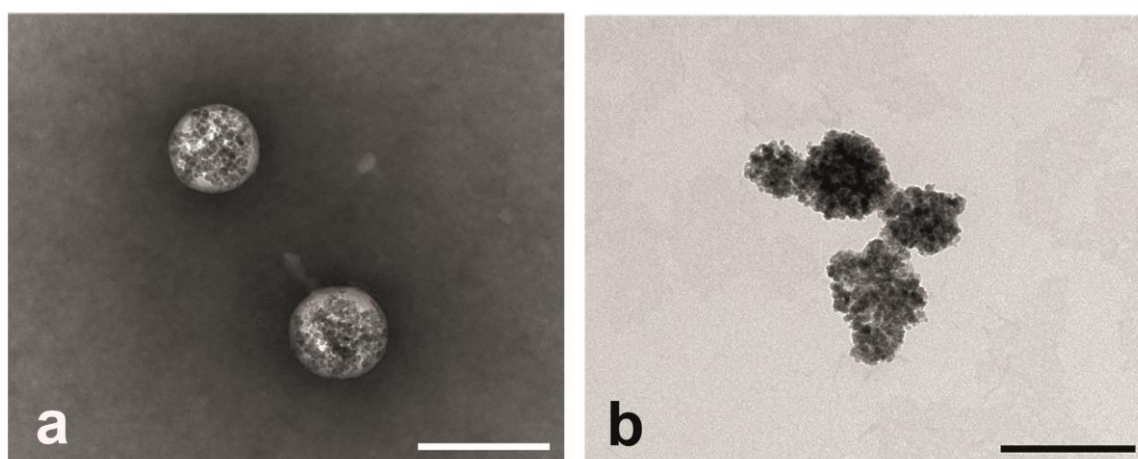
Figure 23 Negative staining transmission electron microscopy of magnetite-loaded PLGA nanoparticles. (a) NP embedded in heavy metal stain (phosphotungstic acid) (b) Nanoparticles from the same sample preparation as in (a), but without a staining film resulting in dehydrated particles. Scalebars = 200 nm.

In Figure 23b) the same NPs are shown, however, no staining was performed in order to mimic the situation in the non-stained biological tissue. Here, the PLGA matrix of the NPs has collapsed during the final drying step, leaving only magnetite particle clusters visible. This information was important to obtain, as such a drying effect is to be expected during the final processing steps of the tissue samples which contain these NPs. Dehydration, as well as plastic embedding, may be a cause of this effect. Nonetheless, the preserved clusters of the magnetite particles give an indication on whether the particles stay intact or not upon penetration.

As has been proposed in literature before, applying the NP suspension onto porcine ear skin, together with a slight massage, resulted in the highest accumulation of NP in (or on) the SC of the infundibulum of the HF (Figure 24ai-av) [76, 83]. Of note, in all magnifications, the homogeneously-sized, spherically-shaped clusters of the magnetite particles are visible; hence particles stay intact upon penetration.
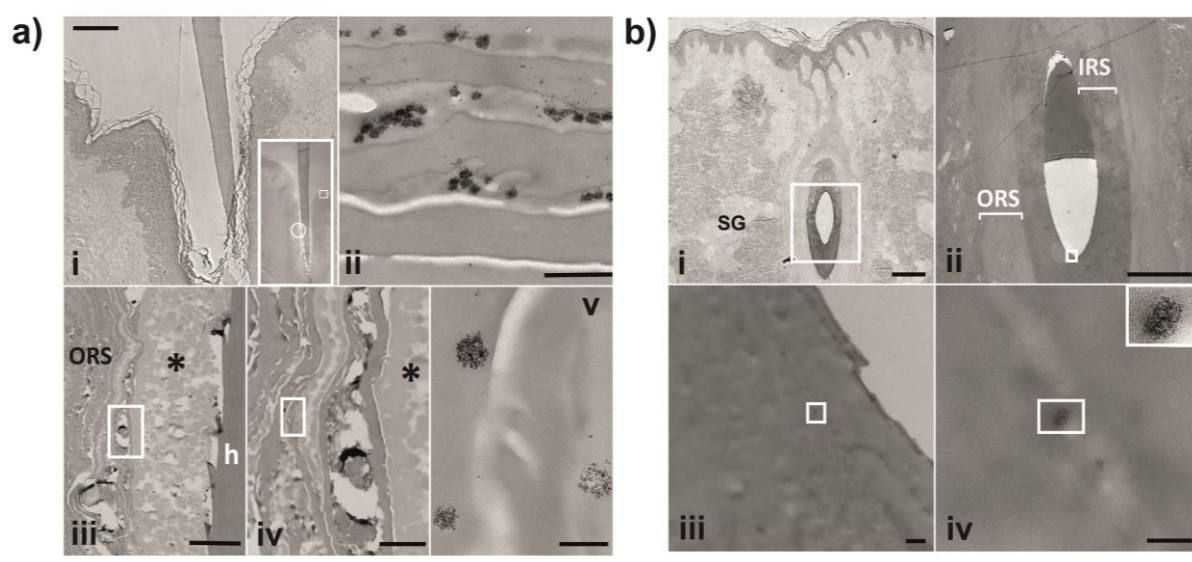

Figure 24: Localization of PLGA-NP in infundibulum of HF(a) and central region of HF(b). (ai) Light microscopy image of the infundibular region of the HF. Inset: TEM image of a corresponding ultrathin section. Square: *stratum corneum* magnified in (aii); circle: infundibular region magnified in (aiii-av); each image represents a magnification of the previous one; Scalebars = 200 μm, 1 μm, 10 μm, 2 μm, and 200 nm for a-e, respectively. (bi) Light microscopy image of a semi-thin section depicting overview of a diagonally cut HF in upper central region; (bii) corresponding ultrathin section of (bi); (bii-biv) each represent magnification of previous one. Inset in (biv) represents final magnification. Scalebars = 500 μm, 100 μm, 2 μm, and 300 nm, for bi-biv, respectively. *h*=hair, ORS=outer root sheath, *=sebum.

Figure 24bi-iv displays the central region of a HF cut diagonally. Here, individual intact particles (see inset in Figure 24biv for final magnification) did penetrate into the hair shaft, reaching parts of the HF about 500 μm away from the skin surface. These individual particles, embedded in the epithelium, also demonstrated preservation of the PLGA matrix i.e. intactness of the particles upon penetration, revealed by the expected side of the clusters of magnetite particles (see biv including inset). As was expected, the particles appeared in a dried and collapsed state, which is an artifact resulting from the sample preparation process, as was discussed before (Figure 23b). In this study, the particles were mainly observed in the cuticle/Huxley layer of the IRS (Figure 24bii-iv) but a translocation of these individual particles into the ORS, let alone the dermis, was not observed here.

Thus, the detection of majority of the particles in the infundibulum, which was previously shown to be protected by the double-barrier consisting of the SC and TJs, is only reasonable. Few particles were seen in deeper areas of the hair shaft, yet it seems as if they were not able to penetrate past the TJ barrier in those regions. No particles at all were observed in parts of the HF which is not protected by any barrier (i.e. the bulb).

2.2.5. Conclusion

This work shows for the first time the existence of a continuous TJ barrier in the ORS of mammalian HF, ranging from the infundibulum down to the suprabulbar region. While in the lower follicular regions they are likely the only barrier, they seem to act as a second line of defense, next to the SC, in the infundibulum of the HF. The application of model NP to the skin and subsequent analysis using TEM demonstrated that majority of the particles were located in the upper follicular region protected by this double-barrier (SC and TJs). Fewer particles were located in parts of the HF where TJs seem to act as the only barrier. Thus, we hypothesize, that the two follicular barriers, the SC and TJs are organized according to the principle of risk stratification: areas with a high accessibility are protected by two barriers, whereas in areas with lower accessibility, only one barrier is present. Moreover, besides the continuous barrier in the ORS, another TJ barrier was detected in Huxley's layer of the IRS in the suprabulbar region; the bulb, however, seemed to be completely permeable. Therefore, as a result of these different TJ barriers in various regions of the HF, it can be concluded that a compartmentalization of the HF occurs that divides it into areas accessible and non-accessible from the dermal microenvironment. This argues for a potential role of these barriers, not only concerning the invasion of exogenous substances, but also for the loss of solutes, and likely also for HF biology. Finally, expression and co-localization of the investigated TJ proteins in porcine HFs were shown to be equivalent to human skin, indicating suitability of this model regarding TJ barrier experiments, and thereby arguing for a transferability of our results to human HFs.

2.2.6.   Acknowledgement

The above mentioned article was accepted for publication after submission of this doctoral thesis.

2.3. Nanocarriers for Optimizing the Balance Between Interfollicular Permeation and Follicular Uptake of Topically Applied Clobetasol

<u>Personal contributions to this chapter were as follows:</u>

- ❖ Particle preparation and characterization for follicular uptake and skin permeation studies described
- ❖ Performance and analysis of Differential Stripping experiments
- ❖ Analysis and interpretation of described results
- ❖ Writing of chapter

2.3.1. Abstract

Glucocorticoids are essential for the treatment of many dermatological conditions, ranging from inflammatory-based hair disorders to eczema or psoriasis. However, these drugs are known to cause severe systemic as well as local adverse effects even when only applied topically. Optimizing the balance between the release of drug, interfollicular permeation, and follicular uptake may allow minimizing these adverse effects given that one succeeds in targeting a sustained release formulation to the hair follicle. To test this hypothesis, three different polymeric nanocarriers (nanospheres, nanocapsules, lipid-core nanocapsules) encapsulating the potent glucocorticoid Clobetasol propionate (CP) were prepared, all providing a sustained release of drug as was demonstrated by separate *in vitro* experiments. They were each formulated as a suspension and hydrogel and (partially) labeled with Rhodamin B for quantification purposes. Follicular uptake was evaluated using the Differential Stripping method and nanocapsules in suspension were found to achieve the best recovery (4%) after application of a massage. In contrast, only minimal amounts of CP were detected in the hair follicle when applied as free drug in solution or hydrogel, regardless of the use of massage. Skin permeation experiments using heat-separated human epidermis mounted in Franz Diffusion cells revealed similar decreased transdermal permeability for all three nanocarriers when compared to free drug. Summarizing these results, nanocapsules in suspension and applied using massage were shown to be a good candidate for maximizing follicular targeting, minimizing drug permeation, and releasing the drug in a steady and continuous manner. We conclude that such nanoparticle-based formulations offer a viable strategy for achieving more efficient glucocorticoid delivery to the hair follicle, while potentially decreasing adverse effects by releasing the drug in a controlled manner and decreasing interfollicular permeation simultaneously.

2.3.2. Introduction

Glucocorticosteroids are considered to be first-line agents for many diseases in the field of dermatology [173]. Their wide range of therapy includes high-prevalence skin disorders like eczema, atopic dermatitis, or psoriasis to diseases in which the inflamed or diseased hair follicle (HF) serves as the main target, e.g. lichen planopilaris (LPP), alopecia areata (AA), or frontal, fibrosing alopecia (FFA) [95, 174-179]. As has been discussed in Chapter 1, the skin is very effective in limiting xenobiotics access to the body. Nonetheless, some substances can still passively diffuse through the *stratum corneum* (SC), the outermost layer previously identified as the limiting barrier, and reach the viable epidermis and/or systemic circulation [147]. This effect is dependent upon different factors regarding the patient's skin nature (age, application site, hydration level, etc.), the nature of the molecule used (size, lipophilicity, pKa, etc.), and the vehicle itself (lipophilicity, viscosity, interactions

with the drug, ability to release the drug, extent of follicular penetration, possible interaction with the skin, etc.). The most important systemic side effects that occur as a consequence of high glucocorticoid absorption are bodyweight gain, development of diabetes mellitus, production of electrolyte imbalance, hypertension, Cushing's syndrome, osteoporosis, peptic ulcer, growth retardation in infants and children, and suppression of the hypothalamic-pituitary-adrenal axis [180, 181]. Within the local adverse events the most common one observed is cutaneous atrophy [181]. A typical disease pattern for this condition is a characteristic reduction in epidermis and SC thickness, a decreased number of keratinocytes, changes in the organization of elastin and collagen fibers, a decreased cellularity in the dermis, elimination of fatty tissue, and loss of mast cells [98, 99]. Although the occurrence of this adverse event is almost unavoidable during frequent application of topical glucocorticoids, the degree of it observed in patients can generally be directly related to factors like the treated skin site ("thicker" on scalp or forearm vs. "thinner" on eyelid), patient's age, potency of the drug used, and usage of occlusion [182]. Besides these adverse events there are other major drawbacks that physicians and patients describe when employing topical glucocorticoid treatment, especially for inflammatory scalp diseases like AA, LPP, or FFA. For example current clinical trials employ therapies which involve the application of an ointment containing a glucocorticosteroid (e.g. Clobetasol Propionate, CP) to the desired site of action under occlusion with a plastic film, or application of a shampoo or cream several times a day [95, 96, 183]. Because these conditions are very tedious and time-consuming they are generally not well accepted by the patients resulting in decreased patient compliance. Moreover, reaching the desired site of action, e.g. the inflamed region of the hair follicle in patients suffering from AA or LPP in a more direct and efficient manner, presents itself as being extremely difficult as normal formulations like creams gels do not penetrate well into the hair shaft.

One way to minimize the risk of developing the above mentioned adverse events would be to limit dermal permeation as well as limiting the exposure of the skin to high drug concentrations. In literature it has been shown that polymeric nanoparticles (NPs) are able to serve as a controlled drug release system [100-106]. Hence, a sustained drug release and the resulting avoidance of a burst effect would protect the epidermal epithelial regenerative cells from the sudden encounter of high drug concentrations, resulting in a reduced risk of developing local cutaneous atrophy and enhanced regeneration. Furthermore, Lademann *et al.* described that poly(lactic-co-glycolic acid) NPs accumulate in porcine HFs, and in that sense may serve as a drug delivery system to target this annex [184]. They also demonstrated a so-called `depot effect´ of these particles in the HF for up to 10 days, while the particles located in the SC were detectable for 24 hours. Consequently, besides the above mentioned specific scalp diseases, typical high-prevalence inflammatory skin disorders, e.g. eczema, or psoriasis vulgaris, could also benefit from a NP-based glucocorticoid therapy by achieving an

accumulation of particles in the hair shaft of vellus and/or terminal HFs, and simultaneously penetrating into upper epidermal layers, where they exhibit a steady release of drug over time.

Due to the above mentioned arguments, it is hypothesized that a NP-based sustained-release formulation for CP, a very potent glucocorticosteroid, that decreased skin permeation and facilitates follicular targeting is a new and improved strategy to reach the desired site of action for the above mentioned conditions in a more efficient and direct way. It is believed that it could decrease, or even diminish, those described side effects due to release kinetics and decreased permeation, and potentially increase patient compliance in the future. Hence, in this chapter, three different types of polymeric NPs (nanospheres (NS), nanocapsules (NC), lipid-core nanocapsules (LNC)) were prepared and characterized. The particles were formulated either as an aqueous suspension or as Carbopol® hydrogel (HG). Targeted delivery to the HF of the different types of NPs and formulations was quantified to determine differences in the extent of follicular uptake between the particles and/or formulations. Furthermore, the influence of massage on follicular uptake was evaluated. Lastly, experiments with excised human skin were performed to evaluate skin permeation under conditions where follicular uptake is considered to be minimal [185].

2.3.3. Materials and Methods

2.3.3.1. Materials

Poly(-ε-caprolactone), Clobetasol propionate, Caprylic/capric triglyceride mixture, Polysorbate 80, Polyethylene glycol 5400, and sorbitan monostearate were purchased from Sigma-Aldrich (St. Louis, MO, USA. Dialysis bags (Spectra Por 7, 10 Kd, Spectrum Laboratories, USA) were purchased from Bioagency (SaoPaulo, Brazil) and acetone from Nuclear (Sao Paulo, Brazil). Carbopol® Ultrez 10 was purchased from Ginama (Valencia, Spain). Human skin was kindly donated by the Hospital 9 de Octubre, Valencia, Spain, and Caritaskrankenhaus, Lebach, Germany, after previous signed consent of patients. Pig ears were obtained from Emil Faerber GmbH & Co. KG Zweibrücken (Zweibruecken, Germany). Methanol, acetonitrile and ethanol solvents were of HPLC quality and purchased by Scharlau (Barcelona, Spain). HPLC water was obtained by MilliQ-purification.

2.3.3.2. Preparation of Different Nanoparticles in Suspension and Hydrogel

Drug-free and CP-loaded NS, NC, and LNC were prepared using the nanoprecipitation-solvent evaporation technique, previously described by Fessi *et al.* [186], which has been successfully applied

to poly(-Ɛ-caprolactone) (PCL) [15, 103, 104]. This polymer was chosen because it is biodegradable and has previously been approved by the Food and Drug Administration (FDA) for drug delivery specific purposes [187]. The NS represent a matricial system, meaning that the drug is physically and uniformly dispersed in the polymer matrix (Figure 25a). The NC and LNC are representative vesicular systems, which consist of a polymer shell and an inner core (here consisting of a liquid or an organogel, respectively) in which the drug is dissolved (Figure 25b-c).
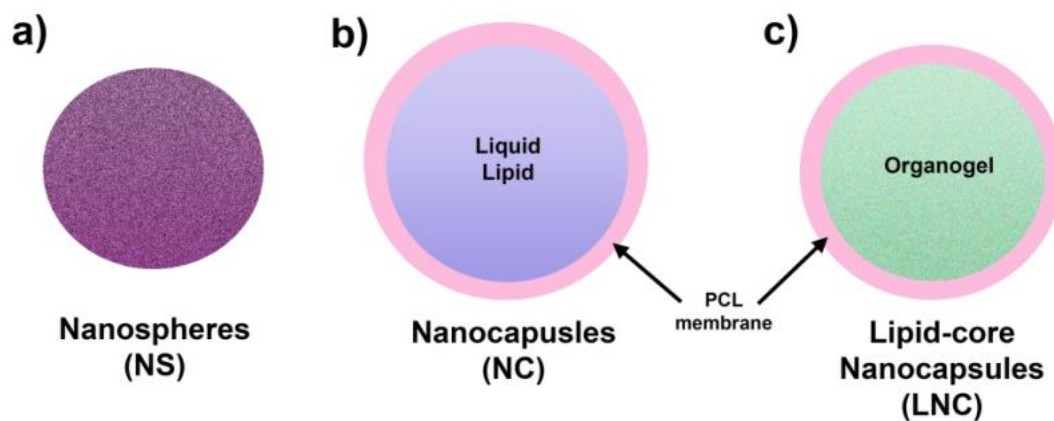
Figure 25: Depiction of the three different types of nanoparticles prepared. a) shows the nanospheres (NS), which give rise to a matrix system, b) nanocapsules (NC), and c) lipid-core nanocapsules (LNC). The latter two consist of a core-and-shell structure.

For the preparation of NS, sorbitan monostearate was dissolved in the organic phase along with the polymer. NC contained PCL as the polymeric shell and capric/caprylic triglycerides (CCT) as a liquid lipid core, and the LNC consisted of PCL as the polymeric shell, and CCT plus the lipophilic surfactant sorbitan monostearate dispersed in the core, forming an organogel [188]. Exact concentrations of all components for the three nanocarriers are given in Table 2.

The LNC suspensions were prepared by dissolving PCL (unlabeled and/or Rhodamin-B labeled as has previously been described by Poletto et. al [189]), sorbitan monostearate, and CCT (plus CP in the case of the drug-loaded particles) in acetone. This organic solution was injected at a stable, continuous speed into the aqueous phase, containing polysorbate 80, under moderate stirring. NS were prepared in the same manner minus the addition of the oil phase (medium chain triglycerides), and for the preparation of NC, no sorbitan monostearate was added. Acetone was removed using a rotational evaporator, and the formulation was concentrated to reach a final volume of 10 ml at 40ºC under reduced pressure. As a control, free CP in water/ethanol (50:50) was prepared. All formulations were made in triplicates and stored at room temperature (25º C) in amber glass flasks in order to protect the fluorescently-labeled polymer from light degradation.

Table 2: Concentrations of components of nanospheres (NS), nanocapsules (NC), and lipid-core nanocapsules (LNC) in aqueous suspension

	Type of Particle	PCL unlabeled (mg/ml)	PCL labeled (mg/ml)	SM (mg/ml)	CCT (mg/ml)	Polysorbate 80(mg/ml)	CP (mg/ml)
10% labeled PCL, CP-loaded	NS	9	1	3.8	-	7.7	0.5
	NC	9	1	-	16.0	7.7	0.5
	LNC	9	1	3.8	16.0	7.7	0.5
100% labeled PCL, drug-free	NS	-	10	3.8	-	7.7	-
	NC	-	10	-	16.0	7.7	-
	LNC	-	10	3.8	16.0	7.7	-
100% unlabeled PCL, CP-loaded	NC	10	-	-	16.0	7.7	0.5
100% labeled PCL, CP-loaded	NC	-	10	-	16.0	7.7	0.5

PCL, poly(ε-caprolactone); SM, sorbitan monostearate; CCT, capric/caprylic triglyceride; CP, clobetasol propionate

The hydrogel (HG) preparation was done by dispersing Carbopol® Ultrez 10 NF at 0.5 % into the various NP suspensions (drug-free and drug-loaded NS, NC and LNC). The formulations were mixed thoroughly for 5 min to guarantee complete dispersion. To obtain a suitable semisolid formulation for dermal application, triethanolamine (0.2 %; w/w) was added for neutralization purposes. For each type of NP, a corresponding HG was produced as well containing drug-free particles in order to assure that no changes in particle size and polydispersity are brought about via the encapsulation process of drug. Additionally, a control HG containing non-encapsulated/free CP, dissolved in water/ethanol (50:50), was prepared. All HG were prepared in triplicate, protected from light, and stored at room temperature (25°C).

2.3.3.3. Particle Characterization

Size & ζ-potential

For size, polydispersity and ζ-potential measurements of the three types of NPs, a Zetasizer Nanoseries (Malvern Instruments, Worcestershire, UK) was used. The NP suspension-samples and HG-samples were diluted 1:500 in aqua dest. for dynamic light scattering (DLS) analysis to measure size and the polydispersity index (PDI), and 1:500 in 10 mM NaCl for computing the ζ-potential. Of each formulation, three replicates were measured at room temperature. Results are given as mean ± standard deviation (SD).

Morphology Study

Morphology of all three types of particles was analyzed using scanning electron microscopy (SEM) and transmission electron microscopy (TEM).

SEM was only possible after a 20.000-fold dilution of the suspension, due to a thick film covering the particles, most likely a result of excess polysorbate 80. For the preparation, 10 µl of the diluted NP suspensions were added onto supports with carbon-glue, and coated with gold under an argon atmosphere using a gold sputter module in a high-vacuum evaporator. Samples were then measured at a magnification of 30 k for NS, and 25 k for NC and LNC. The SEM instrument used was an EVO LS, Carl Zeiss AG, Oberkochen, Germany.

Transmission electron microscopy (TEM) images were taken on a transmission electron microscope (TEM, JEOL JEM-2011; Jeol GmbH, Munich, Germany; available at the Experimental Physics Department, Saarbrücken, Germany), using a voltage of 200 kV at a magnification of 20 k. The NP suspensions were first diluted 1:100 in aqua dest., 10 µl were added onto the carbon coated grid and left to dry for 2-3 min. Excess of water was removed from the grid using a piece of filter paper. After 3-5 min, the deposited sample was negatively stained by addition of 10 µl of a 1% phosphotungstic acid solution. After 3-5 min, excess of liquid was removed again using a piece of filter paper and the samples were allowed to air dry before measuring.

2.3.3.4. Drug Content and Encapsulation Efficiency

In order to assure that no drug loss occurred during the production of the NP suspensions, CP content of all three particle suspensions was analyzed following a slightly modified version of the method described by Fontana *et al.* [190]. Hence, 1 ml of each suspension, or 1 mg of each HG, was dissolved in 25 ml acetonitrile (ACN) (instead of methanol), and the mixture was sonicated for 20 min. Samples were analyzed by means of HPLC. Moreover, the encapsulation efficiency of the samples was determined. For that the samples were centrifuged (Ultrafree-MC 10,000 MW, Millipore) at 12,000 rpm for a period of 5 min, and the ultrafiltrate was quantified for CP. To determine CP content in the particles, the difference between the total drug and the ultrafiltrate concentration was calculated. The encapsulation efficiency (EE %) was then calculated by dividing the drug entrapped by the total drug content. All measurements were made in triplicate, and samples were analyzed by means of HPLC. For the analysis a Kromasil® RP-18 column (5 µm particle size, 100 Å pore size, 150 x 4.6 mm) was used as the stationary phase and ACN:H_2O (65:35 v/v) as the corresponding mobile phase with a flow rate of 1 ml/min. UV detection was set at 240 nm with a column temperature of 30°C, and an injection volume of 20 µl.

2.3.3.5. Stability Study

To assure stability of the formulations over a period of time, suspensions in water (0.5 g/ml CP) were stored for 3 months after preparation and monitored in terms of particle size, PDI, ζ-potential, and pH. The samples were stored in amber glass flasks, protected from light, at room temperature.

2.3.3.6. Drug Release Study

For the determination of CP release from the three different particles, experiments were performed by means of the dialysis bag method using water/polysorbate 80/PEG 400 (60:0.5:40 v/v) as the receptor medium [191]. This receptor medium was chosen for comparison purposes due to previously published release data, in which the same particles loaded with a different drug were used [190]. The components polysorbate 80 and PEG 400, at the concentrations stated above, were added in order to assure sink conditions during the experiment [102]. Stability of CP in the above described release medium was previously evaluated using HPLC, and no degradation of CP was observed for up to 72 hours (data not shown). In short, 1 ml (0.5 mg/ml CP) of each NP suspension was pipetted into a dialysis bag (Spectra Por 7, 10 Kd). This dialysis membrane (molecular weight cut off: 10,000 Dalton) was chosen because it is only permeable to free CP, but not to the NPs. Hence, only free drug that has been released from the particles and permeated into the receptor medium will be quantified. The bag filled with sample was then placed into a 250 ml Erlenmeyer flask containing 200 ml of the previously mentioned receptor medium. 1 ml samples of this medium were withdrawn after 2, 4, 6, 8, 24, 30, 48, 54, and 72 hours and immediately replaced by fresh medium. The CP concentration of each sample was determined via HPLC using the same method as described above [190]. As a control, 0.5 mg/ml CP dissolved in an ethanolic solution was prepared and tested accordingly.

2.3.3.7. Follicular uptake studies

The extent of follicular uptake for each type of particle (NS, NC, and LNC in suspension and in HG) was analyzed and assessed quantitatively on porcine ear skin based on the differential stripping (DS) method [118]. As a control, free drug in solution and free drug in HG were tested, too, in order to determine whether CP delivery to the HF is in fact enhanced by means of encapsulation.

Differential Stripping Method

The differential stripping (DS) method is the most straightforward technique to determine follicular uptake quantitatively, as has recently been described by Raber *et al*. [86]. Since it has already been introduced in Chapter 1, it is only described here shortly.The formulation is first applied onto a predetermined area on the skin, followed by an optional 3 min massage, depending on the desired

experimental setup. The massage is performed using a gloved forefinger and massaging in a circular motion (60 rpm) for 3 min with applied pressure (~2 N). To minimize deviation, all DS experiments were done by one well-trained person. After 1 hour incubation, 10 subsequent tape strips (Tesa® adhesive tape) are taken to clean the skin surface by removing the SC layer by layer, followed by 2 cyanoacrylate skin surface biopsies which enable the removal of the entire follicular content [192]. All tape strips and cyanoacrylate biopsies were pressed onto the skin using a roller to stretch the skin surface and guarantee reaching the skins wrinkles and furrows [193]. For quantification and mass-balance purposes, all tape strips and cyanoacrylate biopsies, along with all used application devices and skin rest, were extracted in ACN, centrifuged at 20°C using 12.000 rpm for five minutes, and analyzed for fluorescence (Rhodamin-B labeled PCL) or CP content (see Section: Quantification Methods for Follicular Uptake Studies for specifics on analytic).

Follicular Uptake of Drug-free Particles

Preliminary follicular uptake studies of drug-free NS, NC, and LNC were performed in order to determine whether the type of nanocarrier and their differeing molecular architecture affect the uptake into the HF. Quantification of these drug-free particles was possible via fluorescence measurements, as Rhodamin-B labeled PCL was used for the preparation. Previous experiments had demonstrated that the amount of labeled PLC in the HF was below the detection limit when NPs were prepared using only 10% of the Rhodamin-B labeled PCL and 90% unlabeled (as was used for skin permeation experiments below), therefore all nanocarriers used for follicular penetration studies that were quantified via fluorescence were prepared using 100% labeled PCL. The composition of all particles is given in Table 2. Besides determining the influence of the type of particle and type of formulation on follicular penetration, the influence of a 3 min massage was evaluated as well. Each formulation was tested on two separate pig ears, each ear containing three areas of formulation, and one blank. n=6 for each.

Follicular Uptake of Clobetasol-loaded Nanocapsules

After these preliminary experiments using drug-free particles, NC in suspension were chosen as the best formulation for obtaining the highest follicular uptake. To evaluate delivery of encapsulated CP to the HF, this formulation loaded with 0.5 mg/ml CP was then tested using the DS method (including a 3 min massage) and follicular uptake was quantified based on CP content using LC-MS, rather than the fluorescently labeled polymer. n=6.

Follicular Uptake of Clobetasol and Polymer Simultaneously

To investigate whether changes in size influence the extent of follicular uptake, smaller CP-loaded NCs were prepared by increasing the stirring speed during the addition of the organic phase into the aqueous phase. As we were interested in co-tracking drug and polymer simultaneously, the CP-loaded particles were prepared using 100% Rhodamin-B labeled polymer. Follicular uptake was quantified based on drug content and labeled polymer for the same sample set. n=6.

Follicular Uptake of Free Clobetasol in Solution and Hydrogel

For control experiments free CP in an ethanolic solution (0.5 mg/ml) and free CP in HG (0.5 mg/g) were applied onto porcine ear skin and follicular uptake was evaluated. n=6.

Quantification Methods for Follicular Uptake Studies

Fluorescence

All fluorescence measurements were performed using a Cytofluor II fluorescence plate reader (λexc = 560 nm, λem = 662 nm) [189]. The lower limit of quantification (LLOQ), important for determining the analytical limitations of the quantification method [86], was calculated based on the fluorescence of the blanks plus the background fluorescence of the different types of matrices (tape strips, application devices, cyanoacrylate biopsies). The LLOQ was previously determined for each type of matrix.

LC-MS

LC-MS analysis and quantification for follicular uptake of the CP-loaded NC was carried out using a TSQ Quantum Access Max (Thermo Fisher Scientific) tandem quadrupole mass spectrometer coupled to an Accela UHPLC system. The whole system consists of a quaternary mixing pump with a built-in solvent degassing system, thermostated autosampler and column oven. An Accucore RP-MS column (150 mm x 2.1 mm, 2.6 µm, Thermo Fisher Scientific, Waltham, MA, USA) was implemented, which was set at 30°C during the experimental run. The system was operated by the standard software Xcalibur. A method described by Nam *et al.* was used with slight modification [194]. The LC system was run isocratically for 5 minutes at 400 µl/min using acetonitrile + 0.1% formic acid and water + 0.1% formic acid (65:35). Heated-electrospray ionization (H-ESI) in positive mode was used. The optimized H-ESI conditions were: capillary voltage of 4500 V, vaporizer temperature of 500 °C, ion transfer tube temperature of 350 °C. Nitrogen was used as sheath and auxiliary gas, and the settings were of 40 and 5 (arbitrary units), respectively. Quantitation was performed operating in selective reaction monitoring (SRM) mode. Observed ions were as follows (values are given for mother ion [m/z]; collision energy [V]; product ion [m/z]; scan time [s]; scan width [m/z]: 467; 12; 355; 0.2; 0.02.

The method was previously validated over a concentration range of 3.0-200.0 ng/ml (samples were diluted prior to measuring accordingly) with a correlation coefficient of $r^2 = 0.9995$.

Recovery (%)

Total recovery (%) was calculated for each performed experiment using a mass-balance. Based on the guidelines of the Scientific Committee on Consumer Safety (SCCS) only data which fit the recovery limits of 85-115% were evaluated [195].

2.3.3.8. Skin Permeation Studies

The skin was obtained from the Hospital 9 de Octubre, Valencia, Spain, and from the Department of Plastic and Hand Surgery at the Caritaskrankenhause in Lebach, Germany, after written consent was obtained from the patients. The epidermis was separated from the dermis using the well-adapted method first described by Kligmann *et al.* in 1963 [196]. In short, a previously cut skin section (25 mm in diameter) is placed into 60°C aqua dest. for 90 sec to weaken epidermal-dermal junction. Next, the epidermis is carefully peeled off using two anatomical forceps and placed into PBS buffer until use. This study was approved by the ethical commission of Saarland, Germany (Aerztekammer des Saarlandes, 204/08).

The acceptor compartment of the Franz cells was filled with an ethanol/phosphate buffer solution mixture (50:50) to assure sink conditions, and placed into a preheated incubator at 32°C to maintain the physiologic temperature of the skin throughout the experiment. The previously heat-separated epidermis (HSE) was placed onto a Whatman® filter[6] with the SC facing upwards for additional support, and positioned on top of the acceptor compartment to separate it from the donor compartment (refer to Figure 6). After a 30 min acclimatization period, 1 ml of each nanoparticle suspensions (NS, NC, and LNC) or control were pipetted into the donor compartment of the cells. The gels (0.5 g), in contrast, were evenly spread onto the membrane surface to cover the complete diffusion area. Both compartments were held together using a clamp. In addition, the donor compartment was sealed off using Parafilm® to avoid evaporation of the ethanol in the receptor medium. Samples were taken from the receptor compartment after predetermined time intervals followed by an immediate replacement of the removed volume by fresh buffer. Subsequently the samples were analyzed by HPLC using the method described above and the cumulative amounts of CP permeated into the receptor compartment were calculated [190]. n≥6 for each formulation.

---

[6] Previous experiments had demonstrated that this filter membrane did not limit permeability of the substance (data not shown)

2.3.3.9. Statistical Analysis

Results are expressed as the arithmetic mean ± SD. Significant differences between formulations were investigated by means of one-way analysis of variance (ANOVA) and two-way ANOVA (using 95% confidence interval) for all follicular uptake data, and Student's t-test (two-sided, unpaired, with Welch's correction, $p < 0.5$) for determination of intra-individual variability of permeability data *in vitro*. All statistical analysis was done using the software SigmaPlot (version 12.5, from Systat Software, Inc., San Jose California USA).

2.3.4.　　Results and Discussion

2.3.4.1. Size Distribution and ζ-Potential

The sizes measured for the three different types of particles ranged between ~100 - 260 nm (see Table 3 for exact values). As previously mentioned, a smaller sized-set of CP-loaded NC particles (106 nm) was prepared to evaluate if size is a key factor in deciding the extent of follicular penetration.

Table 3: Size distribution, PDI values, and ζ-potential of nanospheres (NS), nanocapsules (NC), and lipid-core nanocapsules (LNC) in suspension using dynamic light scattering (DLS) analysis; mean ± standard deviation.

	Type of Particle	DLS (nm)	PDI	ζ-potential (mV)	CP Content (mg/ml)	Encapsulation Efficiency (%)
10% labeled PCL	NS	176 ± 07	0.12 ± 0.04	-12.17 ± 1.11	0.48 ± 0.02	98.46 ± 1.0
90% unlabeled PCL	NC	218 ± 02	0.18 ± 0.01	-10.38 ± 0.69	0.50 ± 0.01	98.25 ± 0.8
CP-loaded	LNC	222 ± 14	0.19 ± 0.06	-12.03 ± 1.12	0.51 ± 0.01	97.92 ± 0.3
	NS	128 ± 02	0.17 ± 0.02	-13.59 ± 0.73	-	-
100% labeled PCL drug-free	NC	257 ± 11	0.15 ± 0.01	-14.42 ± 1.09	-	-
	LNC	157 ± 04	0.14 ± 0.01	-13.29 ± 1.27	-	-
100% unlabeled PCL, CP-loaded	NC	221 ± 07	0.06 ± 0.03	-12.21± 0.73	0.50 ± 0.03	98.45 ± 0.4
100% labeled PCL CP-loaded	NC	106 ± 01	0.08 ± 0.01	-13.22 ± 0.34	0.51 ± 0.01	98.76 ± 0.7

PCL, poly(ε-caprolactone); CP, clobetasol propionate

NC and LNC gave rise to a generally larger size when compared to NS. This can be explained by the presence of the oil phase [197] leading to a core-and-shell structure for NC and LNC instead of a matrix system (NS). All suspensions had a PDI between 0.06 and 0.19 confirming a homogeneous size

distribution. The ζ-Potential of all three types of NPs was negative, ranging from -10.0 to -14.5 mV. This negative potential is most likely caused by the polymeric wall formed by poly(ε-caprolactone) [198]. The stability of the particles in suspension is, thus, a result of steric hindrance of the surfactant between the two phases preventing coalescence [199].

2.3.4.2. Drug Content & Encapsulation Efficiency

The CP content quantified was approximately 0.5 mg/ml for all three nanocarriers, showing that no drug was lost during the preparation step for NS, NC, or LNC. Moreover, the encapsulation efficiency (EE %) measured was close to 100%, regardless of the type of particle (for exact values please refer to Table 3). Hence, no significant differences regarding the ability to encapsulate the drug were observed between NS, NC, or LNC, although the preparation processes and components used were slightly different.

2.3.4.3. Morphology

Scanning electron microscopy (SEM) and transmission electron microscopic (TEM) analysis were feasible for all three types of particles (see Figure 26).
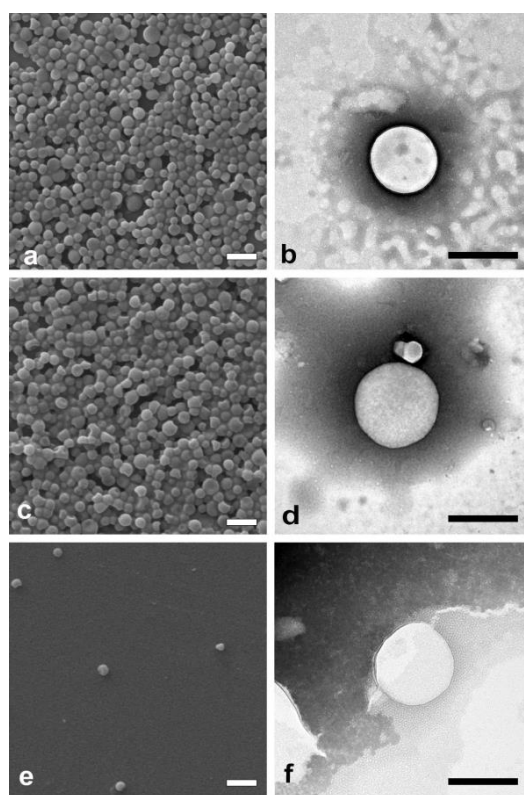
Figure 26: SEM images of NS (a), NC (c), and LNC (e) in suspension; TEM images of NS (b), NC (d), and LNC (f) in suspension. Scalebars in a, c, and e represent 400 nm and image was taken with 25 k magnification. Scalebars in b, d, and f represents 200 nm and image was taking using a voltage of 200 kV at a magnification of 20 k.

However, for LNC the imaging was more difficult, most likely due to the presence of the organogel. Both methods confirmed the expected morphology. All particles were spherical in shape, revealed a smooth surface, and a homogeneous size distribution. Figure 26 displays SEM (a,c,e) and TEM (b,d,f) images of all three particles (NS, NC, and LNC) in suspension, respectively.

2.3.4.4. Stability Study

Stability of the NPs in suspension was tested for a period of 3 months in terms of size, polydispersity, ζ-potential, and pH (see Table 4). After this period a slight increase in particle size was observed, most likely due to aggregation or agglomeration. However, this effect was minimal and negligible. The ζ-potential varied marginally over time with no general trend observed. The pH study demonstrated that the pH values obtained were suitable for application on the skin over the entire period of three months, as the pH stayed between pH 5.1 - 6.1. A slight reduction in pH was observed, but still remained adequate for topical application. This effect has previously been explained as a possible degradation of the polymer due to a release of free ϵ-hydroxycaproic, as well as a hydrolysis of the medium chain triglycerides, leading to an increase of free fatty acids [199]. Thus, all measurements confirmed that no noteworthy changes in size, polydispersity, ζ-potential, or pH occurred over time.

Table 4: Physiochemical characteristics of nanospheres (NS), nanocapsules (NC), and lipid-core nanocapsules (LNC) suspensions tracked for 3 months; mean ± SD (size measured using DLS analysis)

Type of Particle	Month	Size (nm)	PDI	ζ -Pot (mV)	pH
NS	0	158 ± 2	0.09 ± 0.02	-14.40 ± 1.75	6.12 ± 0.23
NS	1	169 ± 1	0.12 ± 0.03	-11.90 ± 1.59	5.86 ± 0.13
NS	2	167 ± 9	0.14 ± 0.05	-11.47 ± 1.84	5.53 ± 0.26
NS	3	173 ± 7	0.14 ± 0.03	-13.49 ± 1.09	5.50 ± 0.14
NC	0	195 ± 4	0.08 ± 0.02	-12.10 ± 1.93	5.99 ± 0.23
NC	1	218 ± 3	0.16 ± 0.02	-10.30 ± 1.71	5.92 ± 0.19
NC	2	208 ± 4	0.13 ± 0.03	-13.63 ± 0.65	5.42 ± 0.12
NC	3	223 ± 10	0.14 ± 0.04	-13.39 ± 2.57	5.25 ± 0.13
LNC	0	193 ± 3	0.08 ± 0.04	-10.60 ± 3.43	6.11 ± 0.21
LNC	1	217 ± 3	0.15 ± 0.03	-12.46 ± 2.52	5.90 ± 0.11
LNC	2	209 ± 3	0.16 ± 0.02	-14.31 ± 1.91	5.92 ± 0.19
LNC	3	216 ± 10	0.16 ± 0.04	-12.11 ± 1.64	5.11 ± 0.10

PDI, polydispersity index ζ –Pot, zeta potential

2.3.4.5. Hydrogel Characterization

A summary of the hydrogel characterization is given in Table 5. The pH values of the Carbopol® HG measured were between 5.6 and 6.7, yielding a suitable pH for topical administration of semisolid formulations [200].

Table 5: Hydrogel (HG) Characterization; mean ± SD.

	Type of Particle	pH	Size (nm)	CP content (mg/g)
10% labeled PCL CP-loaded	NS-HG	5.61 ± 0.22	183 ± 17	0.51 ± 0.01
	NC-HG	6.05 ± 0.11	219 ± 15	0.51 ± 0.01
	LNC-HG	5.90 ± 0.12	230 ± 18	0.52 ± 0.03
	CP-HG	5.87 ± 0.18	-	-
100% labeled drug-free	NS-HG	5.92 ± 0.31	185 ± 2.05	-
	NC-HG	6.73 ± 0.57	206 ± 2.61	-
	LNC-HG	6.03 ± 0.42	143 ± 1.11	-

NS, nanospheres, NC, nanocapsules, LNC, lipid-core nanocapsules, CP, Clobetasol propionate, PCL, poly(ε-caprolactone)

The presence of the drug did not alter the pH of the HGs for any of the formulations ($p > 0.05$ for each formulation). The sizes of the particles in the HGs were still in the same range as the original suspensions, and drug content remained close to the desired CP concentration of 0.5 mg/g for all formulations.

2.3.4.6. Drug Release Study

To determine whether the encapsulation process results in a sustained release of drug, the dialysis bag method was applied. Figure 27 depicts the release profiles of the three different NPs in suspension (NS, NC, LNC) vs. free drug in an ethanolic solution as a control. As can clearly be seen in Figure 27, no significant differences were observed between the release profiles of the three nanocarriers NS, NC, or LNC ($p > 0.05$). However, as was anticipated, all three CP-loaded particles revealed a sustained release of the drug, as after 24 h only approximately 50% of the encapsulated drug was released for all three carriers. Even at the end of a 72 h period, the mean amount of released drug still remained below 80%. Free drug, in contrast, revealed a fast release profile with ~80% of CP already being detected after only 5h.
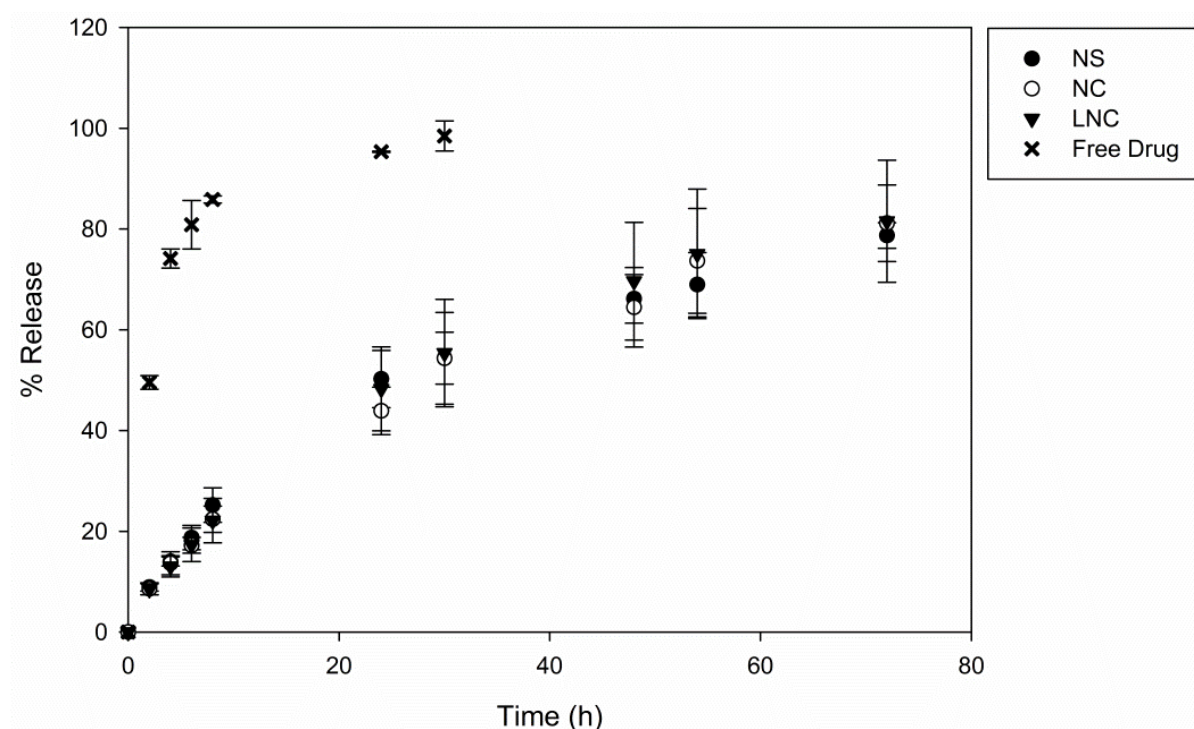
Figure 27: Release profiles of Clobetasol (CP) from nanoparticle formulations nanocapsules (NC), nanospheres (NS), lipid-core nanocapsules (LNC) compared to free drug (CP) (mean ± SD).

2.3.4.7. Follicular Uptake Studies

The detection limit of quantification for all three NPs in suspension was as low as 0.3-0.7%, and for the particles in HGs ≤ 0.2% of the total amount applied in all matrices (tape strips, cyanoacrylate biopsies, application devices, skin rest). Thus, the goal to detect < 1.0%, set due to previous results in follicular uptake studies [86], was achieved for all NPs in suspension, as well as in HG.

Follicular Uptake of Drug-Free Particles

Follicular uptake of the drug-free particles, with and without the application of a massage, is depicted in Figure 28. Figure 28a) displays the recovery (w/w %) in the HF of the total amount applied for the three types of drug-free nanocarriers (NS, NC, LNC; suspension vs. HG) when no massage was applied. For this specific experimental setup NC presented a significantly higher recovery in the HF for both formulations in comparison to NS and LNC (two-way ANOVA, $p < 0.05$) (also see Table 6 for exact values). However, no significant difference was observed between the two types of dosage forms.
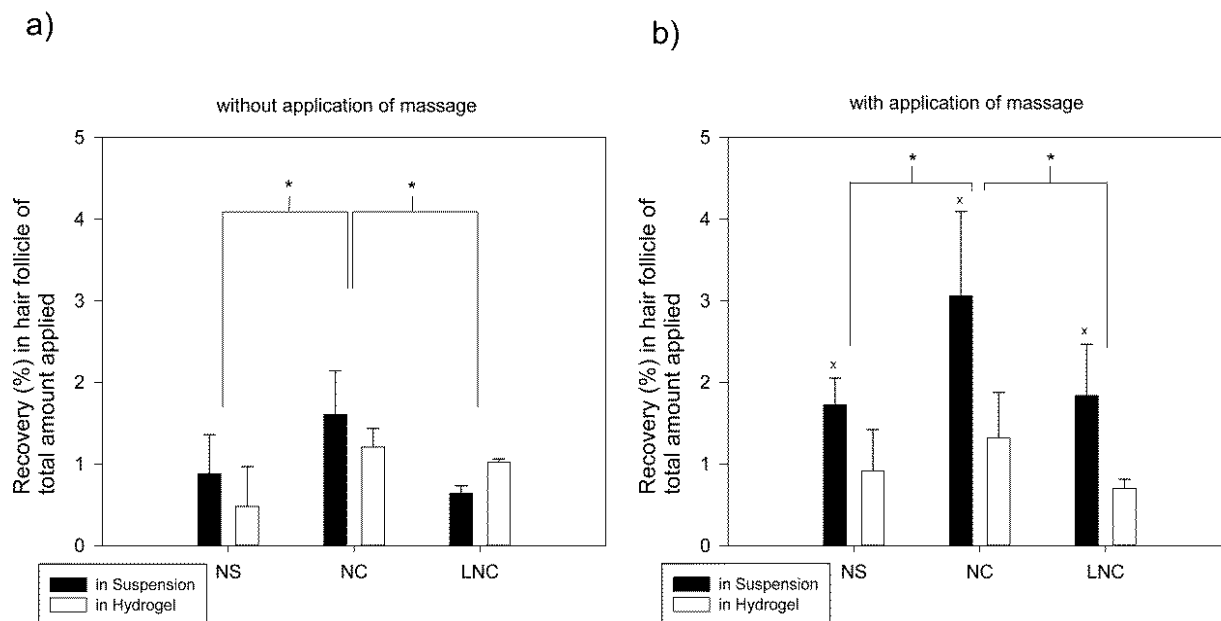
Figure 28: Recovery (%) in hair follicles of total amount applied of blank NS, NC, and LNC formulated as suspension and hydrogel without application of massage in a) and after application of massage depicted in b); * represents statistical significance between types of particles (NC vs. NS and NC vs. LNC), ˣ represents statistical significance between formulation (in suspension vs. in hydrogel)

Figure 28b) displays the results obtained for the follicular uptake experiments when a 3 min massage was performed before incubation. A similar trend with a generally higher recovery of the particles in the HF can be seen with the additional massage. Again, NC demonstrated a significantly higher follicular uptake when compared to NS and LNC (two-way ANOVA, $p < 0.05$) for both formulations. Moreover, the positive effect of a massage on follicular penetration, which was also observed in this study, has previously been discussed in literature by Lademann *et al.* [184]. In this work the authors hypothesize that the moving of the hair, which is an effect caused by the massage, acts like a so-called 'gear pump', resulting in an increased transport or translocation of the particles into the hair shaft. It therefore mimics the natural movement of the hair.

A reason for the higher accumulation of NCs as opposed to NS in the HF shaft could be related to the differences in their supramolecular organization. NCs represent a rather flexible core-and-shell structure, whereas NS give rise to a rigid matrix system. Differences in follicular penetration between the two core-and-shell systems, NC and LNC, could be attributed to the difference in the core viscosity and resulting flexibility. The NC core consists of mainly oil (medium chain triglycerides), resulting in a liquid lipid, whereas the LNC core additionally contains the lipophilic surfactant sorbitan monostearate. This surfactant, in presence of the oil, acts like a low molecular mass organic gelator, resulting in the formation of an organogel [198, 201, 202] (see Figure 25 for schematic depiction of particles). In a previous study using almost equivalent NC and LNC particles (only differing in the drug encapsulated), it was shown that the LNC, comprising this organogel core, exhibited a stiffness

(based on the calculated Young's modulus MPa) almost twice as high as was measured for the NC using atomic force microscopy (AFM) [198]. Thus, it can be speculated that a higher follicular penetration may be achieved by using more flexible particles. Regarding the dosage form, the particles formulated in a HG resulted in an overall statistically significant lower uptake in comparison to particles formulated in a suspension regardless of the application of massage (two-way ANOVA, $p<0.05$). This could be related to viscosity differences which may lead to difficulties of the NPs leaving the more viscous matrix during the incubation time.

Table 6: Recovery in hair follicle (w/w%) of total amount applied for different types of particles with and without application of massage as well as controls (CP in solution vs. CP in hydrogel); mean ± standard deviation.

Particle Information		Recovery (%) in hair follicle without massage		Recovery (%) in hair follicle with massage	
		Aqueous Suspension	Hydrogel	Aqueous Suspension	Hydrogel
NS	drug free	0.88 ± 0.48	0.48 ± 0.49	1.73 ± 0.33 [x]	0.91 ± 0.51
NC	drug free	1.61 ± 0.54*	1.21 ± 0.23*	3.06 ± 1.03 [x,*]	1.32 ± 0.56*
LNC	drug free	0.64 ± 0.09	1.02 ± 0.04	1.84 ± 0.63 [x]	0.70 ± 0.11
		Recovery (%) in hair follicle without massage		Recovery (%) in hair follicle with massage	
CP in ethanolic solution		< LLOQ		< LLOQ	
CP in hydrogel		< LLOQ		< LLOQ	

*represents statistically significant difference between types of particles (NC vs. NS and NC vs. LNC) $p<0.05$
x represents statistical significant difference between formulation (in suspension vs. in hydrogel) $p<0.05$

Follicular Uptake of Clobetasol-loaded Nanocapsules, and Free Clobetasol in Solution and Hydrogel

To confirm that the amount of polymer which we have quantified in the HF is also representative of the amount of encapsulated drug reaching the desired site of action, we compared the uptake of similarly sized drug-free NC and drug-loaded NC in suspension via fluorescence and LC-MS, respectively. A very good correlation was observed for the detected amount of polymer and drug, as can be seen in Table 7 (3.06 ± 1.03 % vs. 3.29 ± 0.53 % recovery in HF of total amount applied). Also, the smaller NC with an average size of 106 nm were taken up similarly as the original NC of size 257 nm (2.98 ± 0.65 % and 3.09 ± 0.17 % vs. 3.06 ± 1.06 %). Lastly, no significant difference in the amount detected was observed when comparing the two quantitation methods (fluorescence vs. LC-MS) for the same sample set of the smaller NCs ($p>0.05$).

Table 7: Type of formulation and recovery (w/w %) in hair follicle of total amount applied for differently formulated and quantified nanocapsules (NC) in suspension; mean ± SD.

Type	PCL	Size (nm)	Quantification Method	Recovery (%) in hair follicle of total amount applied
drug-free NC	100% labeled	257	Fluorescence	3.06 ± 1.03
CP-loaded NC	100% unlabeled	221	LC-MS	3.29 ± 0.53
CP-loaded NC	100% labeled	106	Fluorescence	2.98 ± 0.65
			LC-MS	3.09 ± 0.17

CP, Clobetasol propionate

*represents statistically significant difference between types of particles (NC vs. NS and NC vs. LNC NC vs. controls) p<0.05

x represents statistical significant difference between formulation (in suspension vs. in hydrogel) p<0.05

Although a size-dependent effect in the extent of follicular penetration was expected due to previous studies by other groups [84], the small range in particle size (106 - 257 nm) investigated in this study may be the reason that this effect was not observed. To investigate this topic further, a larger range in particle size, e.g. ~100 nm – 2 μm, should be tested in the future.

As for the controls, follicular recovery (%) of the total amount applied of free CP in solution and free CP in HG, with and without the application of massage, was below the lower limit of quantification (LLOQ) and thus negligible [86, 184, 203]. This confirms that by means of encapsulation a more targeted delivery to the HF was achieved.

Recovery

Total mass balance was calculated for each above mentioned experiment, and the total recovery (w/w %) for all included formulations ranged between 86-110%, fitting well within the limits of recovery of 85-115% given by the SCCS [195].

Summarizing this section, follicular penetration studies revealed that all three types of nanocarriers are able to achieve a better and more targeted delivery to the HF when compared to free drug in solution or HG. It was demonstrated that the three types of nanocarriers exhibited different penetration behaviors, with NCs achieving the highest follicular recovery of up to 4% when applied as an aqueous suspension. This only further emphasizes the possible influence of molecular organization on the penetration into the HF. This uptake effect was even amplified after application of a massage, as was expected. One thing to consider regarding the potential of these particles from a clinical perspective is that all follicular uptake studies described herein were performed on the porcine ear skin model. As previously mentioned, *in vitro* follicular uptake experiments on excised human skin are not feasible, as

excision results in immediate contraction and closure of the HFs [185]. So even though an excellent correlation between pig ear tissue *in vitro* and human forearm skin *in vivo* has been established by our group regarding the penetration of nanoparticles into the HF [86], the amount of terminal HFs available for this kind of therapy on the average human scalp (site of action for most inflammatory-based hair disorders) is much higher than what is seen on porcine ear skin (124-200 hairs/cm^2 on human occipital scalp vs. 11-25 hairs/cm^2 on porcine ear skin) [109, 204, 205]. In that sense a substantially higher follicular recovery is to be expected *in vivo,* only further corroborating the potential of this form of application for hair disorders like AA, LPP, or FFA.

2.3.4.8. Skin Permeation Studies

As a substantial amount of formulation was shown to not penetrate into the HF, and we were interested in testing the ability to lower dermal permeation in general, Franz Diffusion cell studies were performed using HSE assuming that the follicular pathway is negligible [185, 206]. Figure 29 displays the resulting permeation profiles (exact amounts can be found in Table 8).
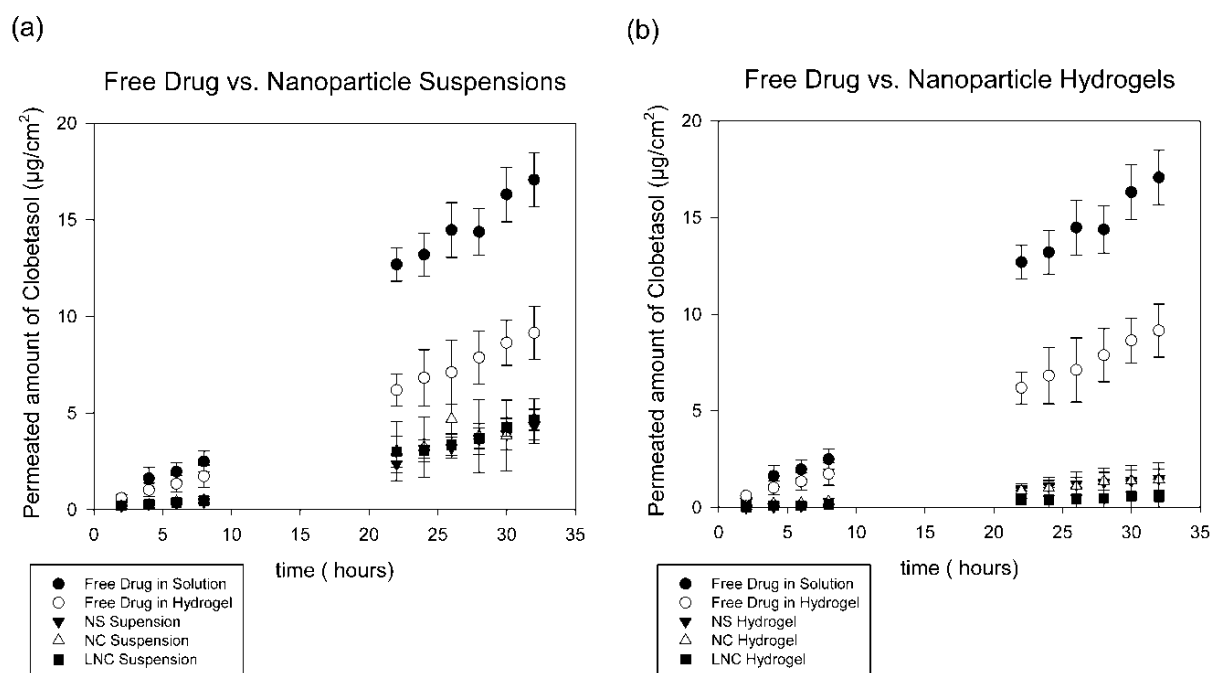
Figure 29: a) depicts permeability through HHSE of free Clobetasol (CP) in solution, free CP in Hydrogel, and CP encapsulated into three nanocarriers (nanospheres, NS; nanocapsules, NC; lipid-core nanocapsules, LNC) formulated as suspensions; b) shows permeability through HHSE of free CP in solution, free CP in Hydrogel, and CP encapsulated into NS, NC, and LNC formulated as Hydrogels (mean ± SD).

Figure 29a) depicts the permeated amount of free CP in solution and free CP in HG vs. permeated CP after being encapsulated into the three nanocarriers (NS, NC, LNC) and formulated as suspensions. Figure 29b) shows the same scenario, except here the nanocarriers are formulated as a HG as opposed to a suspension. In both, Figure 29a) and b), the incorporation of free CP into a HG results in a significantly less amount of permeated CP to about 50% with respect to free CP in solution, hence the rate of permeation is decreased ($p < 0.05$). Similarly, among the three nanocarriers a statistically significant lower cumulative amount was observed when the viscosity of the medium was increased, yielding a decreased permeation ($p < 0.05$). Nonetheless, between the three types of particles no significant differences were detected when they were formulated alike ($p > 0.05$). These results are in accordance with the previously discussed release profiles of CP from NS, NC, and LNC, in which also no differences was to be detected. Comparing the permeation profiles of the drug after it has been encapsulated into the particles and non-encapsulated CP in solution, however, a clear and significant decrease in dermal permeation was achieved by means of encapsulation, as was desired.

Table 8: Mean cumulative amounts of Clobetasol (CP) permeated ($\mu g/cm^2$) for nanospheres (NS), nanocapsules (NC), and lipid-core nanocapsules (LNC) in suspension as well as in hydrogel. Results presented as mean ± SD.

	Cumulative amount of Clobetasol permeated ($\mu g/cm^2$)							
Sample Time (hour)	Free Drug Solution	Free Drug Hydrogel	NS Suspension	NC Suspension	LNC Suspension	NS Hydrogel	NC Hydrogel	LNC Hydrogel
2	0.46 ± 0.03	0.60 ± 0.16	0.20 ± 0.01	0.17 ± 0.10	0.21 ± 0.05	0.00 ± 0.00	0.07 ± 0.03	0.00 ± 0.00
4	1.62 ± 0.56	1.02 ± 0.35	0.31 ± 0.03	0.25 ± 0.13	0.27 ± 0.06	0.03 ± 0.02	0.19 ± 0.09	0.01 ± 0.01
6	1.96 ± 0.48	1.34 ± 0.44	0.36 ± 0.02	0.42 ± 0.15	0.36 ± 0.07	0.08 ± 0.07	0.21 ± 0.08	0.03 ± 0.02
8	2.49 ± 0.53	1.73 ± 0.58	0.41 ± 0.07	0.49 ± 0.20	0.46 ± 0.10	-	0.29 ± 0.16	-
22	12.69 ± 0.87	6.19 ± 0.83	2.37 ± 0.47	3.03 ± 1.53	3.00 ± 0.80	0.94 ± 0.07	0.85 ± 0.38	-
24	13.20 ± 1.13	6.82 ± 1.46	3.14 ± 0.48	3.33 ± 1.57	3.06 ± 0.58	1.10 ± 0.06	1.00 ± 0.39	1.16 ± 0.26
26	14.48 ± 1.42	7.12 ± 1.66	3.20 ± 0.54	3.69 ± 0.77	3.37 ± 0.58	1.19 ± 0.14	1.09 ± 0.45	1.39 ± 0.32
28	14.38 ± 1.22	7.88 ± 1.38	3.66 ± 0.80	3.81 ± 1.90	3.69 ± 0.53	1.31 ± 0.06	1.35 ± 0.46	1.55 ± 0.35
30	16.32 ± 1.41	8.64 ± 1.17	3.90 ± 0.80	3.83 ± 1.83	4.28 ± 0.48	1.40 ± 0.05	1.36 ± 0.58	1.60 ± 0.32
32	17.07 ± 1.41	9.15 ± 1.37	4.33 ± 0.89	4.79 ± 1.07	4.66 ± 0.54	1.49 ± 0.04	1.43 ± 0.55	1.77 ± 0.41

One thing to keep in mind is that all results described in this study were done under *in vitro* conditions and may not be 100 % predictive of the *in vivo* situation, as results obtained under these conditions are known to generally overestimate the observed effect [207]. This is most likely due to the non-existing clearance *in vitro*, as well as the ongoing desquamation process in living tissue. Nonetheless, the general trend observed is indeed representative and to be expected under real-life conditions. Thus, the

observed decreased interfollicular permeation of CP that is achieved via encapsulating the drug into the various nanocarriers is beneficial in two ways. For one, less free drug is available to diffuse through the skin and enter the blood stream resulting in adverse events, and secondly the particles which to penetrate into the skin (or hair shaft) reside in the upper epidermal layers where they release the drug steadily over time.

2.3.4.9. Interplay of Follicular Uptake and Non-follicular Permeation

Modulating the interplay of non-follicular permeation and follicular uptake via the application of nanocarriers could be a new, revolutionizing strategy to treat many different skin and/or scalp diseases in the future. As was previously hypothesized, the data obtained from the follicular uptake and skin permeation studies confirmed that it is indeed possible, depending on the type of carrier and/or vehicle used, to vary the treatment based on the desired therapy. For example, one can maximize follicular uptake, and simultaneously decrease skin permeation and release of drug into the interfollicular epidermis, by using a carrier with the highest follicular delivery, decreased skin permeation, and a simultaneous sustained release effect, as in the case of the NC suspension. This could be revolutionizing for the treatment of various hair disorder therapies like AA, LPP, or scalp psoriasis, as well as more prevalent conditions like atopic dermatitis and psoriasis [95-97, 183].

2.3.5. Conclusion

In conclusion, the potent glucocorticosteroid CP could successfully be formulated into three different types of poly-Ɛ-caprolactone NPs. All particles exhibited a sustained release of drug over a period of 72 h, as was desired. Concerning targeted delivery to the HF, a reoccurring difference in the degree of follicular uptake between the various types of NPs could be detected, with NC displaying a significantly higher uptake when compared to NS and LNC, in suspension as well as in HG. A formulation-dependent trend was also observed, with a generally higher uptake for particles formulated as a suspension rather than a HG. This effect was even amplified by the application of a 3 min massage before incubation. Inter-follicular skin permeation was reduced in an equivalent manner for all three types of NPs. Thus, the information learned from this study about the possibility of modulating the interplay between follicular uptake and non-follicular skin permeation could be applied to provide a more patient-specific and desired therapy under optimized conditions in the future. For now, the information obtained from the present *in vitro* study is a good start for facilitating the translation of CP nanocarriers as a means to minimize adverse effects into clinical testing.

2.3.6.   Acknowledgement

The above mentioned article was accepted for publication after submission of this doctoral thesis.

3. General Conclusion & Discussion

The presented work illuminates the suitability and applicability of the porcine ear skin model for the testing of follicular tight junction (TJ) functionality and the evaluation of nanoparticle-based delivery systems via the hair follicle. Special emphasis was placed on the comparison and equivalency between the porcine and human hair follicle, as all obtained data *in vitro* and/or *ex vivo* should ideally help the investigators to gain insight on the *in vivo* situation. Furthermore, the combination of acquired knowledge about the suitability, along with predictions gained from the accumulated data *in vitro,* is crucial when considering the translation of follicular uptake experiments of any kind into clinical testing.

The determination of suitability and equivalency of the porcine ear skin model in comparison to human skin was one of the main aims of this work. Thus, as presented in the first section of this thesis, a chemically selective and non-destructive analysis of human and porcine hair follicles was performed using the novel technique confocal Raman microscopy. Based on the acquired Raman spectra, we could identify and differentiate between the four main components of the hair follicle (hair, epidermis, dermis and sebum) in both species, and conclude that their chemical compositions were nearly equivalent. Especially the sebum, which represents the release medium for substances taken up via the transfollicular pathway, showed no significant differences. Advantages of this methodology, as opposed to a normal staining procedure, regarding specificity and accuracy of component distribution, were also shown. Furthermore, confocal Raman microscopy in combination with optical profilometry revealed the intactness of individual hair follicles in excised cyanoacrylate skin surface biopsies on a three-dimensional level. This new acquired insight is of great importance because up to now the most common quantification method for determining follicular uptake (Differential Stripping Method) had only been based on the assumption that the entire follicular cast gets removed by means of cyanoacrylate biopsies; we were able to confirm this assumption.

The next section of this thesis focused on the identification and testing of potential barriers in the mammalian hair follicle. Consequently, expression and localization of follicular TJs, known to play a role in epidermal barrier properties, were looked at in the porcine ear skin model. In that sense, suitability of the applied porcine model was investigated again in this section and confirmed, as all examined TJ proteins in the porcine hair follicle were shown to be expressed and distributed similarly in both species by means of qPCR and immunostaining, respectively. Moreover, using an extracellular tracer molecule, the existence of a continuous barrier consisting of TJs was discovered throughout porcine hair follicles located in the outer root sheath (a continuation of the viable epidermis), and another TJ barrier in Huxley's layer of the inner root sheath; in contrast, the bulb was completely permeable. Finally, desired modification, i.e. opening, of this TJ barrier was feasible after administering the TJ modulator EDTA. This could be of relevance for the drug delivery of substances via the transfollicular pathway in the future. The last part of this section dealt with comparing the distribution of the existing barriers present in the hair follicle (the *stratum corneum* in the upper part of the hair follicle, e.g. infundibulum, and the TJ barrier in the outer root sheath) with the distribution of an externally applied model substance – here nanoparticles – in the hair shaft, and the penetration behavior of these types of particles. Thus, transmission electron microscopy was employed to, for one, confirm for the first time that polymeric particles do stay intact upon penetration. Furthermore, it was demonstrated that the majority of these particles accumulated in the infundibulum of porcine hair follicle, the region protected by both barriers, the *stratum corneum* and the TJs. Few intact particles were also discovered past this point in the central region of the hair follicle where TJs are likely the only barrier.

The last section of this work was mainly focused on the applicability of the porcine ear skin model with regard to follicular uptake studies. Three different polymer-based nanoparticles were prepared

and characterized, giving rise to three varying particle structures of differing sizes, yet equivalent surface charge, polydispersity, and encapsulation efficiency of drug. A desired sustained release of drug was achieved by means of encapsulation and this effect was similar for all three nanocarriers. Also, the possibility of decreasing skin permeation, and simultaneous targeting to the hair follicle, was shown. The reduction in skin permeation (as opposed to free drug in solution) was similar for the different particles and was only more reduced by increasing the viscosity of the formulation/release medium. The extent of follicular penetration, however, was dependent upon the molecular architecture of the particles, as well as on the viscosity of the formulation. For all particles, the application of a massage enhanced follicular uptake. The particles were all loaded with Clobetasol propionate, a very potent drug used for many inflammatory-based skin and hair disorders, but also known to cause severe adverse effects even when only applied topically. The information learned from this study could potentially help to minimize adverse effects by (i) releasing the drug in a time-dependent manner and thereby not reaching toxic concentration levels, (ii) by decreasing general skin permeability, plus (iii) via targeting the hair follicle as this type of therapy could revolutionize the disease management of several specific hair disorders (e.g. inflammatory-caused scalp diseases). Furthermore, selection of a specific nanocarrier and/or formulation could achieve a better delivery of the drug to the desired site of action, as well as a more patient-specific treatment.

Overall, this thesis has highlighted various important aspects concerning research in the field of sciences ranging from characterizing and evaluating potential *in vitro/ex vivo* models, to performing basic research that deals with the anatomy of the hair follicle and its barrier properties, and lastly the technological approach of preparing and testing novel drug delivery systems. Combining all of the information learned from the discussed studies, one can say that the porcine ear skin model is indeed

suitable to use as a surrogate for human skin regarding (i) the testing of tight junction distribution and functionality in the hair follicle, and (ii) experiments concerning the uptake and penetration depth of nanoparticle-based drug delivery systems. This confirmation is most useful for the field of pharmaceutical technology, as the necessity and demand for reliable models is a topic of general concern. In that sense, large data sets can be generated on the model and only the most promising candidates (e.g. for drug delivery systems) will advance to be tested *in vivo*. Moreover, the characterization of the tight junction proteins and their barrier function in the hair follicle adds to the information and insight which is already known about the very complex biology of the hair follicle. Whether these structures are in fact a deciding factor regarding nanoparticles uptake or nanoparticle translocation remains to be further elucidated. Hence, more studies with a wider variety of particles need to be performed. Moreover, the described follicular uptake studies using the nanocarriers loaded with the potent glucocorticosteroid Clobetasol propionate reveal that the nanoparticle-based drug delivery approach is very promising not only for the recently much discussed topic of non-invasive transfollicular vaccination [90, 92, 145, 146], but also for the field of dermatology, especially with regard to inflammatory-based scalp diseases.

4. Outlook

In the future, the penetration behavior of particles ranging in size (nano-micro), molecular architecture (core-and-shell particles, nanospheres, liposomes, solid lipid nanoparticles), and surface charge should be further assessed with the goal of i) obtaining a higher follicular recovery, and ii) gaining more insights on what parameters are deciding regarding the location in the hair follicle that is reached. For these studies, transmission electron microscopy (similarly to what was done here), fluorescence microscopy, and/or the Differential Stripping method *in vitro* as well as *in vivo* would be of aid.

Additionally, the ability to modulate follicular and/or epidermal TJs, which was shown to be feasible in this work, should be further optimized. Especially the use of more specific TJ modulators (e.g. Occludin mimetic peptides, Sodium caprate, Chitosan, Clostridium perfringens enterotoxin, etc.) should be tested to determine whether it is possible to regulate the opening and closing of this TJ barrier, as has been described for other epithelia before. Moreover, combining this TJ modulation with particle-based delivery to the hair follicle would be an intriguing approach. For example, in the field of non-invasive transfollicular vaccination the major challenges seen consist of delivering the antigen to the peri-follicular antigen presenting cells located mainly in the infundibulum of the hair follicle [145, 146, 203]. Thus, the possibilities of i) encapsulating a specific TJ modulator along with an antigen and adjuvant, or ii) co-administering a specific TJ modulator along with the encapsulated antigen and adjuvant should be further explored.

5.   List of Abbreviations

A	area of application
AA	Alopecia areata
ACN	acetonitrile
ANOVA	analysis of variance
AUC	area under the curve
Biotin-SH	EZ-Link^{TM}-Sulfo-NHS-LC-Biotin
C	cortex
CI	confidence interval
CL	companion cell layer
CCL	central cell layer
CCT	capric/caprylic triglycerides
Cldn	claudin
Ct	cycle threshold
Cu	cuticular layer of hair shaft
CP	clobetasol propionate
C_0	average initial concentration
D	apparent diffusion coefficient
DLS	dynamic light scattering
DS	Differential Stripping
DP	dermal papilla
DMEM	Dulbecco's Modified Eagle Medium
EDTA	Ethylenediaminetetraacetic acid
EE	encapsulation efficiency
FDA	Food and Drug Administration
FFA	Frontal, fibrosing alopecia
h	length of the apparent diffusion path
He	Henle's layer of the inner root sheath
He*	fully differentiated and highly keratinized cells in Henle's layer of the inner root sheath
H&E	haematoxylin & eosin
H-ESI	heated-electrospray ionization
HF	hair follicle
HG	hydrogel
HSE	heat-separated epidermis

Hu	Huxley's layer of the inner root sheath
icu	cuticle of the inner root sheath
IRS	inner root sheath
Jss	steady-state flux
K	vehicle/barrier partition coefficient
Kp	permeability coefficient
LNC	lipid-core nanocapsules
LLOQ	lower limit of quantification
LPP	Lichen planopilaris
M	medulla
MC	matrix cells
M(t)	accumulated mass of substance
NC	nanocapsules
NP	nanoparticle
NS	nanospheres
Ocln	occludin
OECD	Organization for Economic Co-Operation and Development
ORS	outer root sheath
PBS	phosphate buffered saline
PCL	poly(-ε-caprolactone)
PDI	polydispersity index
PLGA	Poly-D,L-lactide-co-glycolide
ROI	region of interest
SC	stratum corneum
SCCS	Scientific Committee on Consumer Safety
SD	standard deviation
SEM	scanning electron microscopy
SM	sorbitan monostearate
SRM	selective reaction monitoring
TER	transepithelial resistance
TEM	transmission electron microscopy
TJ	tight junction
ZO-1	zonula occludens protein 1

6. List of Figures

7.   List of Tables

References

[1] J.M. Baron, H.F. Merk, Drug metabolism in the skin, Curr Opin All Clin, 1 (2001) 287-291.

[2] K.A. Walters, M.S. Roberts, The structure and function of skin, Drugs and the pharmaceutical Sciences, 119 (2002) 1-40.

[3] J. McGrath, J. Uitto, Anatomy and organization of human skin, Rook's Textbook of Dermatology, 8, (2010) 1-53.

[4] P.M. Elias, E.R. Cooper, A. Korc, B.E. Brown, Percutaneous transport in relation to stratum corneum structure and lipid composition, J Invest Dermatol, 76 (1981) 297-301.

[5] S. Pfeiffer, G. Vielhaber, J.P. Vietzke, K.P. Wittern, U. Hintze, R. Wepf, High-pressure freezing provides new information on human epidermis: simultaneous protein antigen and lamellar lipid structure preservation. Study on human epidermis by cryoimmobilization, J Invest Dermatol, 114 (2000) 1030-1038.

[6] S.B. Hoath, D. Leahy, The organization of human epidermis: functional epidermal units and phi proportionality, J Invest Dermatol, 121 (2003) 1440-1446.

[7] R. Moll, I. Moll, W.W. Franke, Identification of Merkel cells in human skin by specific cytokeratin antibodies: Changes of cell density and distribution in fetal and adult plantar epidermis, Differentiation, Res Biol Div, 28 (1984) 136-154.

[8] A. Haake, G.A. Scott, K.A. Holbrook, Structure and function of the skin: overview of the epidermis and dermis, The biology of the skin, 2001 (2001) 19-45.

[9] R. Paus, G. Cotsarelis, The biology of hair follicles, New Eng J Med, 341 (1999) 491-497.

[10] M.H. Hardy, The secret life of the hair follicle, TIG, 8 (1992) 55-61.

[11] M.R. Schneider, R. Schmidt-Ullrich, R. Paus, The Hair Follicle as a Dynamic Miniorgan, Curr Biol, 19 (2009) 132-142.

[12] E. Kam, M. Hodgins, Communication compartments in hair follicles and their implication in differentiative control, Development, 114 (1992) 389-393.

[13] R. Lavker, A. Bertolino, I. Freedberg, T. Sun, Biology of hair follicles, Dermtaol in Gen Med, 1 (1999) 230-238.

[14] L.C. Sperling, S.E. Cowper, E.A. Knopp, An atlas of hair pathology with clinical correlations, CRC Press, 2012.

[15] D.V. Chebotaev, A.Y. Yemelyanov, R.M. Lavker, I.V. Budunova, Epithelial cells in the hair follicle bulge do not contribute to epidermal regeneration after glucocorticoid-induced cutaneous atrophy, J Invest Dermatol, 127 (2007) 2749-2758.

[16] K.L. Baquerizo Nole, R.S. Kirsner, Hair Follicles and Their Potential in Wound Healing, Exp Dermatol, (2014).

[17] I. Driskell, F. Oeztuerk-Winder, P. Humphreys, M. Frye, Genetically Induced Cell Death in Bulge Stem Cells Reveals Their Redundancy for Hair and Epidermal Regeneration, Stem cells, (2014).

[18] M.-S. Ma, M. Czepiel, T. Krause, K.-H. Schäfer, E. Boddeke, S. Copray, Generation of Induced Pluripotent Stem Cells from Hair Follicle Bulge Neural Crest Stem Cells, Cellular Reprogram, 16 (2014) 307-313.

[19] M. Ohyama, Hair follicle bulge: a fascinating reservoir of epithelial stem cells, J Dermatol Sci, 46 (2007) 81-89.

[20] M.R. Schneider, R. Paus, Deciphering the functions of the hair follicle infundibulum in skin physiology and disease, Cell Tissue Res, 358 (2014) 697-704.

[21] A.C. Gilliam, I.B. Kremer, Y. Yoshida, S.R. Stevens, E. Tootell, M.B.M. Teunissen, C. Hammerberg, K.D. Cooper, The human hair follicle: A reservoir of CD40(+) B7-deficient Langerhans cells that repopulate epidermis after UVB exposure, J Invest Dermatol 110 (1998) 422-427.

[22] R.B. Baleeiro, K.H. Wiesmuller, Y. Reiter, B. Baude, L. Dahne, A. Patzelt, J. Lademann, J.A. Barbuto, P. Walden, Topical vaccination with functionalized particles targeting dendritic cells, J Invest Dermatol, 133 (2013) 1933-1941.

[23] U. Blume-Peytavi, A. Vogt, Human hair follicle: reservoir function and selective targeting, British J Dermatol, 165 Suppl 2 (2011) 13-17.

[24] L. Langbein, M.A. Rogers, S. Praetzel, N. Aoki, H. Winter, J. Schweizer, A novel epithelial keratin, hK6irs1, is expressed differentially in all layers of the inner root sheath, including specialized huxley cells (Flugelzellen) of the human hair follicle, J Invest Dermatol, 118 (2002) 789-799.

[25] W. Montagna, The Structure and Function of Skin 3E, Elsevier, 2012.

[26] S. Aijaz, M.S. Balda, K. Matter, Tight junctions: molecular architecture and function, Int Rev Cytol, 248 (2006) 261-298.

REFERENCES

[27] M.A. Deli, Potential use of tight junction modulators to reversibly open membranous barriers and improve drug delivery, BBA-Biomembranes, 1788 (2009) 892-910.

[28] L. Paris, L. Tonutti, C. Vannini, G. Bazzoni, Structural organization of the tight junctions, Biochim Biophysica Acta, 1778 (2008) 646-659.

[29] M.G. Farquhar, G.E. Palade, Junctional complexes in various epithelia, J Cell Biol, 17 (1963) 375-412.

[30] J.M. Brandner, M. McIntyre, S. Kief, E. Wladykowski, I. Moll, Expression and localization of tight junction-associated proteins in human hair follicles, Arch Dermatol Res, 295 (2003) 211-221.

[31] C.M. Niessen, Tight junctions/adherens junctions: basic structure and function, J Invest Dermatol, 127 (2007) 2525-2532.

[32] D.R. Raleigh, A.M. Marchiando, Y. Zhang, L. Shen, H. Sasaki, Y. Wang, M. Long, J.R. Turner, Tight Junction–associated MARVEL Proteins MarvelD3, Tricellulin, and Occludin Have Distinct but Overlapping Functions, Molecular biology of the cell, 21 (2010) 1200-1213.

[33] V. Wong, B.M. Gumbiner, A synthetic peptide corresponding to the extracellular domain of occludin perturbs the tight junction permeability barrier, J Cell Biol, 136 (1997) 399-409.

[34] M. Furuse, T. Hirase, M. Itoh, A. Nagafuchi, S. Yonemura, S. Tsukita, S. Tsukita, Occludin: a novel integral membrane protein localizing at tight junctions, J Cell Biol, 123 (1993) 1777-1788.

[35] M.S. Balda, C. Flores-Maldonado, M. Cereijido, K. Matter, Multiple domains of occludin are involved in the regulation of paracellular permeability, J Cell Biochem, 78 (2000) 85-96.

[36] M. Saitou, M. Furuse, H. Sasaki, J.D. Schulzke, M. Fromm, H. Takano, T. Noda, S. Tsukita, Complex phenotype of mice lacking occludin, a component of tight junction strands, Mol Biol of Cell, 11 (2000) 4131-4142.

[37] J.D. Schulzke, A.H. Gitter, J. Mankertz, S. Spiegel, U. Seidler, S. Amasheh, M. Saitou, S. Tsukita, M. Fromm, Epithelial transport and barrier function in occludin-deficient mice, Biochim Biophys Acta, 1669 (2005) 34-42.

[38] J.M. Brandner, Tight junctions and tight junction proteins in mammalian epidermis, Eur J Biopharm Pharm, 72 (2009) 289-294.

[39] M.K. Findley, M. Koval, Regulation and roles for claudin-family tight junction proteins, IUBMB life, 61 (2009) 431-437.

[40] M. Furuse, K. Fujita, T. Hiiragi, K. Fujimoto, S. Tsukita, Claudin-1 and -2: novel integral membrane proteins localizing at tight junctions with no sequence similarity to occludin, J Cell Biol, 141 (1998) 1539-1550.

[41] D. Gunzel, A.S. Yu, Claudins and the modulation of tight junction permeability, Physiol Rev, 93 (2013) 525-569.

[42] C. Wray, Y. Mao, J. Pan, A. Chandrasena, F. Piasta, J.A. Frank, Claudin-4 augments alveolar epithelial barrier function and is induced in acute lung injury, Am J Physiol-Lung C, 297 (2009) L219-L227.

[43] N. Kirschner, P. Houdek, M. Fromm, I. Moll, J.M. Brandner, Tight junctions form a barrier in human epidermis, Eur J Cell Biol, 89 (2010) 839-842.

[44] S. Milatz, S.M. Krug, R. Rosenthal, D. Günzel, D. Müller, J.-D. Schulzke, S. Amasheh, M. Fromm, Claudin-3 acts as a sealing component of the tight junction for ions of either charge and uncharged solutes, Biochim Biophys Acta, 1798 (2010) 2048-2057.

[45] S.L. Kominsky, B. Tyler, J. Sosnowski, K. Brady, M. Doucet, D. Nell, J.G. Smedley, B. McClane, H. Brem, S. Sukumar, Clostridium perfringens enterotoxin as a novel-targeted therapeutic for brain metastasis, Cancer Res, 67 (2007) 7977-7982.

[46] Y. Matsuda, S. Semba, J. Ueda, T. Fuku, T. Hasuo, H. Chiba, N. Sawada, Y. Kuroda, H. Yokozaki, Gastric and intestinal claudin expression at the invasive front of gastric carcinoma, Cancer Sci, 98 (2007) 1014-1019.

[47] C.B. Coyne, T.M. Gambling, R.C. Boucher, J.L. Carson, L.G. Johnson, Role of claudin interactions in airway tight junctional permeability, Am J Physiol-Lung C, 285 (2003) L1166-L1178.

[48] M.N. Tatari, B. De Craene, B. Soen, J. Taminau, P. Vermassen, S. Goossens, K. Haigh, S. Cazzola, J. Lambert, D. Huylebroeck, J.J. Haigh, G. Berx, ZEB2-transgene expression in the epidermis compromises the integrity of the epidermal barrier through the repression of different tight junction proteins, Cell Mol Life Sci, 71 (2014) 3599-3609.

[49] L. González-Mariscal, R. Tapia, D. Chamorro, Crosstalk of tight junction components with signaling pathways, Biochim Biophys Acta, 1778 (2008) 729-756.

[50] L. Guillemot, S. Paschoud, P. Pulimeno, A. Foglia, S. Citi, The cytoplasmic plaque of tight junctions: a scaffolding and signalling center, Biochim Biophys Acta, 1778 (2008) 601-613.

[51] J.M. Anderson, C.M. Van Itallie, A.S. Fanning, Setting up a selective barrier at the apical junction complex, Curr Opin Cell Biol, 16 (2004) 140-145.

[52] K. Umeda, J. Ikenouchi, S. Katahira-Tayama, K. Furuse, H. Sasaki, M. Nakayama, T. Matsui, S. Tsukita, M. Furuse, S. Tsukita, ZO-1 and ZO-2 independently determine where claudins are polymerized in tight-junction strand formation, Cell, 126 (2006) 741-754.

[53] A.S. Breathnach, An atlas of the ultrastructure of human skin: development, differentiation, and post-natal features, Churchill Livingstone, 1971.

[54] P.M. Elias, D.S. Friend, The permeability barrier in mammalian epidermis, J Cell Biol, 65 (1975) 180-191.

[55] P.M. Elias, N.S. Mcnutt, D.S. Friend, Membrane alterations during cornification of mammalian squamous epithelia: A freeze-fracture, tracer, and thin-section study, The Anatomical Record, 189 (1977) 577-593.

[56] Y. Yoshida, K. Morita, A. Mizoguchi, C. Ide, Y. Miyachi, Altered expression of occludin and tight junction formation in psoriasis, Arch Dermatol Res, 293 (2001) 239-244.

[57] S. Tsukita, M. Furuse, Claudin-based barrier in simple and stratified cellular sheets, Curr Opin Cell Biol, 14 (2002) 531-536.

[58] M. Furuse, M. Hata, K. Furuse, Y. Yoshida, A. Haratake, Y. Sugitani, T. Noda, A. Kubo, S. Tsukita, Claudin-based tight junctions are crucial for the mammalian epidermal barrier: a lesson from claudin-1-deficient mice, J Cell Biol, 156 (2002) 1099-1111.

[59] Y.-h. Chen, C. Merzdorf, D.L. Paul, D.A. Goodenough, COOH terminus of occludin is required for tight junction barrier function in early Xenopus embryos, J Cell Biol, 138 (1997) 891-899.

[60] T. Yuki, H. Yoshida, Y. Akazawa, A. Komiya, Y. Sugiyama, S. Inoue, Activation of TLR2 enhances tight junction barrier in epidermal keratinocytes, J Immunol, 187 (2011) 3230-3237.

[61] S. Igawa, M. Kishibe, M. Murakami, M. Honma, H. Takahashi, H. Iizuka, A. Ishida-Yamamoto, Tight junctions in the stratum corneum explain spatial differences in corneodesmosome degradation, Exp Dermatol, 20 (2011) 53-57.

[62] M. Furuse, M. Hata, K. Furuse, Y. Yoshida, A. Haratake, Y. Sugitani, T. Noda, A. Kubo, S. Tsukita, Claudin-based tight junctions are crucial for the mammalian epidermal barrier: a lesson from claudin-1-deficient mice, J Cell Biol, 156 (2002) 1099-1111.

[63] T. Sugawara, N. Iwamoto, M. Akashi, T. Kojima, J. Hisatsune, M. Sugai, M. Furuse, Tight junction dysfunction in the stratum granulosum leads to aberrant stratum corneum barrier function in claudin-1-deficient mice, J Dermatol Sci, 70 (2013) 12-18.

[64] T. Yamamoto, Y. Saeki, M. Kurasawa, S. Kuroda, S. Arase, H. Sasaki, Effect of RNA interference of tight junction-related molecules on intercellular barrier function in cultured human keratinocytes, Arch Dermatol Res, 300 (2008) 517-524.

[65] G. Imokawa, Lipid abnormalities in atopic dermatitis, J Am Acad Dermatol, 45 (2001) S29-32.

[66] A. De Benedetto, N.M. Rafaels, L.Y. McGirt, A.I. Ivanov, S.N. Georas, C. Cheadle, A.E. Berger, K. Zhang, S. Vidyasagar, T. Yoshida, M. Boguniewicz, T. Hata, L.C. Schneider, J.M. Hanifin, R.L. Gallo, N. Novak, S. Weidinger, T.H. Beaty, D.Y. Leung, K.C. Barnes, L.A. Beck, Tight junction defects in patients with atopic dermatitis, J allerg Dermatol, 127 (2011) 773-786 e771-777.

[67] R. Gruber, J.L. Sugarman, D. Crumrine, M. Hupe, T.M. Mauro, E.A. Mauldin, J.P. Thyssen, J.M. Brandner, H.-C. Hennies, M. Schmuth, Sebaceous Gland, Hair Shaft, and Epidermal Barrier Abnormalities in Keratosis Pilaris with and without Filaggrin Deficiency, Am J Path, 185 (2015) 1012-1021.

[68] N. Kirschner, C. Poetzl, P.V. von den Driesch, E. Wladykowski, I. Moll, M.J. Behne, J.M. Brandner, Alteration of Tight Junction Proteins Is an Early Event in Psoriasis Putative Involvement of Proinflammatory Cytokines, Am J Path, 175 (2009) 1095-1106.

[69] M.R. Prausnitz, R. Langer, Transdermal drug delivery, Nature biotech, 26 (2008) 1261-1268.

[70] B.W. Barry, Novel mechanisms and devices to enable successful transdermal drug delivery, Eur J Pharm Sci, 14 (2001) 101-114.

[71] R.J. Scheuplein, Mechanism of percutaneous absorption. II. Transient diffusion and the relative importance of various routes of skin penetration, J Invest Dermatol, 48 (1967) 79-88.

[72] P. Talreja, N.K. Kleene, W.L. Pickens, T.F. Wang, G.B. Kasting, Visualization of the lipid barrier and measurement of lipid pathlength in human stratum corneum, AAPS pharmSci, 3 (2001) E13.

[73] P.J. Caspers, A.C. Williams, E.A. Carter, H.G. Edwards, B.W. Barry, H.A. Bruining, G.J. Puppels, Monitoring the penetration enhancer dimethyl sulfoxide in human stratum corneum in vivo by confocal Raman spectroscopy, Pharm Res, 19 (2002) 1577-1580.

[74] A.C. Williams, B.W. Barry, Penetration enhancers, Adv Drug Deliver Rev, 56 (2004) 603-618.

[75] S. Jessy, M. Shripad, S. Mansi, Transdermal penetration enhancers, Current Drug Therapy, 2 (2007) 133-142.

REFERENCES

[76] T.W. Prow, J.E. Grice, L.L. Lin, R. Faye, M. Butler, W. Becker, E.M.T. Wurm, C. Yoong, T.A. Robertson, H.P. Soyer, M.S. Roberts, Nanoparticles and microparticles for skin drug delivery, Adv Drug Deliver Rev, 63 (2011) 470-491.

[77] R. Alvarez-Román, A. Naik, Y. Kalia, R.H. Guy, H. Fessi, Skin penetration and distribution of polymeric nanoparticles, J Control Release, 99 (2004) 53-62.

[78] A.V. Zvyagin, X. Zhao, A. Gierden, W. Sanchez, J.A. Ross, M.S. Roberts, Imaging of zinc oxide nanoparticle penetration in human skin in vitro and in vivo, J Biomed Opt, 13 (2008).

[79] F. Rancan, A. Vogt, Getting under the skin: what is the potential of the transfollicular route in drug delivery?, Therapeutic delivery, 5 (2014) 875-877.

[80] B. Illel, H. Schaefer, J. Wepierre, O. Doucet, Follicles play an important role in percutaneous absorption, J Pharm Sci, 80 (1991) 424-427.

[81] N. Otberg, D. Grone, L. Meyer, S. Schanzer, G. Hoffmann, H. Ackermann, W. Sterry, J. Lademann, Water-filtered infrared-A (wIRA) can act as a penetration enhancer for topically applied substances, German medical science, 6 (2008) Doc08.

[82] A. Teichmann, N. Otberg, U. Jacobi, W. Sterry, J. Lademann, Follicular penetration: development of a method to block the follicles selectively against the penetration of topically applied substances, Skin Pharm PHys, 19 (2006) 216-223.

[83] J. Lademann, H. Richter, A. Teichmann, N. Otberg, U. Blume-Peytavi, J. Luengo, B. Weiss, U.F. Schaefer, C.M. Lehr, R. Wepf, W. Sterry, Nanoparticles--an efficient carrier for drug delivery into the hair follicles, Eur J Pharm Biopharm, 66 (2007) 159-164.

[84] A. Patzelt, H. Richter, F. Knorr, U. Schafer, C.M. Lehr, L. Dahne, W. Sterry, J. Lademann, Selective follicular targeting by modification of the particle sizes, J Control Release, 150 (2011) 45-48.

[85] A. Mittal, A.S. Raber, U.F. Schaefer, S. Weissmann, T. Ebensen, K. Schulze, C.A. Guzman, C.M. Lehr, S. Hansen, Non-invasive delivery of nanoparticles to hair follicles: A perspective for transcutaneous immunization, Vaccine, 31 (2013) 3442-3451.

[86] A.S. Raber, A. Mittal, J. Schafer, U. Bakowsky, J. Reichrath, T. Vogt, U.F. Schaefer, S. Hansen, C.M. Lehr, Quantification of nanoparticle uptake into hair follicles in pig ear and human forearm, J Control Release, 150 (2014).

[87] J. Lademann, H. Richter, U.F. Schaefer, U. Blume-Peytavi, A. Teichmann, N. Otberg, W. Sterry, Hair follicles - a long-term reservoir for drug delivery, Skin Pharm Phys, 19 (2006) 232-236.

[88] L. Mu, R.L. Sprando, Application of Nanotechnology in Cosmetics, Pharmaceut Res, 27 (2010) 1746-1749.

[89] A.A. Date, B. Naik, M.S. Nagarsenker, Novel drug delivery systems: Potential in improving topical delivery of antiacne agents, Skin Pharm Phys, 19 (2006) 2-16.

[90] S. Hansen, C.M. Lehr, Nanoparticles for transcutaneous vaccination, Microb Biotechnol, 5 (2012) 156-167.

[91] V.M. Meidan, M.C. Bonner, B.B. Michniak, Transfollicular drug delivery - Is it a reality?, Int J Biopharm, 306 (2005) 1-14.

[92] B. Combadiere, B. Mahe, Particle-based vaccines for transcutaneous vaccination, Comparative Immunology Microbiology and Infectious Diseases, 31 (2008) 293-315.

[93] J.G. Smith, Topical formulation of low level clobetasol propionate for treating disorders of the skin and mucous membranes, Google Patents, 2012.

[94] C. Charman, H. Williams, The use of corticosteroids and corticosteroid phobia in atopic dermatitis, Clinics in dermatology, 21 (2003) 193-200.

[95] A. Tosti, B.M. Piraccini, M. Pazzaglia, C. Vincenzi, Clobetasol propionate 0.05% under occlusion in the treatment of alopecia totalis/universalis, J Am Acad Dermatol, 49 (2003) 96-98.

[96] P. Lenane, C. Macarthur, P.C. Parkin, B. Krafchik, J. DeGroot, A. Khambalia, E. Pope, Clobetasol Propionate, 0.05%, vs Hydrocortisone, 1%, for Alopecia Areata in Children A Randomized Clinical Trial, Jama Dermatol, 150 (2014) 47-50.

[97] A. Baibergenova, J. Donovan, Lichen planopilaris: update on pathogenesis and treatment, Skinmed, 11 (2013) 161-165.

[98] S. Schoepe, H. Schacke, E. May, K. Asadullah, Glucocorticoid therapy-induced skin atrophy, Exp Dermatol, 15 (2006) 406-420.

[99] B. Havlickova, M. Friedrich, The advantages of topical combination therapy in the treatment of inflammatory dermatomycoses, Mycoses, 51 (2008) 16-26.

[100] L. Mu, S.S. Feng, A novel controlled release formulation for the anticancer drug paclitaxel (Taxol): PLGA nanoparticles containing vitamin E TPGS, J Control Release, 86 (2003) 33-48.

[101] P. Prabu, A.A. Chaudhari, N. Dharmaraj, M.S. Khil, S.Y. Park, H.Y. Kim, Preparation, characterization, in-vitro drug release and cellular uptake of poly(caprolactone) grafted dextran copolymeric nanoparticles loaded with anticancer drug, J Biomed Mater Res A, 90A (2009) 1128-1136.

[102] M. Fontana, K. Coradini, S. Guterres, A. Pohlmann, R. Beck, Nanoencapsulation as a way to control the release and to increase the photostability of clobetasol propionate: influence of the nanostructured system, J Biomed Nanotechnol, 5 (2009) 254-263.

[103] A.F. Ourique, A. Melero, C.D. da Silva, U.F. Schaefer, A.R. Pohlmann, S.S. Guterres, C.M. Lehr, K.H. Kostka, R.C.R. Beck, Improved photostability and reduced skin permeation of tretinoin: Development of a semisolid nanomedicine, Eur J Pharm Bipharm, 79 (2011) 95-101.

[104] A. Melero, A. Ferreira Ourique, S. Staniscuaski Guterres, A. Raffin Pohlmann, C.M. Lehr, R.C. Ruver Beck, U. Schaefer, Nanoencapsulation in Lipid-Core Nanocapsules Controls Mometasone Furoate Skin Permeability Rate and Its Penetration to the Deeper Skin Layers, Skin Pharm Phys, 27 (2014) 217-228.

[105] S.S. Feng, 15. Vitamin E TPGS based nanoparticles of biodegradable polymers for controlled release of anticancer drugs: Original research article: a novel controlled release formulation for the anticancer drug paclitaxel (Taxol): PLGA nanoparticles containing vitamin E TPGS (2003), J Control Release, 190 (2014) 58-60.

[106] J. Panyam, V. Labhasetwar, Biodegradable nanoparticles for drug and gene delivery to cells and tissue, Adv Drug Deliver Rev, 64 (2012) 61-71.

[107] Y. Frum, G.M. Eccleston, V.M. Meidan, In-vitro permeation of drugs into porcine hair follicles: is it quantitatively equivalent to permeation into human hair follicles?, J Pharm Pharmacol, 60 (2008) 145-151.

[108] J. Lademann, H. Richter, M. Meinke, W. Sterry, A. Patzelt, Which skin model is the most appropriate for the investigation of topically applied substances into the hair follicles?, Skin Pharm Phys, 23 (2010) 47-52.

[109] U. Jacobi, M. Kaiser, R. Toll, S. Mangelsdorf, H. Audring, N. Otberg, W. Sterry, J. Lademann, Porcine ear skin: an in vitro model for human skin, Skin Res Technol, 13 (2007) 19-24.

[110] F.H. Sakamoto, Z. Tannous, A.G. Doukas, W.A. Farinelli, N.A. Smith, D. Zurakowski, R.R. Anderson, Porphyrin Distribution After Topical Aminolevulinic Acid in a Novel Porcine Model of Sebaceous Skin, Lasers in Surgery and Medicine, 41 (2009) 154-160.

[111] H. Clowes, R. Scott, J. Heylings, Skin absorption: flow-through or static diffusion cells, Toxicol in vitro, 8 (1994) 827-830.

[112] W. Diembeck, H. Beck, F. Benech-Kieffer, P. Courtellemont, J. Dupuis, W. Lovell, M. Paye, J. Spengler, W. Steiling, Test guidelines for in vitro assessment of dermal absorption and percutaneous penetration of cosmetic ingredients, Food and Chemical Toxicology, 37 (1999) 191-205.

[113] S.-F. Ng, J.J. Rouse, F.D. Sanderson, V. Meidan, G.M. Eccleston, Validation of a static Franz diffusion cell system for in vitro permeation studies, AAPS PharmSciTech, 11 (2010) 1432-1441.

[114] OECD, Guideline for the testing of chemicals. Skin Absorption: in vitro Method, (2004).

[115] R. Alvarez-Roman, A. Naik, Y.N. Kalia, H. Fessi, R.H. Guy, Visualization of skin penetration using confocal laser scanning microscopy, Eur J Pharm Biopharm, 58 (2004) 301-316.

[116] J. Lademann, H. Weigmann, C. Rickmeyer, H. Barthelmes, H. Schaefer, G. Mueller, W. Sterry, Penetration of titanium dioxide microparticles in a sunscreen formulation into the horny layer and the follicular orifice, Skin Pharm Phys, 12 (1999) 247-256.

[117] R. Toll, U. Jacobi, H. Richter, J. Lademann, H. Schaefer, U. Blume-Peytavi, Penetration profile of microspheres in follicular targeting of terminal hair follicles, J Invest Dermatol, 123 (2004) 168-176.

[118] A. Teichmann, U. Jacobi, M. Ossadnik, H. Richter, S. Koch, W. Sterry, J. Lademann, Differential stripping: Determination of the amount of topically applied substances penetrated into the hair follicles, J Invest Dermatol, 125 (2005) 264-269.

[119] A. Teichmann, M. Ossadnik, H. Richter, W. Sterry, J. Lademann, Semiquantitative determination of the penetration of a fluorescent hydrogel formulation into the hair follicle with and without follicular closure by microparticles by means of differential stripping, Skin Pharm Phys 19 (2006) 101-105.

[120] J.L. Madara, Regulation of the movement of solutes across tight junctions, Annual review of physiology, 60 (1998) 143-159.

[121] R.S. Everett, M.K. Vanhook, N. Barozzi, I. Toth, L.G. Johnson, Specific modulation of airway epithelial tight junctions by apical application of an occludin peptide, Mol Pharmacol, 69 (2006) 492-500.

[122] E.K. Anderberg, T. Lindmark, P. Artursson, Sodium Caprate Elicits Dilatations in Human Intestinal Tight Junctions and Enhances Drug Absorption by the Paracellular Route, Pharmaceut Res, 10 (1993) 857-864.

REFERENCES

[123] N. Kirschner, R. Rosenthal, M. Furuse, I. Moll, M. Fromm, J.M. Brandner, Contribution of tight junction proteins to ion, macromolecule, and water barrier in keratinocytes, J Invest Dermatol, 133 (2013) 1161-1169.

[124] EZ-Link Sulfo-NHS-LC-Biotin and Biotinylation Kits, in, Thermo Scientific, Rockford, IL, 61101 USA 2015.

[125] T. Yuki, A. Hachiya, A. Kusaka, P. Sriwiriyanont, M.O. Visscher, K. Morita, M. Muto, Y. Miyachi, Y. Sugiyama, S. Inoue, Characterization of Tight Junctions and Their Disruption by UVB in Human Epidermis and Cultured Keratinocytes, J Invest Dermatol, 131 (2011) 744-752.

[126] N. Kirschner, J.M. Brandner, Barriers and more: functions of tight junction proteins in the skin, Barriers and Channels Formed by Tight Junction Proteins I, 1257 (2012) 158-166.

[127] M.E. Herbig, P. Houdek, S. Gorissen, M. Zorn-Kruppa, E. Wladykowski, T. Volksdorf, S. Grzybowski, G. Kolios, C. Willers, H. Mallwitz, A custom tailored model to investigate skin penetration in porcine skin and its comparison with human skin, Eur J Pharm Biopharm, (2015).

[128] R.L. Bronaugh, R.F. Stewart, E.R. Congdon, Methods for in vitro percutaneous absorption studies. II. Animal models for human skin, Toxi Appl Pharm, 62 (1982) 481-488.

[129] G.W. Lu, S. Valiveti, J. Spence, C. Zhuang, L. Robosky, K. Wade, A. Love, L.Y. Hu, D. Pole, M. Mollan, Comparison of artificial sebum with human and hamster sebum samples, Int J Pharm, 367 (2009) 37-43.

[130] N. Otberg, A. Patzelt, U. Rasulev, T. Hagemeister, M. Linscheid, R. Sinkgraven, W. Sterry, J. Lademann, The role of hair follicles in the percutaneous absorption of caffeine, Brit J Pharm, 65 (2008) 488-492.

[131] A.C. Lauer, C. Ramachandran, L.M. Lieb, S. Niemiec, N.D. Weiner, Targeted delivery to the pilosebaceous unit via liposomes, Adv Drug Deliver Rev, 18 (1996) 311-324.

[132] P.J. Caspers, G.W. Lucassen, E.A. Carter, H.A. Bruining, G.J. Puppels, In vivo confocal Raman microspectroscopy of the skin: noninvasive determination of molecular concentration profiles, J Invest Dermatol, 116 (2001) 434-442.

[133] A. Tfayli, O. Piot, F. Pitre, M. Manfait, Follow-up of drug permeation through excised human skin with confocal Raman microspectroscopy, Eur Biophys J Biophy, 36 (2007) 1049-1058.

[134] G. Zhang, C.R. Flach, R. Mendelsohn, Tracking the dephosphorylation of resveratrol triphosphate in skin by confocal Raman microscopy, J Control Release, 123 (2007) 141-147.

[135] C. Adlhart, W. Baschong, Surface distribution and depths profiling of particulate organic UV absorbers by Raman imaging and tape stripping, Int J Cosmic Scie, 33 (2011) 527-534.

[136] G. Zhang, L. Senak, D.J. Moore, Measuring changes in chemistry, composition, and molecular structure within hair fibers by infrared and Raman spectroscopic imaging, J Biomed Opt, 16 (2011) 056009-056009-056007.

[137] B. Barry, H. Edwards, A. Williams, Fourier transform Raman and infrared vibrational study of human skin: assignment of spectral bands, J Raman Spectros, 23 (1992) 641-645.

[138] L. Franzen, C. Mathes, S. Hansen, M. Windbergs, Advanced chemical imaging and comparison of human and porcine hair follicles for drug delivery by confocal Raman microscopy, J Biomed Opt, 18 (2013).

[139] L. Silveira, F.L. Silveira, B. Bodanese, R.A. Zangaro, M.T.T. Pacheco, Discriminating model for diagnosis of basal cell carcinoma and melanoma in vitro based on the Raman spectra of selected biochemicals, J Biomed OPt, 17 (2012) 077003-077003.

[140] H. Edwards, D. Hunt, M. Sibley, FT-Raman spectroscopic study of keratotic materials: horn, hoof and tortoiseshell, Spectrochimica Acta Part A, 54 (1998) 745-757.

[141] A. Nasir, A. Friedman, S. Wang, Nanotechnology in dermatology, Springer Science & Business Media, 2012.

[142] S.F. Zakrzewski, Environmental toxicology, Oxford University Press, 2002.

[143] L.W. Zhang, W.W. Yu, V.L. Colvin, N.A. Monteiro-Riviere, Biological interactions of quantum dot nanoparticles in skin and in human epidermal keratinocytes, Toxicol Appl Pharmacol, 228 (2008) 200-211.

[144] B. Mahe, A. Vogt, C. Liard, D. Duffy, V. Abadie, O. Bonduelle, A. Boissonnas, W. Sterry, B. Verrier, U. Blume-Peytavi, B. Combadiere, Nanoparticle-based targeting of vaccine compounds to skin antigen-presenting cells by hair follicles and their transport in mice, J Invest Dermatol 129 (2009) 1156-1164.

[145] A. Mittal, K. Schulze, T. Ebensen, S. Weissmann, S. Hansen, C.M. Lehr, C.A. Guzman, Efficient nanoparticle-mediated needle-free transcutaneous vaccination via hair follicles requires adjuvantation, Nanomed-Nanotechnol, (2014) 11.1:147-154.

[146] A. Mittal, K. Schulze, T. Ebensen, S. Weissmann, S. Hansen, C.A. Guzmán, C.-M. Lehr, Inverse micellar sugar glass (IMSG) nanoparticles for transfollicular vaccination, J Control Release, (2015).

[147] P.M. Elias, Epidermal Lipids, Barrier Function, and Desquamation, J Invest Dermatol, 80 (1983) S44-S49.

[148] J.M. Brandner, M. Zorn-Kruppa, T. Yoshida, I. Moll, L.A. Beck, A. De Benedetto, Epidermal tight junctions in health and disease, Tissue Barriers, 3 (2014) e974451.

[149] A. Kubo, K. Nagao, M. Amagai, Epidermal barrier dysfunction and cutaneous sensitization in atopic diseases, J Clin Invest, 122 (2012) 440-447.

[150] C.A. O'Neill, D. Garrod, Tight junction proteins and the epidermis, Exp Dermatol, 20 (2011) 88-91.

[151] T. Yuki, A. Komiya, A. Kusaka, T. Kuze, Y. Sugiyama, S. Inoue, Impaired tight junctions obstruct stratum corneum formation by altering polar lipid and profilaggrin processing, J Dermatol Sci, 69 (2013) 148-158.

[152] F. Rancan, Z. Afraz, B. Combadiere, U. Blume-Peytavi, A. Vogt, Hair Follicle Targeting with Nanoparticles, Nanotechnol in Dermatol, Springer, 2013, pp. 95-107.

[153] L. Langbein, C. Grund, C. Kuhn, S. Praetzel, J. Kartenbeck, J.M. Brandner, I. Moll, W.W. Franke, Tight junctions and compositionally related junctional structures in mammalian stratified epithelia and cell cultures derived therefrom, Eur J Cell Biol, 81 (2002) 419-435.

[154] T.C. Troy, R. Rahbar, A. Arabzadeh, R.M.K. Cheung, K. Turksen, Delayed epidermal permeability barrier formation and hair follicle aberrations in Inv-Cldn6 mice, Mech Develop, 122 (2005) 805-819.

[155] L. Alibardi, N. Bernd, Immunolocalization of junctional proteins in human hairs indicates that the membrane complex stabilizes the inner root sheath while desmosomes contact the companion layer through specific keratins, Acta histochem, 115 (2013) 519-526.

[156] S. Hadj-Rabia, L. Baala, P. Vabres, D. Hamel-Teillac, E. Jacquemin, M. Fabre, S. Lyonnet, Y. de Prost, A. Munnich, M. Hadchouel, Claudin-1 gene mutations in neonatal sclerosing cholangitis associated with ichthyosis: a tight junction disease, Gastroenterology, 127 (2004) 1386-1390.

[157] M. Paganelli, X. Stephenne, A. Gilis, E. Jacquemin, A.H. Caude, M. Girard, E. Gonzales, N. Revencu, R. Reding, C. Wanty, Neonatal ichthyosis and sclerosing cholangitis syndrome: extremely variable liver disease severity from claudin-1 deficiency, J Pediatr Gast Nutr, 53 (2011) 350-354.

[158] V. Kassis, J. Søndergaard, Heat-separation of normal human skin for epidermal and dermal prostaglandin analysis, Arch Dermatol Res, 273 (1982) 301-306.

[159] J.M. Brandner, S. Kief, C. Grund, M. Rendl, P. Houdek, C. Kuhn, E. Tschachler, W.W. Franke, I. Moll, Organization and formation of the tight junction system in human epidermis and cultured keratinocytes, Eur J Cell Biol, 81 (2002) 253-263.

[160] W. Wu, Q. He, C. Jiang, Magnetic iron oxide nanoparticles: synthesis and surface functionalization strategies, Nanoscale Res Lett, 3 (2008) 397-415.

[161] R.A. Jain, The manufacturing techniques of various drug loaded biodegradable poly(lactide-co-glycolide) (PLGA) devices, Biomaterials, 21 (2000) 2475-2490.

[162] M. Laue, Electron microscopy of viruses, Methods in cell biology, 96 (2010) 1-20.

[163] J.H. Schefe, K.E. Lehmann, I.R. Buschmann, T. Unger, H. Funke-Kaiser, Quantitative real-time RT-PCR data analysis: current concepts and the novel "gene expression's CT difference" formula, J Molec Med, 84 (2006) 901-910.

[164] K. Yoshida, M. Yokouchi, K. Nagao, K. Ishii, M. Amagai, A. Kubo, Functional tight junction barrier localizes in the second layer of the stratum granulosum of human epidermis, J Dermatol Sci, 71 (2013) 89-99.

[165] A. Ishida-Yamamoto, M. Kishibe, M. Murakami, M. Honma, H. Takahashi, H. Iizuka, Lamellar granule secretion starts before the establishment of tight junction barrier for paracellular tracers in mammalian epidermis, PloS one, 7 (2012).

[166] M. Saitou, K. Fujimoto, Y. Doi, M. Itoh, T. Fujimoto, M. Furuse, H. Takano, T. Noda, S. Tsukita, Occludin-deficient embryonic stem cells can differentiate into polarized epithelial cells bearing tight junctions, J Cell Biol, 141 (1998) 397-408.

[167] J.A. Tunggal, I. Helfrich, A. Schmitz, H. Schwarz, D. Günzel, M. Fromm, R. Kemler, T. Krieg, C.M. Niessen, E-cadherin is essential for in vivo epidermal barrier function by regulating tight junctions, The EMBO journal, 24 (2005) 1146-1156.

[168] N. Kirschner, C. Poetzl, P. von den Driesch, E. Wladykowski, I. Moll, M.J. Behne, J.M. Brandner, Alteration of tight junction proteins is an early event in psoriasis: putative involvement of proinflammatory cytokines, J Invest Dermatol, 129 (2009) S57-S57.

[169] N. Kirschner, C. Bohner, S. Rachow, J.M. Brandner, Tight junctions: is there a role in dermatology?, Arach Dermatol Res, 302 (2010) 483-493.

[170] E. Kam, M.B. Hodgins, Communication Compartments in Hair-Follicles and Their Implication in Differentiative Control, Development, 114 (1992) 389-393.

[171] E. Windsor, G.E. Cronheim, Gastro-intestinal absorption of heparin and synthetic heparinoids, Nature, 190 (1961) 263-264.

[172] M.A. Deli, Potential use of tight junction modulators to reversibly open membranous barriers and improve drug delivery, Biochim Biophys Acta, 1788 (2009) 892-910.

[173] X. Huang, H. Tanojo, J. Leon, C. Cuesico, Impact of vehicle on clobetasol propionate skin permeation and drug distribution in vitro, J Am Acad Dermatol, 50 (2004) P178-P178.

[174] A. Tosti, M. Iorizzo, G.L. Botta, M. Milani, Efficacy and safety of a new clobetasol propionate 0.05% foam in alopecia areata: a randomized, double-blind placebo-controlled trial, J Eur Acad Dermatol, 20 (2006) 1243-1247.

[175] P. Lenane, C. Macarthur, P.C. Parkin, B. Krafchik, J. DeGroot, A. Khambalia, E. Pope, Clobetasol Propionate, 0.05%, vs Hydrocortisone, 1%, for Alopecia Areata in Children: A Randomized Clinical Trial, Jama Dermatol, 150 (2014) 47-50.

[176] V. Lajevardi, S.Z. Ghodsi, A. Goodarzi, P. Hejazi, A. Azizpour, S. Beygi, Comparison of Systemic Mycophenolate Mofetil with Topical Clobetasol in Lichen Planopilaris: A Parallel-Group, Assessor- and Analyst-Blinded, Randomized Controlled Trial, Am J Clin Dermatol, 16 (2015) 303-311.

[177] J. Aubert, H. Lui, P. Reiniche, P.E. Fogel, Y. Poulin, Gene expression profiling in psoriatic scalp hair follicles: Clobetasol propionate shampoo 0.05% normalizes psoriasis disease markers, J Am Acad Dermatol, 64 (2011) Ab8-Ab8.

[178] L. Abal-Diaz, X. Soria, J.M. Casanova-Seuma, [Scarring alopecia], Actas dermo-sifiliograficas, 103 (2012) 376-387.

[179] C.F. Faulkner, N.J. Wilson, S.K. Jones, Frontal fibrosing alopecia associated with cutaneous lichen planus in a premenopausal woman, Aust J Dermatol, 43 (2002) 65-67.

[180] H.C. Korting, M.J. Kerscher, M. Schaferkorting, Topical Glucocorticoids with Improved Benefit Risk Ratio - Do They Exist, J Am Acad Dermatol, 27 (1992) 87-92.

[181] S. Dhar, J. Seth, D. Parikh, Systemic side-effects of topical corticosteroids, Indian J Dermatol, 59 (2014) 460-464.

[182] A. Coondoo, M. Phiske, S. Verma, K. Lahiri, Side-effects of topical steroids: A long overdue revisit, Indian Dermatol J, 5 (2014) 416-425.

[183] J. Aubert, P. Reiniche, P. Fogel, Y. Poulin, H. Lui, C. Lynde, J. Shapiro, H. Villemagne, P. Soto, J.J. Voegel, Gene expression profiling in psoriatic scalp hair follicles: clobetasol propionate shampoo 0.05% normalizes psoriasis disease markers, J Eur Acad Dermatol, 24 (2010) 1304-1311.

[184] J. Lademann, H. Richter, A. Teichmann, N. Otberg, U. Blume-Peytavi, J. Luengo, B. Weiss, U.F. Schaefer, C.M. Lehr, R. Wepf, W. Sterry, Nanoparticles - An efficient carrier for drug delivery into the hair follicles, Eur J Pharm Biopharm, 66 (2007) 159-164.

[185] J. Lademann, A. Patzelt, H. Richter, S. Schanzer, W. Sterry, A. Filbry, K. Bohnsack, F. Rippke, M. Meinke, Comparison of two in vitro models for the analysis of follicular penetration and its prevention by barrier emulsions, Eur J Pharm Biopharm, 72 (2009) 600-604.

[186] H. Fessi, F. Puisieux, J.P. Devissaguet, N. Ammoury, S. Benita, Nanocapsule Formation by Interfacial Polymer Deposition Following Solvent Displacement, Int J Pharm, 55 (1989) R1-R4.

[187] M.A. Woodruff, D.W. Hutmacher, The return of a forgotten polymer-Polycaprolactone in the 21st century, Prog Polym Sci, 35 (2010) 1217-1256.

[188] E. Jager, C.G. Venturini, F.S. Poletto, L.M. Colome, J.P.U. Pohlmann, A. Bernardi, A.M.O. Battastini, S.S. Guterres, A.R. Pohlmann, Sustained Release from Lipid-Core Nanocapsules by Varying the Core Viscosity and the Particle Surface Area, J Biomed Nanotechnol, 5 (2009) 130-140.

[189] F.S. Poletto, L.A. Fiel, M.V. Lopes, G. Schaab, A.M. Gomes, S.S. Guterres, B. Rossi-Bergmann, A.R. Pohlmann, Fluorescent-Labeled Poly (-caprolactone) Lipid-Core Nanocapsules: Synthesis, Physicochemical Properties and Macrophage Uptake, J Colloid Sci Biotech, 1 (2012) 89-98.

[190] M. Fontana, J. Rezer, K. Coradini, D. Leal, R. Beck, Improved efficacy in the treatment of contact dermatitis in rats by a dermatological nanomedicine containing clobetasol propionate, Eur J Pharm Biopharm, 79 (2011) 241-249.

[191] F.Q. Hu, H. Yuan, H.H. Zhang, M. Fang, Preparation of solid lipid nanoparticles with clobetasol propionate by a novel solvent diffusion method in aqueous system and physicochemical characterization, Int J Pharm, 239 (2002) 121-128.

[192] H.J. Weigmann, J. Lademann, H. Meffert, H. Schaefer, W. Sterry, Determination of the horny layer profile by tape stripping in combination with optical spectroscopy in the visible range as a prerequisite to quantify percutaneous absorption, Skin Pharm Phys, 12 (1999) 34-45.

[193] J. Lademann, H.J. Weigmann, S. Schanzer, H. Richter, H. Audring, C. Antoniou, G. Tsikrikas, H. Gers-Barlag, W. Sterry, Optical investigations to avoid the disturbing influences of furrows and wrinkles quantifying penetration of drugs and cosmetics into the skin by tape stripping, J Biomed Opt, 10 (2005) 054015.

[194] Y.S. Nam, I.K. Kwon, K.-B. Lee, Monitoring of clobetasol propionate and betamethasone dipropionate as undeclared steroids in cosmetic products manufactured in Korea, Forensic Scie Int, 210 (2011) 144-148.

[195] SCCNFP, Basic criteria for the in vitro assessment of dermal absorption of cosmetic ingredients, (2003).

[196] A.M. Kligman, E. Christophel, Preparation of Isolated Sheets of Human Stratum Corneum, Arch Dermatol, 88 (1963) 702-&.

[197] U.M. Agency, Guideline on validation of bioanalytical methods, (2009).

[198] L.A. Fiel, L.M. Rebelo, T.D. Santiago, M.D. Adorne, S.S. Guterres, J.S. de Sousa, A.R. Pohlmann, Diverse deformation properties of polymeric nanocapsules and lipid-core nanocapsules, Soft Matter, 7 (2011) 7240-7247.

[199] W. Abdelwahed, G. Degobert, H. Fessi, A pilot study of freeze drying of poly(epsilon-caprolactone) nanocapsules stabilized by poly(vinyl alcohol): formulation and process optimization, Int J Pharm, 309 (2006) 178-188.

[200] H. Wagner, K.-H. Kostka, C.-M. Lehr, U.F. Schaefer, pH profiles in human skin: influence of two in vitro test systems for drug delivery testing, Eur J Pharm Biopharm, 55 (2003) 57-65.

[201] T.L. De Brum, L.A. Fiel, R.V. Contri, S.S. Guterres, A.R. Pohlmann, Polymeric Nanocapsules and Lipid-Core Nanocapsules Have Diverse Skin Penetration, J Nanosci Nanotechno, 15 (2015) 773-780.

[202] F.S. Poletto, C.P. De Oliveira, H. Wender, D. Regent, B. Donida, S.R. Teixeira, S.S. Guterres, B. Rossi-Bergmann, A.R. Pohlmann, How sorbitan monostearate can increase drug-loading capacity of lipid-core polymeric nanocapsules, J Nanosci Nanotechno, 15 (2015) 827-837.

[203] A. Mittal, A.S. Raber, C.M. Lehr, S. Hansen, Particle based vaccine formulations for transcutaneous immunization, Hum Vacc Immunother, 9 (2013) 1950-1955.

[204] F. Jimenez, J.M. Ruifernandez, Distribution of human hair in follicular units - A mathematical model for estimating the donor size in follicular unit transplantation, Dermatol Surg, 25 (1999) 294-298.

[205] F. Pouradier, C. Celine, D. Marie-Florence, F. Frederic, P. Segolene, D. Stephane, L. Genevieve, Functional and structural age-related changes in the scalp skin of Caucasian women, Skin Res Technol, 19 (2013) 384-393.

[206] X. Liu, J.E. Grice, J. Lademann, N. Otberg, S. Trauer, A. Patzelt, M.S. Roberts, Hair follicles contribute significantly to penetration through human skin only at times soon after application as a solvent deposited solid in man, Brit J Clin Pharm, 72 (2011) 768-774.

[207] S. Kuchler, K. Struver, W. Friess, Reconstructed skin models as emerging tools for drug absorption studies, Expert Opin Drug Met, 9 (2013) 1255-1263.

Curriculum Vitae

PERSONAL INFORMATION

Name	Christiane Mathes
Date of Birth	06.11.1986

SECONDARY AND HIGHER EDUCATION

02/20112 – 04/2015	**Doctoral Thesis** at Saarland University, Saarbruecken, Germany. Supervised by Prof. Dr. Claus-Michael Lehr
11/2010 – 12/2011	**Master Thesis** at University of Valencia, Valencia, Spain. Supervised by Prof. Dr. Teresa Garrigues, "Initial Evaluation of QSPeR Analysis Based on Skin Permeability Coefficients"
08/2007 – 05/2010	**Bachelor** of Science in Pharmaceutical Sciences with a Minor in Chemistry at the University of Missouri Kansas City (UMKC), Kansas City, Missouri, USA
08/2005 – 05/2007	**General Studies** at University of Missouri, Columbia (MU), Columbia, Missouri, USA
09/2001 – 05/2005	**Secondary Education** at Lee's Summit North High School, Lee's Summit, Missouri, USA

INTERNSHIPS

08 – 10/2010	**8 Week Intensive Spanish Language Course** offered by Costa de Valencia, Escuela de Español, in Valencia, Spain
06 – 07/2009	**Pharmaceutical Internship** in the department Pharmaceutical Quality Control at Bayer HealthCare in Shawnee, Kansas, USA

AWARDS

02/2014	**Poster Award** at International Biological Barriers Conference at Saarland University, Saarbruecken, Germany for work entitled: „Uptake of three different poly-caprolactone nanoparticles into the hair follicle"
11/2014	**Poster Award** at Doktorandentag der Fakultät 8, Universität des Saarlandes, Saarbruecken, Germany for work entitled: „Expression and localization of tight junction proteins and tight junction barrier function in porcine hair follicles"

Scientific Output

Articles published in Peer-reviewed Journals

L. Franzen[*], **C. Mathes**[*], S. Hansen, M. Windbergs, Advanced chemical imaging and comparison of human and porcine hair follicles for drug delivery by confocal Raman microscopy, *Journal of Biomedical Optics*, 18 (2013).

C. Mathes[*], J.M. Brandner[*], M. Laue, S.S. Raesch, S. Hansen, A.V. Failla, S. Vidal, I. Moll, U.F. Schaefer, C.M. Lehr, Tight junctions form a barrier in porcine hair follicles, *European Journal of Cell Biology*, 95 (2016) 89-99.

C. Mathes, A. Melero, P. Conrad, T. Vogt, L. Rigo, D. Selzer, W. Prado, C. De Rossi, T. Garrigues, S. Hansen, S.S. Guterres, A.R. Pohlmann, R.C. Beck, C.M. Lehr, U.F. Schaefer, Nanocarriers for optimizing the balance between interfollicular permeation and follicular uptake of topically applied clobetasol to minimize adverse effects, *Journal of Controlled Release*, 223 (2016) 207-214.

[*] the authors contributed equally to this work

Posters & Oral Presentations

C. Mathes, A. Melero, P. Conrad, T. Vogt, L. Rigo, D. Selzer, W. Prado, C. De Rossi, T. Garrigues, S. Hansen, S.S. Guterres, A.R. Pohlmann, R.C. Beck, C.M. Lehr, U.F. Schaefer, *Uptake of three different poly-caprolactone nanoparticles into the hair follicle*.

Has been presented at:

- ❖ HIPS Symposium 2013, Saarbrücken, (DE): Poster
- ❖ CIFARP Congress 2013, Ribeirão Preto (BRA): Poster & Oral Presentation
- ❖ 5th Meeting of the Pharmaceutical Sciences Graduate Program 2013, UFRGS, Porto Alegre (BRA): Oral Presentation
- ❖ Biological Barriers 2014, Saarbrücken (DE): Poster**

C. Mathes, J.M. Brandner, M. Laue, S.S. Raesch, S. Hansen, A.V. Failla, S. Vidal, I. Moll, U.F. Schaefer, C.M. Lehr, *Expression and localization of tight junction proteins and tight junction barrier function in porcine hair follicles*.

Has been presented at:

- ❖ HIPS Symposium 2014, Saarbrücken (DE): Poster
- ❖ E2BRN Conference 2014, Copenhagen (DK): Oral Presentation
- ❖ ESDR Annual Conference 2014, Copenhagen (DK): Poster
- ❖ DPhG Annual Conference 2014, Frankfurt (DE): Poster
- ❖ 6th Meeting of the Pharmaceutical Sciences Graduate Program 2014, UFRGS, Porto Alegre (BRA): Oral Presentation
- ❖ Doktorandentag der Fakultät 8 (2014), Saarland University, Saarbrücken (DE): Poster**
- ❖ GradUS Workshop 2015, Saarland University, Saarbrücken (DE): Poster
- ❖ Annual Meeting 2015 of the Controlled Release Society, Edinburgh (SCO): Poster

**won Poster Award

Acknowledgements

As I am sitting here on the last Friday night before handing in my PhD thesis and reminiscing about the last three and a half years, I am trying to think about who all I owe a thank you to for helping me get here. What I have come to realize is that getting to the point of writing this final section, would have never been possible if it wasn't for so many different people.

First and foremost I want to thank Prof. Dr. Claus-Michael Lehr, my `Doktorvater´, for giving me the chance and opportunity to take on this project and be a part of our beloved DDEL team. He has helped me advance and grow in so many different ways, professionally and personally, and never failed to encourage me when things were getting rough. Alongside of him I also have to take a second to give a huge thank you to apl. Prof. Dr. Ulrich Schäfer, "Uli", who took it upon himself, shortly after retiring, to agree and supervise me during the last year and a half of my PhD time. Between the three of us we had many very fruitful, productive, and intense conversations about research and I am so very thankful to both of them for that. Besides, that, Uli gave me the chance to work in a cooperation project between the University of Porto Alegre (UFRGS), the University of Valencia (UV), and us, funded by the BMBF and CNPq/Brazil. This project ultimately gave me so much more than I ever expected. Besides accumulating a lot of good data, learning many new techniques, and being able to write a manuscript about the results, I got to go to and travel within the beautiful country of Brazil not just once, but twice within two years with my travel buddy, colleague, and dear friend Ana. Big thanks to her for making those two trips amazing! During our travels there I got to meet many special places and people, especially everybody in Porto Alegre. Ruy, Silvia, Adriana, and their whole UFRGS crew welcomed us with open arms and made the whole experience unforgettable. During my first trip to Brazil I was also able to attend the CIFARP conference in Ribeirão Preto, where I was not only invited to present my work in form of a Poster and Oral Presentation, but also met Maze, my boyfriend, partner in crime and best friend! So, Uli, for all of that, your never-ending patience, wisdom, and kind words, and so much more, I want to thank you here and now!

To Prof. Dr. Vogt and the entire thesis committee, I also want to extend my gratitude to for agreeing on giving their expert opinions on my thesis and helping me with this final step.

To Dr. Steffi Hansen, my first PostDoc/supervisor who was the one to initiate my PhD project, thank you for the guidance throughout the first year and a half. Our weekly meetings within "Team Steffi", consisting of Ankit, Anne, Christina, her, and myself taught me so very much about what doing research is all about. Every single one of them always had an open ear and never turned me down when I came to ask your help.

ACKNOWLEGEMENTS

Eidesstattliche Erklärung

"Hiermit versichere ich an Eides statt, dass ich diese Arbeit 'Drug Delivery to the Hair Follicle: Role of Follicular Tight Junctions as a Biological Barrier and the Potential for Targeting Clobetasol Nanocarriers' selbstständig und nur unter Angabe der angegebenen Quellen und Verweise angefertigt habe. Die aus anderen Quellen oder indirekt übernommenen Daten und Konzepte sind unter Angabe der Quellen gekennzeichnet. Ich habe diese Arbeit bisher weder im In- noch im Ausland in gleicher oder ähnlicher Form in einem Verfahren zur Erlangung eines akademischen Grades vorgelegt."

Saarbrücken, November 2015

Christiane Mathes